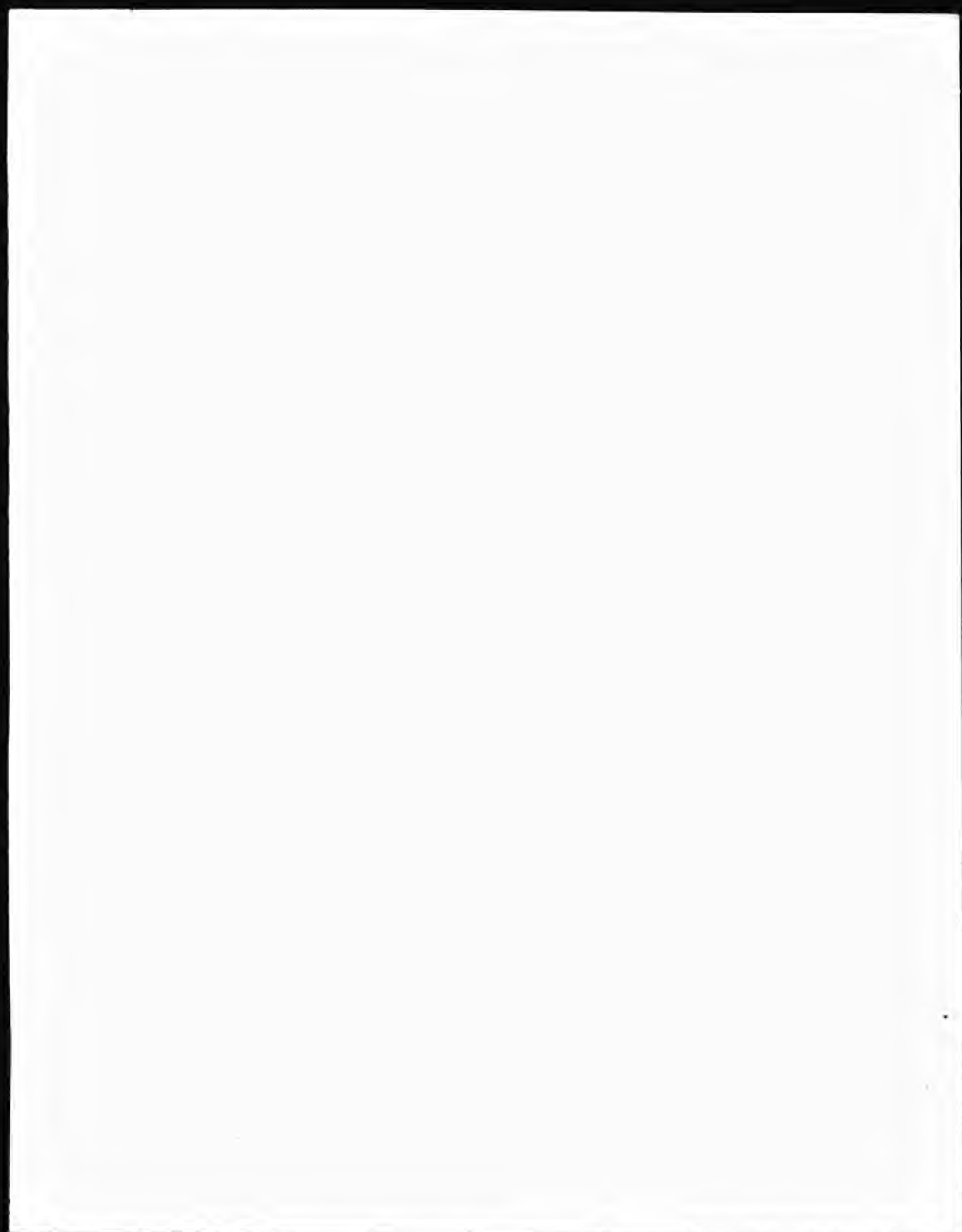


This PDF was created from the British Library's microfilm copy of the original thesis. As such the images are greyscale and no colour was captured.

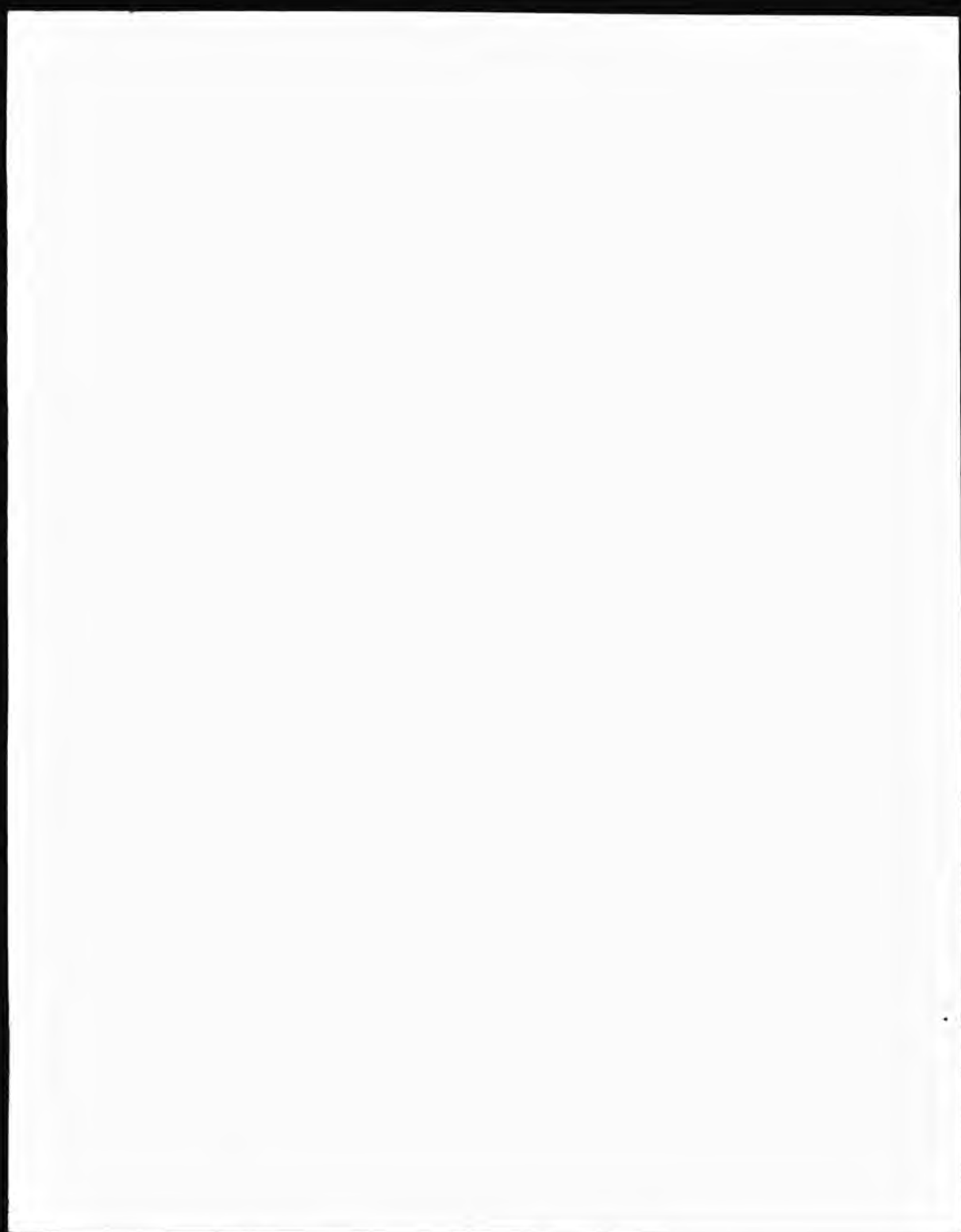
Due to the scanning process, an area greater than the page area is recorded and extraneous details can be captured.

This is the best available copy



DX

96473



THE BRITISH LIBRARY DOCUMENT SUPPLY CENTRE

TITLE

DIFFUSION PROBLEMS AND DEGRADATION OF HEARING OVERLAYS

AUTHOR

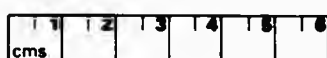
Prakash Shashikant Patel

INSTITUTION
and DATE

C.N.A.A. City of London Polytechnic
1989

Attention is drawn to the fact that the copyright of this thesis rests with its author.

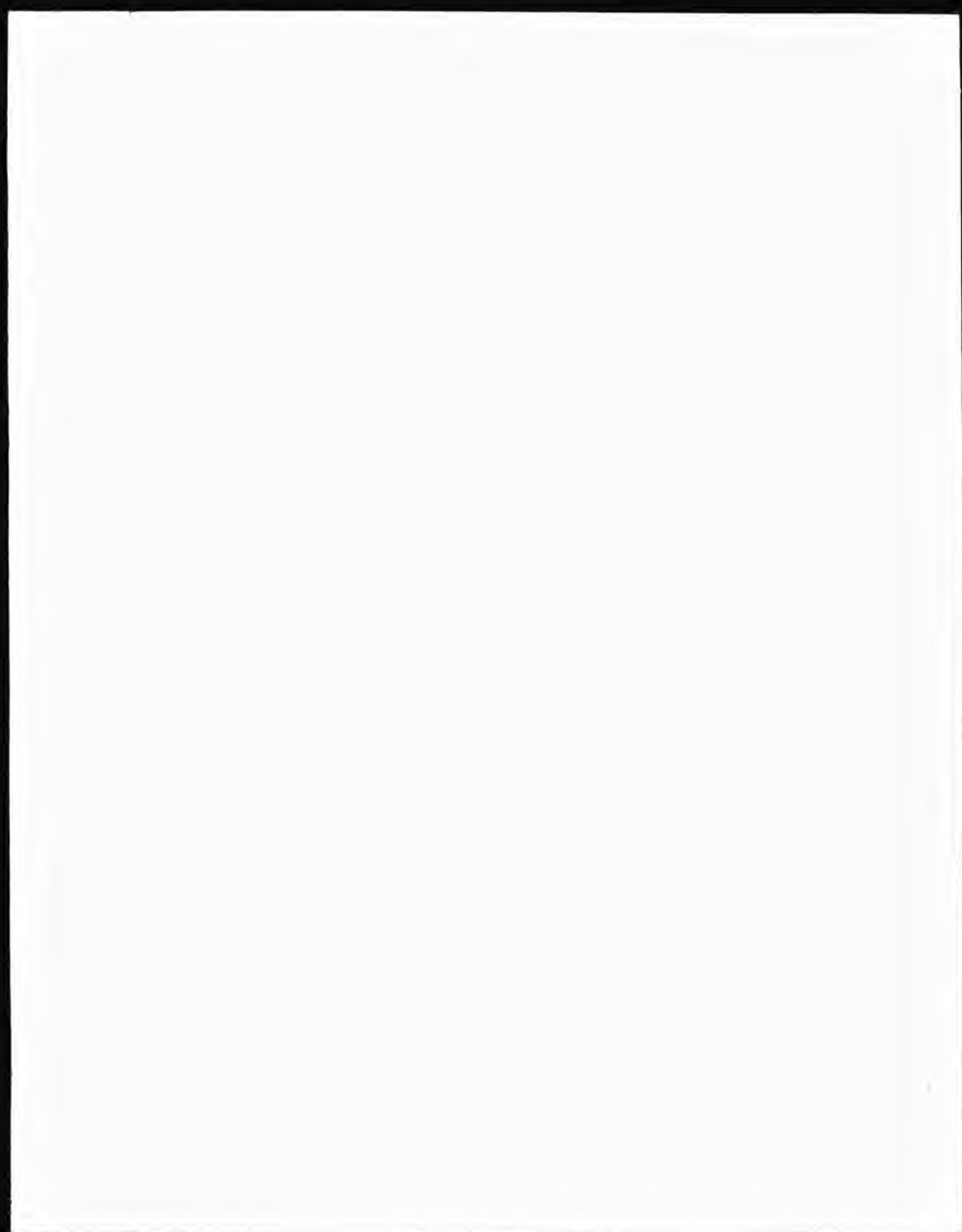
This copy of the thesis has been supplied on condition that anyone who consults it is understood to recognise that its copyright rests with its author and that no information derived from it may be published without the author's prior written consent.



CAM. 9

THE BRITISH LIBRARY
DOCUMENT SUPPLY CENTRE
Boston Spa, Wetherby
West Yorkshire
United Kingdom

REDUCTION X 21



DIFFUSION PROBLEMS AND DEGRADATION OF BEARING OVERLAYS

A thesis submitted to the Council for National Academic
Awards for the degree of Doctor of Philosophy

by

Prakash Shashikant Patel

Sponsoring Establishments

Department of Metallurgy and
Materials Engineering
City of London Polytechnic
Central House
Whitechapel High Street
London E1 7PF.

Shell Research Limited
Thornton Research Centre
PO Box 1
Chester CH1 3SH.

THE BRITISH LIBRARY DOCUMENT SUPPLY CENTRE

BRITISH THESES N O T I C E

The quality of this reproduction is heavily dependent upon the quality of the original thesis submitted for microfilming. Every effort has been made to ensure the highest quality of reproduction possible.

If pages are missing, contact the university which granted the degree.

Some pages may have indistinct print, especially if the original pages were poorly produced or if the university sent us an inferior copy.

Previously copyrighted materials (journal articles, published texts, etc.) are not filmed.

Reproduction of this thesis, other than as permitted under the United Kingdom Copyright Designs and Patents Act 1988, or under specific agreement with the copyright holder, is prohibited.

THIS THESIS HAS BEEN MICROFILMED EXACTLY AS RECEIVED

**THE BRITISH LIBRARY
DOCUMENT SUPPLY CENTRE
Boston Spa, Wetherby
West Yorkshire, LS23 7BQ
United Kingdom**

To my wife

Sanita

Whose is the greater part, the one who achieves,
or the one who forbears that the other may achieve?

CONTENTS

ACKNOWLEDGEMENTS

ABSTRACT

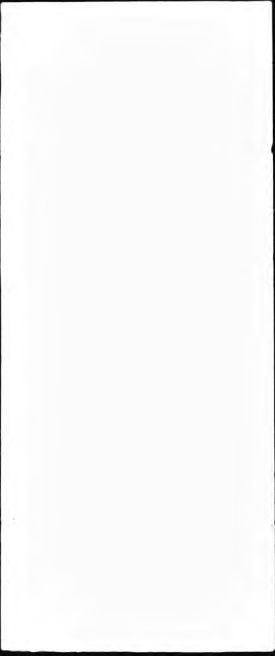
1.0	GENERAL INTRODUCTION	1
2.0	LITERATURE SURVEY	7
2.1	Introduction	
2.2	Bearing Materials	8
2.2.1	Introduction	
2.2.2	White Metal Bearing Alloys	9
2.2.3	Aluminium Bearing Alloys	11
2.2.4	Copper-Lead and Leaded Bronze Alloys	13
2.2.5	Overlay Alloys	15
2.2.6	Degradation of Bearing Overlays	17
2.3	Diffusion	21
2.3.1	Introduction	
2.3.2	Rates of Mass Transport by Diffusion	23
2.3.3	Temperature Dependence of Diffusion	26
2.3.4	Determination of Interdiffusion Coefficients	29
2.3.5	Grube Method	
2.3.6	Boltzmann-Matano Method	
2.3.7	Boltzmann-Matano-Heumann Method	30
2.3.8	Wagner's Method	31
2.4	Reactive Diffusion in Binary Systems	33
2.4.1	Introduction	

2.4.2	Solid State Growth of One Compound Layer	35
2.4.3	One Process in the A-B System	38
2.4.4	Growth of Two Compound Layers	47
2.4.5	Initial Stage of the Growth Process	54
2.4.5.1	Linear Growth	
2.4.5.2	Non-Linear Growth	56
2.4.6	The Role of Critical Thickness in determining the Growth Kinetics of the Layer	57
2.4.6.1	Departures of the Layer Thickness-Time Relationships	
2.4.7	Paralinear Stage of Growth of the Layers	59
2.4.8	Late Stage of Growth of Layers	60
2.5	Intermediate Phases in Barriered Overlay Bearings	62
2.5.1	Nucleation and Growth Kinetics of Intermediate Phases	64
2.6	Diffusion in Amorphous and Crystalline Alloys	67
2.7	Diffusion Barriers	72
2.7.1	Introduction	
2.7.2	Elemental Barriers	73
2.7.3	Single Crystal Barriers	76
2.7.4	Amorphous Diffusion Barriers	79
2.7.5	Stable Diffusion Barriers	81
2.7.6	Partially Stable Barriers	82
2.7.7	Sacrificial Barriers	85
2.7.8	Stuffed Barriers	86
2.8	Electroplating Processes for Plain Bearings	88

2.8.1	Electrodeposition of Lead-Tin Alloys	90
2.8.2	Electrodeposition of Amorphous Alloys	91
3.0	EXPERIMENTAL PROCEDURE	95
3.1	Introduction	
3.2	Electrodeposition Processes	97
3.2.1	Deposition Processes for Cu-P and Cu-B Barriers	100
3.2.2	Deposition Processes for Bi, Pb-P and Pb-Sn-Ni Alloys	103
3.2.3	Deposition of Amorphous Cr-C and Amorphous Ni-P Alloys	104
3.2.4	Deposition Processes for Pb-Sn and Sn	109
3.3	Corrosion Tests and Heat Treatment	111
3.4	Metallography	112
3.4.1	Marker Experiments	113
3.5	SEM and X-Ray Analysis	114
4.0	RESULTS	116
4.1	Introduction	
4.2	Investigation of Pb-Sn Overlayed Cu-P and Cu-B Diffusion Barriers	118
4.2.1	Electrodeposition of Cu-P and Cu-B Diffusion Barriers	
4.2.2	Metallography and Analysis	119
4.2.3	Growth Kinetics of Cu-Sn Diffusion Compounds	133

4.2.4	Corrosion of Pb Overlay in Presence of Cu-P barrier	139
4.3	Investigation of Pb-P and Bi Barriers and Pb-Sn-Ni overlays	
4.4	Investigation of Pb-Sn Overlayed Ni and Amorphous Ni-P Diffusion Barriers	143
4.4.1	Metallography and Analysis	
4.4.2	Marker Studies	149
4.4.3	Analysis of Ni and Amorphous Ni-P Diffusion Barriers	155
4.4.3.1	X-Ray Diffraction Studies	
4.4.3.2	Compositional Analysis of Ni/Sn and Ni-P/Sn Diffusion Couples	156
4.4.3.3	Compositional Analysis of Ni-P/Pb-Sn Diffusion Couples	165
4.4.4	Growth Kinetics of Ni-Sn Compounds	168
4.5	Determination of Interdiffusion Coefficients in Intermetallic Compounds	172
5.0	DISCUSSION	175
5.1	Introduction	
5.2	Investigation of Cu-P and Cu-B Barriers	177
5.3	On The Nucleation and Growth of Ni-Sn Compounds: Crystalline Ni vs Amorphous Ni-P Barrier.	182
5.3.1	The growth of Ni-Sn Compounds	186
5.3.2	Growth of Ni-Sn Compounds on Amorphous Ni-P Barrier Overlayed with Pb-20 wt/o Sn Alloy	191

5.4	Suppression of NiSn ₃ Compound in Amorphous Ni-P/Sn Diffusion Couples	194
5.4.1	Duplex Ni-Sn Compounds on Crystalline Ni Barrier	195
5.4.2	Single NiSn Compound on Amorphous Ni-P Barrier	199
5.5	Technological Importance of Amorphous Ni-P Barrier	204
5.6	Conclusions	206
5.7	Suggestions for Further Work	209
	REFERENCES	210



ACKNOWLEDGMENTS

I would like to express my sincere gratitude to my supervisors Dr R A Jarman, Mr M N Richards and Dr G W Roper for their encouragement and support throughout the course of this research, and in particular Dr S P Wach who initiated this project but passed away before its completion.

I am also indebted to Shell Research Limited for financing this research.

My thanks are also due to Dr M Clarke and Dr C J L Booker for useful discussions.

ABSTRACT

The corrosion and degradation of Pb-Sn bearing overlays is a bilateral process. During service, the lubricant becomes corrosive due to the breakdown of inhibitors with subsequent oxidation occurring at operating temperatures (120-170°C). At the same time the interdiffusion of Cu and Sn between the substrate and the overlay continues to sustain the growth of Cu-Sn intermetallic compounds, which depletes the Sn content of the overlay below the threshold limit of 3-4 wt/o and thus renders it liable to corrosion. In the worst instance the overlay is lost due to corrosion and/or fatigue failure along the layer of brittle Cu-Sn intermetallic compounds with the consequential seizure of the engine.

The interdeposition of a Ni diffusion barrier between the substrate and the overlay is a widely accepted practice. This offers some relief but, Ni-Sn compound formation occurs although, to a lesser extent than Cu-Sn compounds.

Recently, it was claimed that Cu-P and Cu-B diffusion barriers based on impurity co-deposition of P and B completely prevents the nucleation and growth of Cu-Sn intermetallic compounds. These claims and the theoretical basis upon which these barriers were founded were subject to scrutiny and shown to be incongruous.

An alternative diffusion barrier based on amorphous Ni-P alloy has been identified in which only Ni_3Sn_4 compound was found to grow when Ni-P/Sn couples were annealed. The growth rate of this compound was approximately one third less compared to that on a crystalline Ni barrier which results in the growth of duplex ($\text{Ni}_3\text{Sn}_4 + \text{NiSn}_2$) compounds. It is found that the Ni-P barrier partially crystallises before the nucleation of Ni_3Sn_4 compound; however, when the barrier was examined with a Pb-20 wt/o Sn overlay the onset of crystallisation was prolonged during which the extent of interdiffusion was also found to be markedly less compared to that in the Ni-P/Sn system.

1.0 GENERAL INTRODUCTION

Since the advent of the wheel, man has strived to devise means to reduce wear and friction so as not to impede the rotational movement of the wheel. The earliest illustrated application of lubrication of bearing surfaces was that of the moving of the stone statue of the Pharaoh Ramesses II in which one sees the pouring of a liquid, probably a vegetable oil, on to the tracks along which the statue was sliding. In about 1500AD [1], Leonardo Da Vinci described the use of a Sn alloy for optimum bearing properties for low friction ball and roller bearings. Many years later in 1839, Isaac Babbitt first patented the use of a Sn-based alloy which led to the arrival of "white metal" plain bearings.

White metal bearings have been one of the major successes of the 19th century engineering innovation. They virtually provided all the car engine bearing requirements for the first half of the 20th century and continued, until very recently, to provide most of the engine bearings for the American market. The development of thin wall bearings in the 1930's, which rapidly replaced its cast-in predecessor for good economic reasons, made possible a new lease of life for

white metal as progressive increase in engine loads led to premature fatigue failure. This was brought about by deliberately reducing the thickness of the bearing metal layer so that the steel backing could increase the apparent strength whilst reducing the local strains in the white metal.

Eventually, increasing engine loads led to the substitution of stronger materials for white metals. Development tended to follow two separate paths. In each case however, the prescription has either been to provide harder particles in a softer matrix, as in the case of white metal Al-Si bearings, or the reverse, as in the case of Al-Sn or Cu-Pb bearings [2].

Plain bearings may be defined as those in which the moving members are sliding by contrast with the rolling motion of the rolling element bearings. In plain bearing assemblies, the surfaces of the moving parts may either be permitted to rub together in conditions of boundary lubrication, as in marginally lubricated bearings e.g. during engine starts and stops, or be separated by a film of lubricant through which the applied load is transmitted, as in the fluid film bearings, during normal engine operating conditions. The criteria of performance in both cases is the transmission of load with maximum efficiency, which necessitates minimum friction, minimum wear of the

mating surfaces and maximum resistance to seizure, fatigue fracture or corrosion under the operating conditions.

High stiffness and damping characteristics coupled with low friction at high surface velocities under hydrodynamic mode of operation make plain bearings a preferred choice for engine main and big-end bearings.

Plain bearings may be subdivided into two main classifications; direct-lined housings or insert liners. The former consists of housings lined with white metals or, more rarely, Cu-Pb or Pb-bronze and find applications in large plant machinery and large diesel engines. The latter type covers the largest range of applications from the smallest automotive to the largest marine diesel engines and are available as solid inserts or lined inserts. Insert liners consist of backing material such as steel, cast iron, or Cu alloy which has been lined with bearing alloys of white metal, a Cu alloy or an Al alloy.

In recent years there have been considerable developments in engines for passenger cars and trucks as well as for ships and stationary machinery [3]. In addition to an improvement in efficiency, the main considerations were an increase in specific performance and improvement in comfort in the case of passenger car

engines. With engines for trucks and industry, priority was given to improving efficiency and durability. In a number of cases this aim was at least partly achieved by increasing the power output and optimising the fuel economy of engines already in existence. For example, with regard to service life, trucks are expected to have a mean service life of about 750,000 km and in some cases 1-1.2 M km under good service conditions without any engine component replacement.

Against the background of these ongoing developments, manufacturers of plain bearings are faced with the task of adapting the 'three-layer' materials mainly used today for the increasing requirements. These bearings comprise a steel backing sintered with a bearing alloy of Cu-Pb or Al which, in turn, is galvanically coated with a thin (15-20 μm) layer of Pb-Sn, Pb-Sn-Cu or Pb-In as an overlay. Between the two, a very thin (1-5 μm) Ni layer is interposed which in the case of Cu-Pb bearings performs the function of a diffusion barrier, whereas in the case of Al bearings, it serves as a bonding layer between the other two layers. The main purpose of an overlay is to provide a better degree of conformability and embeddability than would be achieved with the base lining material. It also serves to prevent seizure. For Cu-Pb and Pb-bronze types of linings the overlay serves an additional function of protection against corrosion, which is only

afforded if a sufficient level of Sn (2-3wt/o) or In (5-6wt/o) is maintained in the overlay during the lifespan of the bearing.

In modern highly - rated engines, bearings are subjected to temperatures varying from 90°C up to as high as 170°C. Such elevated operating temperatures inevitable promote the formation of Cu-Sn intermetallic compounds at the substrate/overlay interface by means of rapid diffusion of Cu and Sn, thus rendering the overlay susceptible to corrosive attack.

Furthermore, elevated operating temperatures can readily lead to the formation of acidic products in the lubricant by chemical degradation. Under condition of infrequent oil change, bearing failure occurs by corrosion and erosion of the overlay. If in such situations there are operating difficulties, i.e. dirt accumulation or brief lack of lubrication this can lead to the fracturing or splintering of the now exposed brittle intermetallic layer and as a result lead to the failure of the engine by seizure.

The problem of diffusion and corrosive degradation of Pb-Sn overlayed Cu-Pb and Pb-bronze bearings have been recognised over the last two to three decades. Accordingly, a Ni diffusion barrier is most widely employed. Whilst this retards diffusion to some extent,

bearing failure has been noted to occur along the Ni-Sn intermetallic compounds by fatigue fracture.

The present programme of research was designed to investigate the problem of diffusion in Pb-Sn overlayed Pb-bronze bearings. Research reports on the mechanisms of diffusion controlled Sn-metal and metal-metal systems of intermetallic compound growth and its control were evaluated. For example, recently it has been claimed that Cu-P and Cu-B barriers retard the diffusion of Sn and therefore completely suppress the growth of Cu-Sn intermetallic compounds [4,5,6]. Thus it became the object of this research to elucidate the beneficial role of P and B and based upon this develop alternative diffusion barriers.

The research falls into the following broad categories:

- a. Evaluation of C-P and Cu-B diffusion barriers and
- b. Development of alternative diffusion barriers based on amorphous coatings.

2.0 LITERATURE SURVEY

2.1 Introduction

The potential of a material for bearing application cannot be deemed from the determination of its mechanical or physical properties, metallurgical structure or chemistry alone, but require extensive laboratory and field tests in actual application. A survey of bearing materials and their development based upon this is presented.

The generally accepted methods of measuring diffusion coefficients are presented together with recently published reports by Dybkov [7,8] on reactive diffusion and growth kinetics of single and two-phase intermetallic compounds. The mechanisms of diffusion in amorphous alloys are also reviewed.

Critical reports on the solutions to the problems of diffusion in Pb-Sn overlayed bearings based on kinetic or thermodynamic principles are not to be found. The practice of interposing a Ni [9], Co [10] or Fe diffusion barrier owes its origins mainly to the work of Semlitsch, Kay and McKay [11,12] and Unsworth and Mackay

[13]. These authors have carried out detailed investigations into the growth kinetics of Ni, Co and Fe-Sn intermetallic compounds but have failed to provide tentative conclusions upon which more efficient barriers with respect to interdiffusion and reaction control could be developed. For this reason literature in the field of semiconducting devices was reviewed extensively in order that inferences may be drawn from the solutions to similar problems of diffusion controlled interfacial reactions encountered in the development of these devices. Finally, methods of electrodeposition pertaining to bearing applications are reviewed.

2.2 Bearing Materials

2.2.1 Introduction

Bearing materials are required to fulfil a number of different roles. The fatigue strength must be adequate to support the imposed loads under dynamic conditions without wiping or extruding at elevated temperatures. Whilst high strength is demanded of bearing materials it is in opposition to the requirements of embeddability which allows foreign particles to be tolerated by embedding them in the bearing and therefore avoid damaging the shaft.

Bearing materials must be conformable so that it adapts to the contour of the shaft if deflection or misalignment occurs in service and thereby prevent metal to metal contact. Bearings are required to have a good ability to retain a film of lubricant so that wear is limited during engine starts and stops. Bearings are also required to possess good corrosion resistance from contaminants or degraded lubricants.

A large number of bearing materials are in common use since no one material has the ideal combination of all the required properties. Inevitably, the selection of a bearing material is based on a compromise.

Bearing materials are classified in the following categories:

- (a). White metals
- (b). Aluminium alloys
- (c). Copper-lead alloys and Leaded bronzes
- (d). Lead-tin and lead-indium overlay alloys

2.2.2 White Metal Bearing Alloys

The traditional white metal alloys are divided according to the metal used as their basis, i.e. Sn-based and Pb-based, with a number of intermediate

alloys which are Sn-Pb based.

In the Sn-rich alloys, the matrix is Sn, solid solution hardened by the presence of Sb up to a content between 7-8wt/o whilst for casting purpose Cu is limited to about 5 wt/o. Hardness and tensile strength increases with Sb and Cu content, while elongation decreases [14]. Fatigue strength is also raised but at a progressively decreasing rate as the amount of alloying increases [15]. The addition of 1wt/o Cd elevates the compressive strength and bulk fatigue rating by about 40% [16] though some commercial alloys are also known to contain Ni, As and Fe.

Lead-based white metals which clearly offer an economic advantage may contain approximately 12-18wt/o Sb and have either a low Sn content (up to 5wt/o) or a high Sn content of about 10wt/o. Up to 2wt/o Cu is usually added but the addition of As, Ni or other elements are made to refine microstructure and improve mechanical strength [17]. At elevated temperatures their mechanical properties are markedly reduced [18]. Pb-rich alloys have an inherently lower resistance to corrosion and seizure.

The group of alloys containing both Sn and Pb cover a wide range with 20-75wt/o Sn and 10-65wt/o Pb. Sb and Cu content is maintained in the range 12-15wt/o and

1-5wt/o, respectively. These alloys are limited to low temperature applications [19] due to the formation of Sn-Pb-Sb eutectic which melts at about 180°C.

White metals have excellent compatibility and have good conformability and embedability. Their corrosion resistance is in general very good. Unfortunately, their resistance to fatigue by the standards of present day engines, is poor and for this reason white metal is being replaced by stronger bearing linings such as Cu-Pb, leaded-bronze or Al-Si and Al-Sn alloys.

2.2.3 Aluminium Bearing Alloys

Al-6wt/o Sn bearing alloys have been in use since their development in the 1930's [15,20] and are often used in solid form and not as bi-metallic shell bearings but require a shaft hardness of 400HV if they are not overlay plated. At the present time, well over one half of the internal combustion engines for private vehicles utilise the Al-20wt/o Sn alloy bearings and nearly all commercial vehicle engines. Al-30wt/o Sn alloy is also in use to some extent. It appears that the fatigue resistance and bearing performance of the 20wt/o Sn alloy is adequate for virtually all automotive applications while the higher Sn alloy has lower fatigue strength but higher seizure resistance.

Recently, an Al-40wt/o Sn bearing alloy has been developed [21,22] specifically for use in marine diesel engines where white metal is not adequate. This alloy has lower fatigue strength than that of Al-20wt/o Sn but retains its strength properties well at elevated temperatures and embeddability is superior, which makes it acceptable for large engines. Other developments have been concerned with the making of aluminium-babbitts [23], or Al-Pb alloy bearings [24], which contains 8wt/o Pb based white metal in a matrix of Al-3wt/o Cd which has an inherently high fatigue strength.

A more recent development in the high strength bearing alloys is the AL-10wt/oSi-1wt/oCu alloy. The fatigue strength of bearing alloys of this type is high, almost equivalent to that of the strongest copper-based alloys. Compatibility is good; however the hardness of the alloy and the relatively poor embeddability requires that bearings be overlay plated for satisfactory performance. This alloy was developed to meet the high load requirements of the turbo-charged diesel engines [25].

Generally, Al based bearings represent a satisfactory compromise between the opposing requirements of high strength and good surface properties. But under dirty

engine conditions shaft wear can be higher than with an overlay plated bearings. Corrosion is virtually unknown under normal engine bearing conditions, these alloys are resistant to engine oil degradation products though water contamination of the oil supply has been known to corrode the bearing surface.

2.2.4 Copper-Lead and Leaded-Bronze Alloys

Cu-Pb alloys with high Pb content in the range 25-50wt/o were first introduced in the USA in the 1930's. The softer Cu-Pb alloys have good surface properties and in fact the 60/40 Cu-Pb alloys can be used in some engines without the benefit of the soft overlay applied to the 70/30 Cu-Pb alloy and leaded-bronzes. The strength of the 60/40 alloy is low; this and its susceptibility to corrosion restricts its usefulness to a relatively small number of engine applications[16]. However, a widely used 70/30 alloy, overlay plated with 25 μ m of Pb-Sn or Pb-In, operates well in a large number of applications. The 70/30 alloy has good fatigue strength and good seizure resistance, both of which are further enhanced by the presence of the overlay. This increase in the effective fatigue strength derives from the partial sacrification of the overlay in the region of thin films associated with maximum oil film pressure. The maximum oil film

pressure is thereby reduced and the effective fatigue strength is increased.

The low Sn-Pb-bronzes, with a Sn content of 1-2wt/o and a Pb content in the range 23-25wt/o, offer a useful advantage in terms of strength over the 70/30 Cu-Pb alloys. The loss in compatibility is acceptable if the bearing is overlay plated. A further increase in strength is achieved if the Sn content of the alloy is increased to 3-4wt/o. In the case of Cu-22wt/o-Pb-4wt/o-Sn sintered alloy, a strong 95/5 bronze matrix is produced with 22wt/o Pb, distributed in the form of interconnected islands. The alloy, as would be expected, has higher fatigue strength than either Cu-Pb or the low Sn-Pb-bronzes.

The use of Cu-22wt/o-Pb-4wt/o-Sn alloy presupposes an arduous engine condition, in which case the overlay thickness must be limited to 25 μ m or less if premature overlay fatigue is not to supervene. The successful application of this alloy is also dependent on the engines ability to eliminate dirt since the alloy is harder and therefore less conforming and less resistant to embeddability [26].

2.2.5 Overlay Alloys

In the late 1930's the practice of Pb or Sn based overlay plating was introduced with the aim of enabling the harder and stronger Pb-bronzes to be used as bearing lining material, in order that the seizure problems posed by these somewhat incompatible alloys be overcome. Normally, overlays are intended to last the life of the bearing, and in some conservatively designed engines running with low oil temperatures, thick film lubrication and good filtration, overlays may survive several hundred thousand miles [26]. However, the life of an overlay can prematurely be terminated in uprated engines, by a combination of fatigue wear and corrosion [27].

Overlays are generally required to prevent the corrosive attack of the bearing alloy and reduce the tendency towards seizure. The latter is a function of compatibility, conformability and embeddability. Compatibility is the ability of the overlay to resist solid phase welding with the shaft whereas conformability is the ability to self-adjust to shaft deflection and misalignment by deformation and wear. The embeddability is the ability to embed small foreign particles in order to avoid scoring and abrasive wear of the shaft or the bearing lining material.

In the UK the common overlay compositions for automotive engines are Pb-(8-12wt/o) Sn and Pb-(6-10wt/o) In. The fatigue resistance and capacity against loads of the binary Pb alloys are not enough for the requirements of recent diesel engines. Accordingly, ternary and quaternary Pb alloys have been introduced where additions of Cu [26,28], Ni [27], Sb, or Tl as well as one element from the group consisting of Mn, Bi, Ca, and Ba are made to improve overlay properties [27]. Pb, which is the major component of the overlay, provides a high degree of conformability. Sn and In are added primarily to guard against corrosion, but also serves to enhance the flowability of Pb so that abrasive wear due to the shaft is minimised. Cu enhances wear resistance most effectively, followed by Ni for the Pb-based alloys containing 5-20wt/o Sn and 0.005-10wt/o In and/or Tl. However, Cu and Ni reduce the corrosion resistance of the Pb-based alloys [27]. The wear resistance enhancing effect of Ca, Ba, Sb and Bi are lower than that of Ni and decreases in that order. While corrosion resistance is enhanced by the addition of Sb, Bi, Ca, Ba and Mn respectively.

2.2.6 Degradation of Bearing Overlays

In considering the degradation processes of bearing overlays, basic properties such as corrosion resistance, fatigue resistance, wear resistance and conformability can all be deemed to have mutual relationships, in that one poor property disadvantageously influences the other, and hence the reliability and the life of the overlay. The margin against some of these properties is eroded in recent diesel engine designs brought about by increased loading, increased operating temperatures, an increase in oil drain intervals and a reduction in minimum oil film thickness [27].

In recent internal combustion engines, the concentration of corrosive organic acids can become high when engines are in use over long periods. Particularly if the oil is likely to be contaminated by water (especially salt water) and products of combustion (heavy or high sulphur fuels). The overlay is therefore quickly corroded. As a result of the corrosive attack the original smoothness (0.5-0.7 μm) of the overlay surface is caused to be uneven which can lead to cavitation erosion by local decrease in the oil film pressure. This is further exacerbated by reduction in oil film thickness due to increased loading which causes

metal to metal contact during engine starts and stops. Once the overlay has been completely removed from the main load carrying area, the ingress of corrosive oil to the underlying bearing alloy can severely corrode the Pb phase of the Cu-Pb or leaded-bronze bearing alloys.

The mechanisms of corrosive attack of bearing overlays has been described by Zuidema [29], Miskinova and Gindin [30] and Wilson and Shone [31]. Wilson and Shone attribute the corrosion of pure Pb in degraded medicinal white oil to reaction between a surface layer of Pb oxide and oil oxidation acids. This initial reaction forms deposits consisting of Pb soaps and organic acids, which in time dissolve to yield uniform corrosion of Pb in the form of severe etching. However, if Sn or In is alloyed with Pb, then corrosion is prevented by the presence of a continuous surface layer of Sn or In oxide. The continuity of this layer is disrupted by the presence of Pb oxide if the Sn or In content is below 3wt/o and 5wt/o respectively, in which case pitting occurs in Pb-Sn alloys, whereas both general and intergranular corrosion occurs in Pb-In alloys, see Fig.1.

There is no danger of corrosion of the overlay so long as the Sn or In content remains at its original level. However at engine temperature, diffusion of Sn or In from the overlay takes place and if the engine

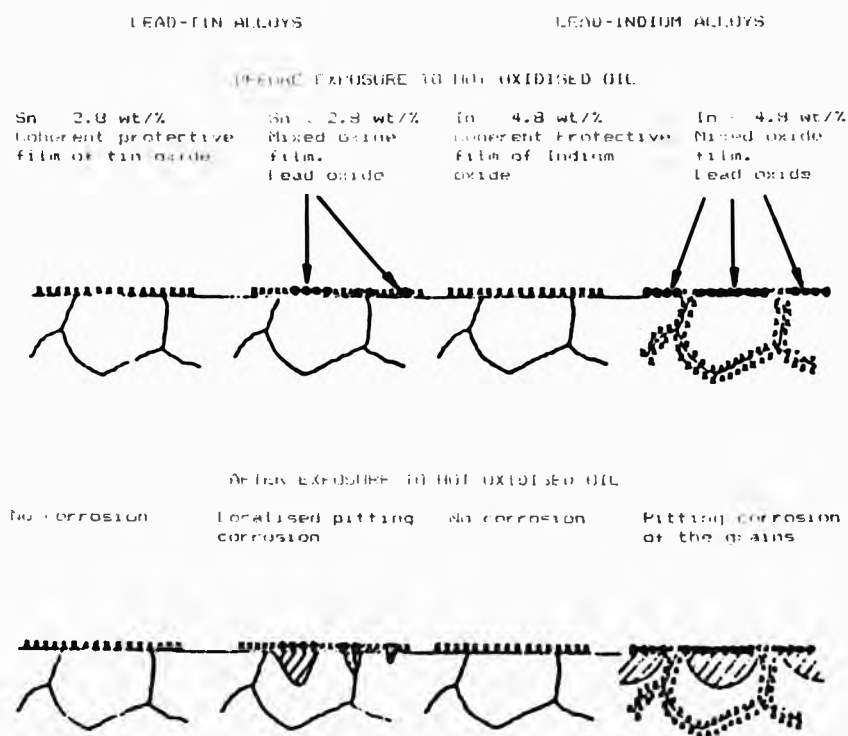


Fig. 1 Schematic representation of the Mechanisms by which Pb-Sn and Pb-In alloys corrode in Medicinal White Oil at 140°C [31]

temperature is high (90-170°C), as in recent engines, diffusion can proceed to the extent that Sn or In falls below the safety level and corrosion sets in as described above. The diffusion phenomena occurring in bearing overlays are well documented [9,10,32].

In the tri-metal bearings interdiffusion results in the formation of Ni-Sn intermetallic compounds (Ni_3Sn_4 and Ni_5Sn_6) on top of the Ni diffusion barrier. The function of the diffusion barrier is to prevent the diffusion of Sn into the underlying lead-bronze bearing alloy. In the absence of a Ni barrier extensive Sn diffusion takes place. Cu-Sn compounds (Cu_3Sn_8 and Cu_5Sn) form at the lead-bronze interface and the loss of Sn is much more serious. In these circumstances bearing failure can occur either by complete removal of the overlay by corrosion or fatigue fracture along the brittle layer of intermetallic compounds. In both cases ultimate seizure ensues by abrasive wear of the exposed intermetallic compounds with the shaft. This problem is also recognised for the Al-Si-Zn overlay-plated bearings used in the turbo-charged diesel engines [25].

2.3 DIFFUSION

2.3.1 Introduction

Diffusion is a process whereby the distribution of each component tends to uniformity [33-43]. Diffusion in solids plays an important role. For instance, the rate of solid state reactions, the growth rate of oxides scales on metals, the sintering rate and the high temperature creep rate of materials are determined by diffusion process.

A crystalline solid consists of a regular array of lattice sites which are low-energy positions for the atoms. A simple concept of diffusion is the atomic movement from one site to another. At room temperature the jump frequency is relatively small, however at higher temperatures it becomes significant leading to readily observable effects. Different jump mechanisms are possible depending on the nature of the moving atom and the nature of the lattice. A number of possible mechanisms are shown in Fig. 2.

Fig. 2a demonstrates the exchange mechanism, where the jump consists of an exchange of two neighbouring atoms. For dilute binary alloys, the diffusion coefficient of individual species are required to be the

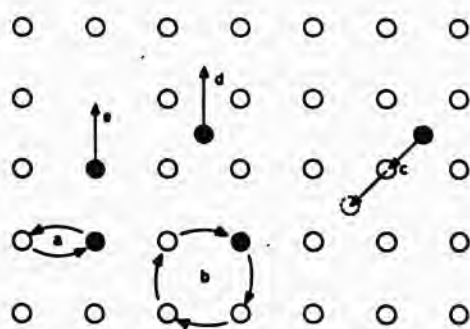


Fig.2 Possible atomic movements contributing to diffusion (a) exchange, (b) ring, (c) interstitialcy, (d) interstitial, (e) vacancy mechanism.

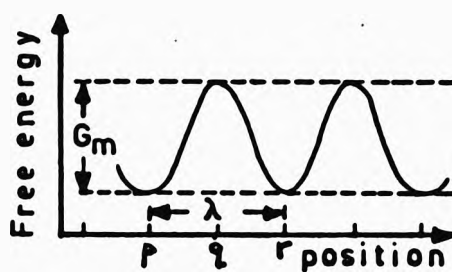


Fig.3 Gigg's energy as a function of position in a lattice, λ is the jump distance.

same. In most cases this mechanism is energetically improbable. Fig.2b is a variant of the exchange mechanism. Fig.2c illustrates the interstitialcy mechanism where an interstitial atom displaces an atom on a lattice site to another interstitial site. Also, a direct jump from one lattice site to another is possible, Fig.2d. This mechanism is assumed to play a major role in the diffusion of noble metals in lead, tin, indium and thallium [44]. Fig.2e demonstrates the most common type of mechanism, the vacancy mechanism in which an atom from a lattice site jumps into an empty neighbouring site. Energetically this mechanism is most favourable and is common in most pure metals and substitutional alloys [45-49], as demonstrated by the study of point defects in some metals e.g. Al[50-51], Cu[52], Ag[53], Au[54], and Pb[55]. Electrodeposited base metal composites are thought to be substitutional systems [33], and diffusion in them occur predominantly by a vacancy mechanism [34,38-40].

2.3.2 Rates of mass transport by diffusion

The atoms in the crystal lattice occupy positions with a relative minimum in the potential energy. In Fig. 3 such positions are p and r. However due to thermal energy they vibrate with a frequency f.

An atom is transferred from position p to r with a probability of $\exp(-G_0/kT)$. The jump frequency is given by

$$P_0 = f \quad (1)$$

in the absence of external force, e.g. concentration gradient. However, under the influence of force the barrier for a jump in the direction of the force is lowered to $(G_0 - \Delta G_0)$, where

$$\Delta G_0 = 1/2 \lambda F \quad (2)$$

Hence, the jump frequency from p to r becomes

$$P_{pr} = P_0 \exp(\Delta G_0/kT)$$

In most cases $\Delta G_0 \ll kT$ so that

$$P_{pr} = P_0 (1 + \Delta G_0/kT)$$

So, to a first order approximation the net jump rate becomes

$$P_{net} = P_{pr} - P_{rp} = P_0 (1 + \Delta G_0/kT)$$

and from equation 2

$$P_{net} = P_0 \frac{F\lambda}{kT}$$

The net velocity of the atoms is λP_{net} ; multiplying this by the number of atoms per unit volume c one obtains the flux J .

$$J = f \frac{F\lambda^2 c}{kT} \exp(-G_a/kT) \quad (3)$$

The flux can be related to concentration gradient so,

$$J = -D \frac{\delta c}{\delta x} \quad (4)$$

This equation is known as Fick's first law.

If the total volume remains constant, the flux of component i across any section, with respect to the origin, can be expressed by

$$J_i = D \frac{\delta c_i}{\delta x} \quad (5)$$

This equation defines the chemical or interdiffusion coefficient.

It is possible to derive an expression for D in terms of jump frequencies by considering two adjacent lattice planes, at a distance λ [56] as

$$D = g\lambda^2 f \exp(-G_a/kT) \quad (6)$$

where g is the geometric factor which often includes a correlation factor.

2.3.3 Temperature dependence of diffusion

The Gibbs energy G_s can be divided into a migration enthalpy H_s and entropy TS_s and substituted into equation 6 which yields

$$D = g\lambda^2 f \exp(S_s/k) \exp(-H_s/kT) \quad (7)$$

to a first approximation for interstitial diffusion.

For vacancy diffusion the temperature dependence of the vacancy concentration and Gibbs energy of formation of defects has to be considered which transforms equation 6 into

$$D = g\lambda^2 f \exp[(S_s+S_v)/kT] \exp[-(H_s+H_v)/kT] \quad (8)$$

Therefore, diffusion coefficients can generally be written in the form

$$D = D_0 \exp(-Q/kT) \quad (9)$$

This is the so-called Arrhenius law where D_0 is the pre-exponential coefficient and Q is the activation enthalpy. The expression is an adequate representation of diffusion in most metals and dilute alloys. Although noticeable exceptions are the anomalous BCC

metals [57].

These exceptions are thought to be due to

- (i) temperature dependence of the activation energy of self diffusion or
- (ii) two or more mechanisms contributing to bulk diffusion.

Seegar and Mehrer [58] and [59] has presented expressions taking into account the above effects.

Fick's second law relates the concentration of the diffusing species to the time and position co-ordinates. If the change in concentration in the given volume equals the net flow into this volume, then

$$\frac{\delta c}{\delta t} = - \frac{\delta}{\delta x} \quad (10)$$

Substitution of Fick's first law into this continuity equation yields

$$\frac{\delta c}{\delta t} = - \frac{\delta}{\delta x} (D \frac{\delta c}{\delta x}) \quad (11)$$

This is the Fick's Second Law. If D is independent of c and x

$$\frac{\delta c}{\delta t} = D \frac{\delta^2 c}{\delta x^2} \quad (12)$$

The solution to Fick's Second Law is

$$c(x,t) = \frac{c_0}{(\pi Dt)^{1/2}} \exp \frac{-x^2}{4Dt} \quad (13)$$

at the following boundary conditions:

$$c(0,0) = c_0 \text{ and } c(x,0) = 0$$

Fig. 4 shows the development of the concentration profile with time. It follows from equation 13 that a plot of $\ln c(x,t)$ vs. x^2 is a straight line with slope $1/4Dt$.

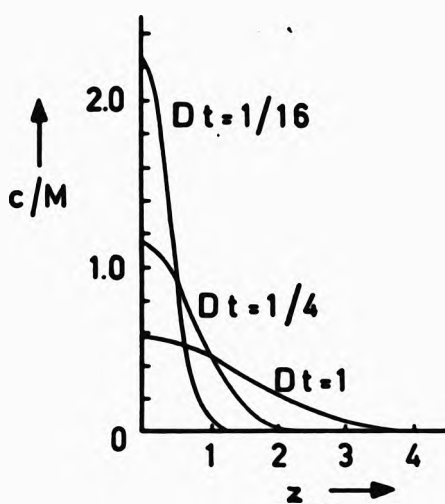


Fig.4 Development of the concentration profile $c(x,t)$ of tracer atoms deposited in an amount $c(0,0) = M$ on the end of a long rod.

2.3.4 Determination of Interdiffusion Coefficients

2.3.5 Grube Method

Measurement of diffusion coefficients are often performed with diffusion couples, e.g. a sandwich of the type AB/A. In these cases the concentration of A at the interface is kept constant during the experiment i.e. the boundary conditions are $c(0,t) = c_0$ and $c(x,0) = 0$ with the solution to equation 12 given by

$$c(x,t) = c_0 \left(1 - \operatorname{erf} \left(\frac{x}{2\sqrt{Dt}} \right) \right) \quad (14)$$

$\operatorname{erf}(y)$ denotes the integral

$$\operatorname{erf}(y) = \frac{2}{\sqrt{\pi}} \int_0^y e^{-x^2} dx \quad (15)$$

the so-called error function. Values for this integral are given in tabular form.

The above treatment is known as the Grube method [60] and is only applicable where D is concentration independent.

2.3.6 Boltzmann-Matano Method

This method allows more accurate determination of D and assumes that D is a function of composition. As with

the Grube method, an accurate determination of concentration penetration profile is required from which the Matano interface is determined graphically. This interface represents a cross-section where the opposing fluxes of species A and B are equal. This interface is located as shown in Fig.5, such that areas N and M are equal. In the absence of porosity and change in molar volume this approximates the original interface.

The Boltzmann solution to Fick's second law is given as

$$D(c_A) = - \frac{1}{2t} \left[\frac{\delta x}{\delta c_A} \right]_{c_A} \int_{c_0}^{c_A} x \, dc_A \quad (16)$$

where, dx/dc_A is the reciprocal of the slope of the concentration profile at a particular composition, c_A , and the integral is the area between the curve and the Matano interface from $c = c_0$ to $c = c_A$.

2.3.7 Boltzmann-Matano-Heumann Method

From the Boltzmann-Matano solution to Fick's second law, Heumann [61] derived an equation that is valid for determination of D in an intermetallic phase if the concentration profile is approximately linear in this phase

$$D = \frac{1}{2t} \frac{d}{(c_{s,1} - c_{s,2})_0} \int_{c_{1/2}}^{c_{1/2}} x dc \quad (17)$$

where

$c_{s,1} - c_{s,2}$ = total conc. difference in the layer

$c_{1/2} = 1/2(c_{s,1} - c_{s,2})$

d = layer thickness of intermetallic phase

$c_{s,1}$ and $c_{s,2}$ are concentrations in phase 2 at the boundaries with phase 1 and 2 (see Fig.6)

The value of D obtained by equation 1 is an average value in intermetallic phase 2 and does not represent the concentration dependence of D .

2.3.8 Wagner's Method

Wagner[62] considered the material transport at the boundaries of the intermetallic phases. From the material balance set up at the phase boundaries the following equation can be derived which is concentration independent:

$$\frac{\Delta c_1}{\Delta c_2} \times \frac{\xi_2}{\xi_1} = \exp \left[\frac{\xi_1 - \xi_2}{4Dt} \right] \quad (18)$$

where

$\Delta c_1, \Delta c_2$ = concentration gap at the left and right phase boundaries, respectively,

ξ_1, ξ_2 = displacements of right and left phase boundary from the Matano interface (Fig.6).

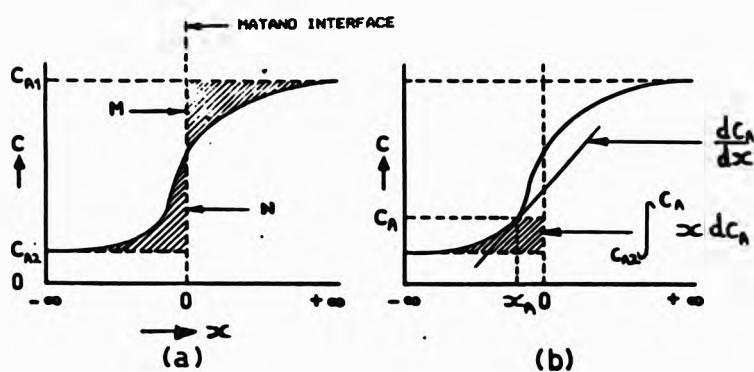


Fig.5 Concentration penetration profiles illustrating the application of Boltzmann-Matano solution for D

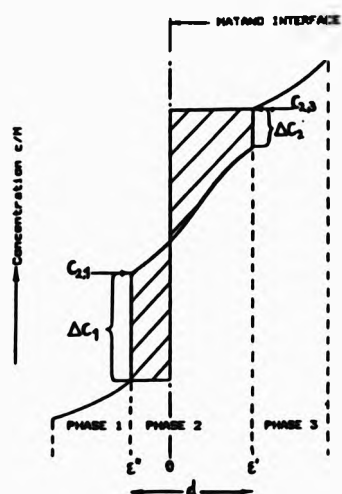


Fig.6 Schematic representation of determination of D in intermediate phases by the application of Boltzmann-Matano-Heumann method and Wagner's method.

2.4 Reactive Diffusion in Binary Systems

2.4.1 Introduction

In a chemical reaction in which one solid reacts with another solid to form a solid product such as a continuous coherent layer of intermetallic compound the reactants become separated from one another. Therefore the rate of diffusional transport of the reacting species become the dominant factor determining the overall reaction rate. Usually the layer growth follows the parabolic law which was first established by Tammann and was then obtained theoretically by Wagner [76,77]. The growth of two compound layers was similarly treated by Arkharov [78], Schroder and Leute [79], Fromhold and Sato [80] and other investigators. They concluded that the thickness of each of the two layers, as well as their total thickness, should increase parabolically with time. In general, this is not the case. The thickness - time relationship in the case of two compound layers is very complex [81,82], and only some portion of the curve is close to a parabola. Moreover, sometimes one of the layers only occurs after a considerable period of time while the others grow from the very beginning of the experiment.

A recent theory developed by Wagner [62], Kidson [83], Heumann [61], Gurov et al [84] and other investigators is based upon Fick's laws (mainly upon Fick's first law) and takes no account of the rate of chemical reaction. There are a number of discrepancies between the existing diffusional theories and the experimental data available in the literature; the main ones are the following according to Dybkov [7,8]:

1. From a diffusional point of view, all the compound layers in a given system are expected to occur and grow simultaneously [84]. This is contrary to the observations. There are a number of binary systems in which up to ten compounds exist in a certain range of temperatures. However the simultaneous growth of say five or six compounds are not reported, the usual number being one to three, and rarely four [2,84].

2. The layer growth is often non-parabolic, especially in those cases where two or more compounds grow simultaneously. In the initial stage the process is non-parabolic, the layer thickness-time relationship being linear [2,84].

3. From diffusional considerations, once a layer forms it cannot then disappear because the smaller the thickness the greater is the layer growth rate, that being inversely proportional to the existing layer

thickness [76,77]. However, this may not be the case; van Loo and Rieck [86] annealed a Ti-Ti₃Al-TiAl-TiAl₃-TiAl₃-Al specimen at 625°C for 15h and found that TiAl and TiAl₃ had vanished completely.

2.4.2 Solid state growth of one compound layer

Consider the case where a single layer of the compound A_pB_q , p and q being positive integers, grows between the elements A and B, Fig.7. The growth of A_pB_q layer between the two mutually insoluble elements, say at temperature T_1 , is due to two parallel processes each of which proceeds in two consecutive steps. Firstly, the B atoms diffuse across the A_pB_q layer and then react with the surface A atoms at the A/ A_pB_q interface (interface 1) according to the equation



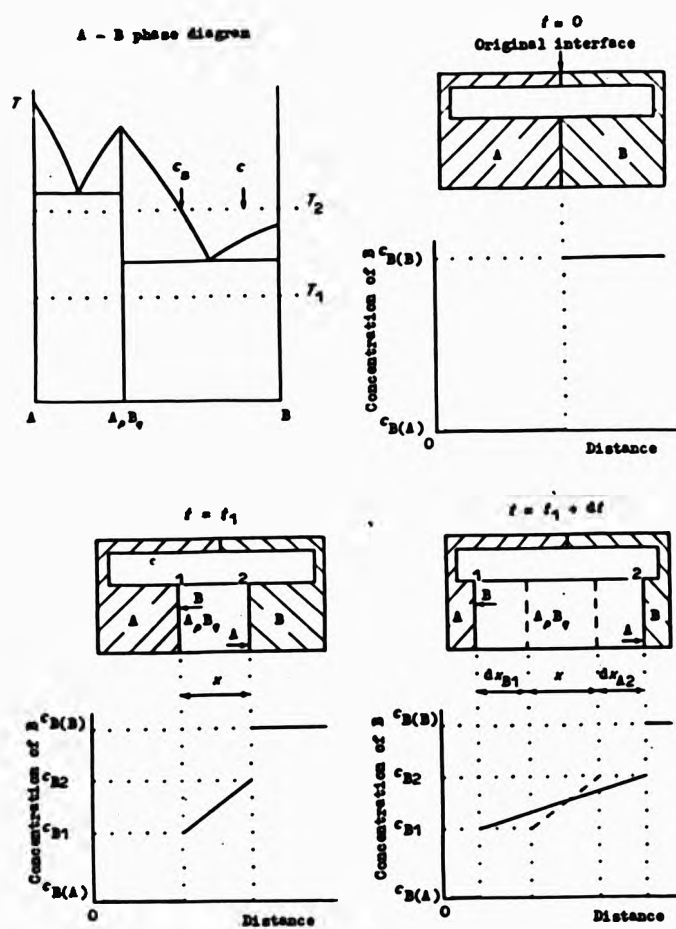


Fig.7 Schematic illustration of the growth of the A_pB_q layer between elements A and B.

Secondly, the A atoms diffuse across in the opposite direction and react at the A/A_2B_3 interface (interface 2) with the surface B atoms according to equation

$$qA(\text{diffusing}) + qB(\text{surface}) = A_2B_3 \quad (20)$$

From the view point of reaction kinetics 19 and 20 are different, while the reacting substances are the same, since the reactants enter in quite different states, namely as diffusing or surface atoms. Both processes involve two consecutive steps [87]: (a) diffusion of atoms through the layer; and (b) chemical reactions with the participation of these atoms taking place at the interface between the layer and either A or B.

The considerations below are based on the following assumptions:

1. the concentrations of components A and B in the layer at boundaries 1 and 2 are equal to the limits of the A_2B_3 homogeneity range;
2. the change in concentration with distance within the A_2B_3 layer is linear
3. during the growth both boundary concentrations and a linear concentration distribution remain unchanged.

These assumptions are usually made to treat the growth kinetics of compound layers [62,61,88]. If these assumptions are satisfied then

$$\frac{\partial c_s}{\partial t} \approx 0 \quad (21)$$

Equation 21 implies that the concentration of A and B within the A_2B_3 layer depend only on position, x and are independent of time, t [2]. This condition is satisfied for stoichiometric compounds having a limited range of homogeneity.

2.4.3 One process in the A-B system

Let reaction 19 be the only reaction in the A-B system. This is the case when diffusion of A within the A_2B_3 is negligible compared to that of B.

In the initial stage of interaction, a number of B atoms are able to reach the A/A_2B_3 interface since the thickness is small and the diffusional transport of B atoms is very fast (in the limit instantaneous). The overall rate of reaction 19 is therefore limited only by the reactivity of the A surface. This reactivity of A surface towards the B atoms, however, remains unchanged during the course of the reaction 1. In such a case the layer growth rate is constant, therefore,

$$\left[\frac{dx}{dt} \right]_{\text{reaction regime}} = k_{001} \quad (22)$$

where x is the thickness of the A_2B_3 layer (m); t the time (sec); k_{001} the rate constant of the layer growth under conditions of reaction control ($m \cdot s^{-1}$). In the subscript 001, 0 indicates the reaction regime of the growth layer, B shows that the B atoms diffuse towards the reaction site and 1 indicates the interface at which reaction takes place.

When the rate of reaction of B atoms with A surface is very fast, the growth of A_2B_3 layer is limited by the rate of transport of B atoms across the layer. This is the diffusional regime, which can be treated with Fick's first law:

$$j_B = -D_B \frac{\partial C_B}{\partial x} \quad (23)$$

where j_B is the flux of the diffusing B atoms across the A_2B_3 layer towards interface 1 ($mol \cdot m^{-2} \cdot s^{-1}$); D_B the diffusion coefficient of B into the A_2B_3 lattice ($m^2 \cdot s^{-1}$); C_B the concentration of component B within the compound layer ($mol \cdot m^{-3}$).

If the concentration distribution is linear (Fig.7), then

$$-\frac{\partial C_B}{\partial x} = \frac{C_{B0} - C_{B1}}{x} \quad (24)$$

Hence,

$$j_s = D_s \frac{C_{s2} - C_{s1}}{x} \quad (25)$$

If the chemical reaction is instantaneous then all the B atoms passing across the layer react at interface 1 to form $A_s B_s$ compound. Thus the thickness of the layer increases by dx . Therefore the flux, j_s , can alternatively be expressed as follows

$$j_s = C_{s1} \left[\frac{dx}{dt} \right]_{\text{diffusional regime}} \quad (26)$$

By equating equations 25 and 26, one obtains

$$\left[\frac{dx}{dt} \right]_{\text{diffusional regime}} = \frac{D_s (C_{s2} - C_{s1})}{C_{s1} x} \quad (27)$$

In this equation

$$k_{1s1} = \frac{D_s (C_{s2} - C_{s1})}{C_{s1}} \quad (28)$$

is the rate constant of the layer growth under conditions of diffusional control. In the subscript 1s1 the first 1 indicates the diffusional regime of the layer growth and the other indexes have the former meanings.

Equations 27 and 28 were first proposed to calculate the diffusion coefficients in growing intermetallic layers by Heumann [61].

In general, the growth rate of the A_2B_3 layer depends on both the rate of diffusion and the rate of chemical reaction since each of these two processes proceeds at finite rate. Therefore, equation 22 and 27 are the limiting cases of a general relationship which can formally be found by summing the reciprocals; thus

$$\frac{dx}{dt} = \frac{k_{\text{eq1}}}{1 + (k_{\text{eq1}}x/k_{\text{is1}})} \quad (29)$$

Integration of equation 29 at the initial condition $x = 0$ at $t = 0$ yields

$$t = \frac{x^2}{2k_{\text{is1}}} + \frac{x}{k_{\text{eq1}}} \quad (30)$$

It is seen that if $k_{\text{eq1}} \ll k_{\text{is1}}/x$ then equation (29) transforms into equation 22. Therefore for small x equation 30 becomes

$$x = k_{\text{eq1}}t \quad (31)$$

Hence, the reaction constant k_{eq1} can be found as the slope of the initial straight line portion of the experimental thickness - time dependence plotted in $x - t$ coordinates.

If however, $k_{\text{eq1}} \gg k_{\text{is1}}/x$ then equation 29 reduces

to equation 27. Accordingly, for large x equation 30 simplifies to

$$x^2 = 2k_{101}t \quad (32)$$

The diffusional constant k_{101} can therefore be found as the slope of the straight portion of the same data, but plotted in $x^2 - t$ coordinates. Another way to find k_{101} is by calculation using known values of D_2 , c_{01} , and c_{02} (equation 28).

Note that the reactivity of the A surface towards the B remains constant whereas the flux of these atoms through the compound layer gradually decreases as the layer thickens. Hence, there exists a single value x^0 , hereafter referred to as (x^0) at which these quantities are equal. Thus

$$\left[\frac{dx}{dt} \right]_{\text{reaction regime}} = \left[\frac{dx}{dt} \right]_{\text{diffusion regime}} \quad (33)$$

from equation 22, 27 and 28 it follows that

$$x^0 = \frac{k_{101}}{k_{001}} \quad (34)$$

At $x < x^0$ the reactivity of the A surface is less than the flux of B atoms and therefore there is an "excess" of these atoms, which can be used to form other chemical compounds. On the other hand, at $x > x^0$ there is a deficit of B atoms because the rate of reaction at the A surface is greater than the flux of B atoms through the

layer, therefore formation of other compound layers is not possible.

Equations 29 and 30 can be interpreted in terms of time, i.e.

$$dt = \left[\frac{x}{k_{191}} + \frac{1}{k_{201}} \right] dx \quad (35)$$

The first term on the right hand side is the time for diffusion of the reacting atoms to the reaction site

$$dt_{\text{diffusion}} = \left[\frac{x}{k_{191}} \right] dx \quad (36)$$

and the second is the time for subsequent chemical transformation

$$dt_{\text{reaction}} = \left[\frac{1}{k_{201}} \right] dx \quad (37)$$

General case: Reaction 19 and 20 proceed simultaneously

The growth of A_2B_2 layer to the left from the original A-B interface is due to reaction 19 whilst its growth to the right is due to reaction 20 (see Fig.7). Taking into account the results from the previous section, one obtains

$$dt = \left[\frac{x}{k_{191}} + \frac{1}{k_{201}} \right] dx_{A_2B_2} \quad (38)$$

and

$$dt = \left[\frac{x}{k_{1a2}} + \frac{1}{k_{0a2}} \right] dx_{a2} \quad (39)$$

where k_{0a2} is chemical constant and k_{1a2} is a diffusional constant which is a function of D_a the diffusion coefficient of A in A_pB_q , and of boundary concentrations c_{a1} and c_{a2} , of A into the layers:

$$k_{1a2} = \frac{D_a(c_{a1} - c_{a2})}{c_{a2}} \quad (40)$$

Reaction 19 and 20 are considered to be independent of each other for the following reasons: (a) they are separated in space; (b) the fluxes, j_a and j_b , across the growing layer appear to be independent of each other. Since each component of the compound forms its own sublattice.

From equations 38 and 39 it follows

$$\frac{dx_{a1}}{dt} = \frac{k_{0a1}}{1 + (k_{0a1}x/k_{1a1})} \quad (41)$$

and

$$\frac{dx_{a2}}{dt} = \frac{k_{0a2}}{1 + (k_{0a2}x/k_{1a2})} \quad (42)$$

A general equation describing the A_pB_q layer growth between A and B phases is the sum of the equations 41 and 42; thus

$$\frac{dx}{dt} = \frac{k_{0a1}}{1 + (k_{0a1}x/k_{1a1})} + \frac{k_{0a2}}{1 + (k_{0a2}x/k_{1a2})} \quad (43)$$

The solution to this equation is

$$R_1 x^2 + R_2 x - R_3 \ln(1 + R_4 x) = t \quad (44)$$

where

$$R_1 = \frac{1}{2(k_{101} + k_{A2})}$$

$$R_2 = \frac{k_{101}^2 k_{A02} + k_{A01} k_{1A2}^2}{k_{A01} k_{A02} (k_{101} + k_{1A2})^2}$$

$$R_3 = \frac{k_{101} k_{1A2} (k_{A01} k_{1A2} - k_{101} k_{A02})^2}{k_{A01}^2 k_{A02}^2 (k_{101} + k_{1A2})^2}$$

$$R_4 = \frac{k_{A01} k_{A02} (k_{101} + k_{1A2})}{k_{101} k_{1A2} (k_{A01} + k_{A02})}$$

Note that there exists another critical value, $x^* = k_{1A2}/k_{A02}$, at which the reactivity of the B surface towards A atoms and the flux of A atoms through the A_2B_2 layer are equal. As previously defined for component B, the growth regime of the A_2B_2 layer is reaction controlled with regard to component A if $x < x^*$ and is diffusional controlled if $x > x^*$. In general,

$$x_A \neq x_B$$

However, if

$$k_{A01} = k_{A02} \text{ and } k_{101} = k_{1A2}$$

then equations 43 and 44 become, respectively,

$$\frac{dx}{dt} = \frac{2k_{001}}{1 + (k_{001}x/k_{101})} \quad (45)$$

and

$$t = \frac{x^2}{4k_{001}} + \frac{x}{2k_{001}} \quad (46)$$

For small values of x , equation 46 reduces to

$$x = 2k_{001}t \quad (47)$$

whereas for large value of x it becomes

$$x^2 = 4k_{101}t \quad (48)$$

This is the case when the contribution of both components to the layer growth are equal. In general, these contributions are different. Nevertheless, an initial portion of the thickness - time relationship is a straight line. Indeed, if $k_{001} \ll k_{101}/x$ and $k_{002} \ll k_{102}/x$ (or, alternatively $x \ll x^0$ and $x \ll x^0$) then

$$\frac{dx}{dt} = k_{001} + k_{002} \quad (49)$$

and therefore

$$x = (k_{001} + k_{002})t \quad (50)$$

Again, for large x the conditions $k_{001} \gg k_{101}/x$ and $k_{002} \gg k_{102}/x$ ($x \gg x^0$ and $x \gg x^0$) are satisfied; thus

$$\frac{dx}{dt} = \frac{k_{101} + k_{102}}{x} \quad (51)$$

and

$$x^2 = 2(k_{101} + k_{102})t \quad (52)$$

Therefore, this long-time portion of the x-t relationship is parabolic.

2.4.4 Growth of two compound layers

A schematic illustration of the growth process of two compound layers at the interface between two elements is shown in Fig. 8. It is assumed that elements A and B are mutually insoluble and that compounds A_2B_3 and A_3B_2 have a narrow range of homogeneity.

The A_2B_3 layer grows as B atoms diffuse through to interface 1 and react with the A surface:



Its thickness increases as A atoms diffuse towards interface 2 and react with A_2B_3 to form A_3B_2 compounds:



The growth of the A_3B_2 layer is due to reactions



and



which take place at interface 2 and 3 respectively.

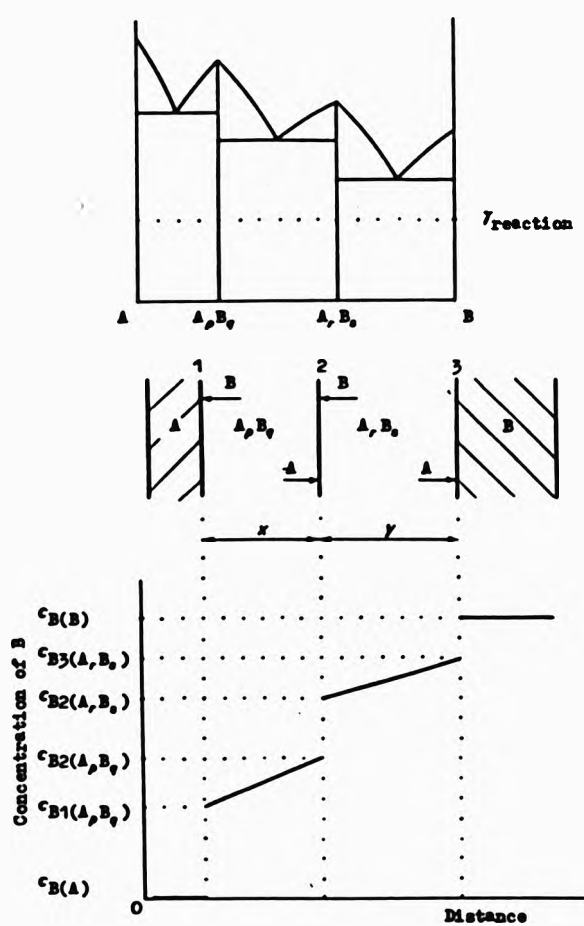


Fig.8 Schematic illustration of the growth of two compound layers

The compound A_2B_3 is the product in reactions 53 and 54 and a reactant in 55. The A_2B_3 compound is the product in reactions 55 and 56 and is the product in 54. Hence the formation of A_2B_3 layer is due to reactions 53 and 54 and the "dissolution" into A_2B_3 due to reaction 55. Similarly, the A_2B_3 layer grows due to reactions 55 and 56 and "dissolves" into the A_2B_3 layer due to reaction 54.

The thickness of A_2B_3 layer will increase by

$$dx_0 = dx_{01} + dx_{02} \quad (57)$$

where dx_{01} is the increase in the layer thickness at interface 1 due to reaction 53 and dx_{02} is the increase in its thickness at interface 2 due to reaction 54 the expression for dx_{01} and dx_{02} can be found from equations 29 and 35 to 37, thus

$$dx_{01} = \frac{k_{001}}{1 + (k_{001} \times / k_{101})} dt \quad (58)$$

where k_{001} is the rate constant of A_2B_3 layer growth under reaction control and k_{101} is the rate constant of its growth under diffusion control. The constant k_{101} is the function of the diffusion coefficient, $D_{B(A_2B_3Q)}$, of B and the boundary concentrations $C_{B1(A_2B_3Q)}$ and $C_{B2(A_2B_3Q)}$ of component B in A_2B_3 layers:

$$k_{101} = \frac{D_2(A_2B_2)[C_{22}(A_2B_2) - C_{21}(A_2B_2)]}{C_{21}(A_2B_2)} \quad (59)$$

Similarly,

$$dx_{A_2} = \frac{k_{202}}{1 + (k_{202}/k_{102})} dt \quad (60)$$

where

$$k_{102} = \frac{D_1(A_1B_1)[C_{11}(A_1B_1) - C_{12}(A_1B_1)]}{C_{12}(A_1B_1)} \quad (61)$$

$D_1(A_1B_1)$ being the diffusion coefficient of A in A_1B_1 and $C_{11}(A_1B_1)$ and $C_{12}(A_1B_1)$ the boundary concentrations at interfaces 1 and 2.

During dt , the A_2B_2 layer thickness will increase by

$$dy_2 = dy_{22} + dy_{23} \quad (62)$$

where dy_{22} is the increase in its thickness at interface 2 due to reaction 55 and dy_{23} is that increase at interface 3 due to reaction 56. The expressions for dy_{22} and dy_{23} are

$$dy_{22} = \frac{k_{202}}{1 + (k_{202}/k_{102})} dt \quad (63)$$

and,

$$dy_{23} = \frac{k_{203}}{1 + (k_{203}/k_{103})} dt \quad (64)$$

where

$$k_{122} = \frac{D_{12}(r_{B_2})[C_{A2}(r_{B_2}) - C_{A2}(r_{B_1})]}{C_{B_2}(r_{B_2})} \quad (65)$$

and,

$$k_{123} = \frac{D_{12}(r_{B_2})[C_{A2}(r_{B_2}) - C_{A2}(r_{B_1})]}{C_{A2}(r_{B_2})} \quad (66)$$

D and c being the diffusion coefficient and boundary concentrations, respectively, of component A and B into the A₂B₂ layer.

During the same time, dt, the thickness of the A₂B₂ layer will decrease by dx. as a result of reaction 55. This decrease can be found from equation 3, in fact;

$$\frac{m_{A_2B_2}}{m_{A_2B_2}} = \frac{rM_{A_2B_2}}{pM_{A_2B_2}} \quad (67)$$

where m is the mass and M the molecular mass of the compound. Since mass is the product of volume and density, ρ,

$$\frac{A_{A_2B_2}dx}{A_{A_2B_2}dx} = \frac{rM_{A_2B_2}}{pM_{A_2B_2}} \quad (68)$$

Hence,

$$dx = \frac{rg}{p} dy_{B_2} \quad (69)$$

where the ratio of the molar volume, V, of A₂B₂ to that of A₂B, is denoted by g, i.e. $g = V_{A_2B_2}/V_{A_2B}$.

By analogy, from equation 54, one obtains

$$dy_- = \frac{q}{sg} dx_{A2} \quad (70)$$

The overall change in the A_2B_2 layer thickness during dt is

$$dx = dx_{B1} + dx_{A2} - dx_- \quad (71)$$

Similarly,

$$dy = dy_{B2} + dy_{A2} - dy_- \quad (72)$$

Therefore a system of differential equations describing the growth kinetics of two compound layers is

$$\begin{aligned} \frac{dx}{dt} &= \frac{k_{B1}}{1+(k_{B1}x/k_{1B1})} + \frac{k_{A2}}{1+(k_{A2}x/k_{1A2})} \\ &\quad - \frac{rg}{p} \frac{k_{B2}}{1+(k_{B2}y/k_{1B2})} \end{aligned} \quad (73a)$$

$$\begin{aligned} \frac{dy}{dt} &= \frac{k_{B2}}{1+(k_{B2}y/k_{1B2})} + \frac{k_{A2}}{1+(k_{A2}y/k_{1A2})} \\ &\quad - \frac{q}{sg} \frac{k_{A2}}{1+(k_{A2}x/k_{1A2})} \end{aligned} \quad (73b)$$

The above differential equations allow some predictions to be made, but there also exists the following critical thicknesses (see eq. 34);

$$x^0 = \frac{k_{101}}{k_{001}} \quad (74)$$

$$x^A = \frac{k_{102}}{k_{002}} \quad (75)$$

$$y^0 = \frac{k_{101}}{k_{002}} \quad (76)$$

$$y^A = \frac{k_{103}}{k_{003}} \quad (77)$$

which divides the $x - t$ and $y - t$ relationship into the reaction and diffusion controlled regimes with regard to component A and B. Some limiting cases of practical interest are presented below.

2.4.5 Initial stage of the growth process

2.4.5.1 Linear growth

Initially the thicknesses of the layers are small and therefore the following conditions are satisfied:

$$k_{001} \ll k_{101}/x, \quad k_{002} \ll k_{102}/x, \quad k_{002} \ll k_{102}/y$$

$$\text{and } k_{003} \ll k_{103}/y$$

Hence, the terms of the form k_{0x}/k_1 and k_{0y}/k_1 can be neglected in comparison with unity. In this case the equations 73a, b simplifies to

$$\frac{dx}{dt} = k_{001} + k_{002} - \frac{rg}{p} k_{002} \quad (78a)$$

$$\frac{dy}{dt} = k_{002} + k_{003} - \frac{q}{sg} k_{002} \quad (78b)$$

$$\text{If } k_{001} + k_{002} > (rg/p) k_{002}$$

$$\text{and } k_{002} + k_{003} > (q/sg) k_{002}$$

then dx/dt and dy/dt are positive and therefore both layers grow linearly with time.

If $k_{d1} + k_{d2} = (rg/p)k_{eq}$ then $dx/dt = 0$.

This means that the thickness of the A_2B_2 layer remains constant since the rate of its growth is equal to its dissolution into A_2B_2 , but A_2B_2 continues to grow linearly.

When the condition

$$k_{d1} + k_{d2} < \frac{rg}{p}k_{eq}$$

is satisfied the A_2B_2 layer cannot grow since $dx/dt < 0$ and therefore only A_2B_2 will grow. If A_2B_2 was initially present then it would dissolve into A_2B_2 until dx/dt becomes positive when it will begin to grow.

Similarly, the A_2B_2 layer thickness remains constant or equal to zero if

$$k_{d1} + k_{d2} = (q/sg)k_{eq}$$

If $k_{d1} + k_{d2} < (q/sg)k_{eq}$

then A_2B_2 is absent.

Note that both layers grow under reaction controlled regime with regard to both components as $x \ll x^s$, $x \ll x^s$, $y \ll y^s$ and $y \ll y^s$

2.4.5.2 Non-linear-linear growth

Thickening of the layers would result in change in their regime of growth. Suppose that A_2B_2 growth is diffusion controlled w.r.t. B ($x \gg x^0$) and assume that A_2B_2 is reaction controlled with respect to A ($x \ll x^0$). The regime of A_2B_2 growth is then regarded as reaction controlled with regards to both components ($y \ll y^0$, $y \ll y^0$). These conditions can be described as follows:

$$k_{001} \gg k_{101}/x, \quad k_{002} \ll k_{102}/x,$$

$$k_{002} \ll k_{102}/y, \quad k_{003} \ll k_{103}/y.$$

Therefore, equations 73a and b become

$$\frac{dx}{dt} = \frac{k_{101}}{x} + k_{002} - \frac{rg}{g} k_{001} \quad (79a)$$

$$\frac{dy}{dt} = k_{002} + k_{003} - \frac{q}{sg} k_{002} \quad (79b)$$

From equation 79b it follows that the A_2B_2 layer grows linearly with time. Whereas the A_2B_2 growth is complicated (parabolic, asymptotic, etc.)

2.4.6 The role of critical thickness in determining the growth kinetics of the layers

2.4.6.1 Departures of layer thickness - time relationships

Suppose that the regime of growth of the A_2B_3 layer becomes diffusion controlled with regards to both components B and A ($x > x^B$, $x > x^A$). In this case, the A_2B_3 layer cannot grow at the expense of component A. Since at $x > x^A$ all A atoms diffusing across A_2B_3 are consumed into A_2B_3 compound at interface 2 according to reaction 2a. Moreover, the thicker the A_2B_3 layer the greater is the deficit of A atoms in comparison with the reactivity of the A_2B_3 ; therefore reaction 4a cannot proceed. At $x > x^A$ this layer grows only at the expense of B. In such a case, the term

$$\frac{k_{A2B3}}{1 + (k_{A2B3}/k_{12B})}$$

in equations 73a and b has no physical meaning. This results in a decrease in the rate of growth of A_2B_3 . Indeed, at $x < x^A$ this layer grows at the expense of both components whereas at $x > x^A$ it grows at the expense of B. Thus a departure of the $y - t$ curve is observed as shown schematically in Fig. 9.

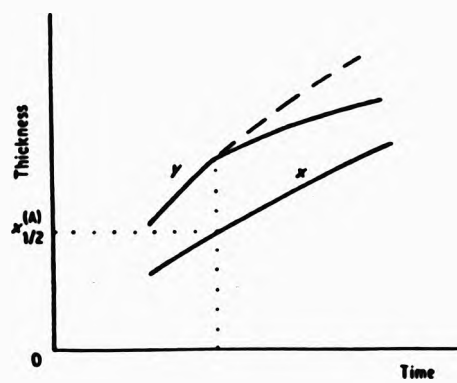


Fig.9 Departure of A_rB_s layer growth due to change in the growth regime of A_pB_q layer.

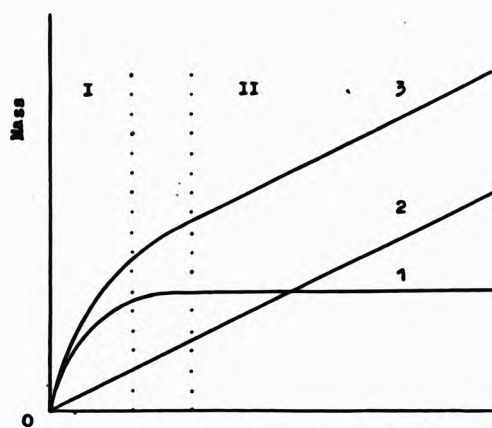


Fig.10 1, Mass of A_pB_q layer, 2, mass of A_rB_s layer, 3, parabolic growth. Region I, parabolic growth, II, linear growth.

2.4.7 Paralinear stage of growth of the layers

If $x \gg x^0$, $x \gg x^*$ and $y \ll y^0$ then equations 73a and b become

$$\frac{dx}{dt} = \frac{k_{101} + k_{102}}{x} - \frac{rg}{p} k_{002} \quad (80a)$$

$$\frac{dy}{dt} = k_{002} - \frac{q}{sg} \frac{k_{102}}{x} \quad (80b)$$

It is seen that the A_2B_3 layer tends to a limiting value defined by the equation

$$x_{\text{lim}} = \frac{(k_{101} + k_{102})p}{rgk_{002}} \quad (81)$$

while A_2B_3 growth at fairly large x becomes linear.

Thus

$$\frac{dx}{dt} = \frac{k_{101} + k_{102}}{x} - \frac{rg}{p} k_{002} \quad (82a)$$

$$\frac{dy}{dt} = k_{002} \quad (82b)$$

Equation of this type were first proposed by Loriers [89-91] and Kofstad [85] which are observed when the diffusion coefficients of the elements in the layers are very different. Such kinetics are usually observed in oxidation of metals and alloys. From equations 80a, b and 82a, b it follows that if

$$\frac{k_{121} + k_{122}}{x} \gg \frac{rg}{p} - k_{222}$$

then the mass - time relationship is almost parabolic whereas the more long - time portion is almost linear, Fig. 10.

2.4.8 Late stage of growth of layers

Eventually, the regime of A₂B₃ layer growth becomes diffusional with respect to component B (y > y^{*}, see Equ.54). In this case, A₂B₃ has no source of B atoms and its further growth proceeds at the expense of A. Thus, at x > x^{*} and y > y^{*} the growth of layers is due to reactions 2a and 3a at interface 2 whereas reactions 1 and 4 cannot proceed, therefore terms

$$k_{222}/[1+k_{222}x/k_{121}] \text{ and } k_{222}/[1+k_{222}y/k_{122}]$$

have no meaning. For the late diffusional region (x >> x^{*} and y >> y^{*}), equations 73a and b become

$$\frac{dx}{dt} = \frac{k_{122}}{x} - \frac{rg}{p} \frac{k_{122}}{y} \quad (83a)$$

$$\frac{dy}{dt} = \frac{k_{122}}{y} - \frac{q}{sg} \frac{k_{122}}{x} \quad (83b)$$

The solutions to these equations are often based on the assumption that the ratio of the rate of growth of the

layers remains constant, i.e.

$$\frac{dx/dt}{dy/dt} = \text{const.}$$

In general, however, this is not the case. The law of growth of two compound layers in the late diffusional stage can, in principle, be found by solving equations 83a and b. But since each stage produces complex expressions it is difficult if not impossible to represent the final result in the form of some simple analytical function.

2.5 Intermediate Phases in Barriered Overlay Bearings

The most common problem in coated structures is the instability which derives from the chemical non-equilibrium between the substrate and the deposited layer. Consequently, the demand for equilibrium drives the interdiffusion and the reaction between the substrate and the coating. Often the configuration which has the minimum free enthalpy after interdiffusion is not of the same crystallographic nature as either of the parent components. In such cases intermetallic compounds are formed which are usually of stoichiometric composition.

Generally, three aspects of intermetallic compound formation can be recognised;

- I. nucleation of the compound
- II. topography of the growth
- III. thermodynamics of formation

For a compound to nucleate in the parent phase, the atoms which predominate the compound must be transferred to the site by a diffusion process. In the Cu-Sn system, the diffusion of Cu through the Cu_3Sn_8 layer is rate controlling [64] and that of Ni in Ni_3Sn_8 for the Ni-Sn system [10].

The topography of the surface of the substrate can influence the alloy growth [65]. There is also evidence that surface treatments can alter the form of individual crystallites [66].

The free enthalpy of formation at the temperature concerned is a relevant factor in the formation of compounds. If more than one compound can form, the one with the highest heat of formation can occur in preference to others.

The intermediate phases in copper-based bearings with Pb-Sn overlay have been identified by Creydt [63] as Cu_3Sn_2 and Cu_2Sn . The Sn rich Cu_3Sn_2 occurs first at the interface, and with time transforms to Cu rich Cu_2Sn . Tin is also known to react with other metals such as Ag, Ni, Co and Fe to form intermetallic compounds. Attempts have been made to utilise Fe and Co as diffusion barriers for bearings, though only Ni has found extensive commercial application. Both Co and Fe form Sn compounds e.g. CoSn_2 [12] and FeSn_2 [11] at temperatures of 170 °C. Nickel however, reacts at room temperature [68] to form Ni_3Sn_2 which then transforms to Ni_2Sn_3 at about 100 °C.

2.5.1 Nucleation and Growth Kinetics of Intermediate Phases

Nucleation of phases in metals and alloys is predominantly heterogeneous. Suitable nucleation sites are non-equilibrium defects such as excess vacancies, dislocations, grain boundaries, stacking faults, and free surfaces, all of which increase the free enthalpy and hence the local activity of the material.

However, the bulk of the transformation product is formed during the growth stage by transfer of diffusants across the parent/product interface. There are two types of interfaces: glissile and non-glissile. Glissile interfaces migrate by dislocation glide resulting in shearing of the parent into the product. Non-glissile interfaces migrate by more-or-less random jumps of individual atoms and are thermally very sensitive. Most interfaces are of non-glissile type, whose parent and product may or may not have the same composition. If the composition remains unchanged the new phase will grow as fast as the atoms cross the interface; as such the transformation is interface controlled. However, when the parent and the product have different composition the growth of the new phase will require long range diffusion. The transformation is interface controlled if the reaction is slow, but

diffusion controlled if the interfacial reaction is fast.

In general, the growth kinetics of intermediate phases are described by the power law of the form

$$x = Kt^{1/n}$$

where, x = thickness of the compound

t = time

K, n = growth constants

Usually the diffusional growth of intermediate phases follows a parabolic law behaviour in which $n=2$. Any deviation from parabolic behaviour is an indication that some mechanism other than bulk diffusion is governing the growth kinetics

Kay and Mackay [11] have measured the rate of growth of Cu_3Sn at room temperature and found that the growth rate was parabolic. Also, they have examined the effect of different basis materials on the compound growth rate against Pb-Sn coatings [12]. They concluded that the growth rate for the total compound was the highest on the Ni-Fe alloy substrate, followed by cobalt, silver, copper, brass and iron at 170°C . The composition and the condition of the coating and the hardness of the copper substrate also have an effect on

the growth rate of the Cu-Sn compounds. They estimate the activation energy for the Cu-Sn system to be 39 KJ mol⁻¹. Tu and Thompson have observed that the growth rate of the Cu₃Sn₈ at room temperature in thin films is linear, and that the dominant diffusant is Cu. However, the rate of growth of Cu₃Sn in the temperature range of 115-150 °C was found to be parabolic with an activation energy of 96.5 KJ mol⁻¹. This entails that the Cu₃Sn₈ phase which nucleates first is interfacial reaction dependent and that diffusion across it is not rate limiting. At the higher temperature of 220 °C, Cogan et al.[67] have reported the growth rate of both Cu₃Sn₈ and Cu₃Sn to be non-parabolic and suggests a grain boundary diffusion mechanism.

2.6 Diffusion in Amorphous and Crystalline Alloys

Until recently there were relatively few investigations of diffusion in amorphous alloys, mainly because of the experimental limitations in measuring small diffusion rates at sufficiently low temperatures to avoid crystallisation.

A tentative comparison of the rates of diffusion in an amorphous alloy with that in an equivalent crystalline alloy cannot be made since a homogeneous closed packed crystal of the same composition as the amorphous alloy usually cannot be manufactured. A crystallised form of the amorphous alloy is readily made but is too complex, consisting of multi-phase crystals separated by a high density of interphase and grain boundaries.

However, sufficient and reliable diffusion data is now available to make a generalised comparison. Fig.11 shows diffusion coefficients of P, Si and Au in a range of Fe, Ni and Pd based amorphous alloys [69]. At a given temperature, diffusion in an amorphous alloy is faster than crystalline self diffusion and substitutional impurity diffusion, but slower than crystalline interstitial impurity diffusion and grain boundary diffusion [69,70]. Diffusion is also affected by structural relaxation when an amorphous alloy is heat

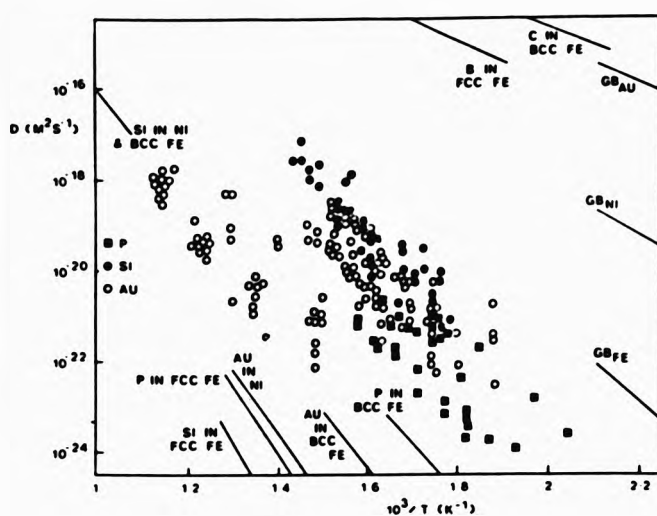


Fig. 11 Au, P and Si diffusion coefficients in amorphous alloys, together with comparable crystalline data.

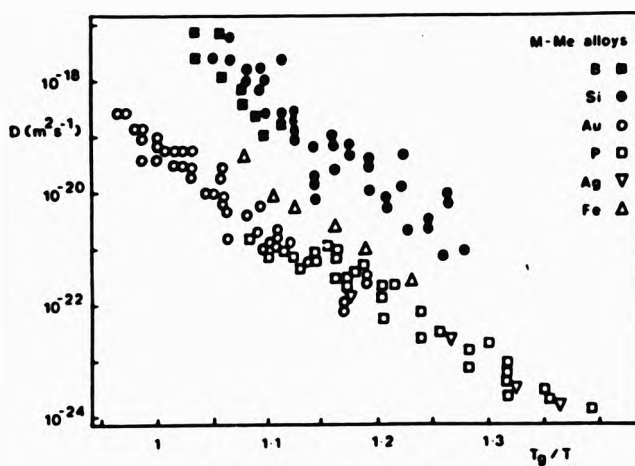


Fig. 12 Comparison of different diffusing species in M-Me amorphous alloys.

treated. Different investigations have shown either a sharp decrease, a small decrease or no effect. These conflicting results may arise from different methods of manufacture [71].

With the exception of B and Si, every amorphous alloy diffusant combinations investigated has displayed an Arrhenius type of behaviour with an approximately constant activation energy, indicative of a single diffusion mechanism operating over the range of temperature studied [69], see Fig.12. However, diffusion in metal-metal (M-M) amorphous alloy is significantly faster than in metal-metalloid (M-Me) amorphous alloys, see Fig.13.

Modelling of the diffusion process in amorphous alloys has proved to be difficult. Attempts have hitherto been made based on the random walk analysis of diffusion of an interstitial atom through an idealised amorphous structure [72]. The treatment is based on the idea that diffusion takes place between the adjacent interstitial sites or voids for lighter elements such as H, Li, B and Si. For the diffusion of heavier atoms, it is generally assumed that migration via the largest interstitials or 'holes' occurs.

Buschow [73] has shown a correlation between the crystallisation temperature of the glass and the calculated enthalpy of formation of holes in a number of

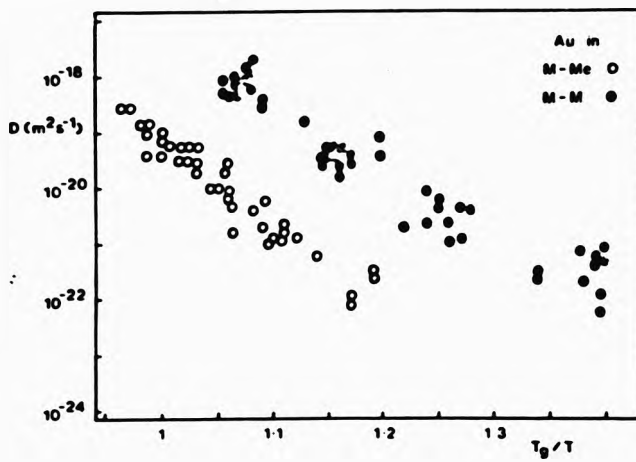


Fig. 13 Comparison of Au diffusion in M-Me and M-M amorphous alloys.

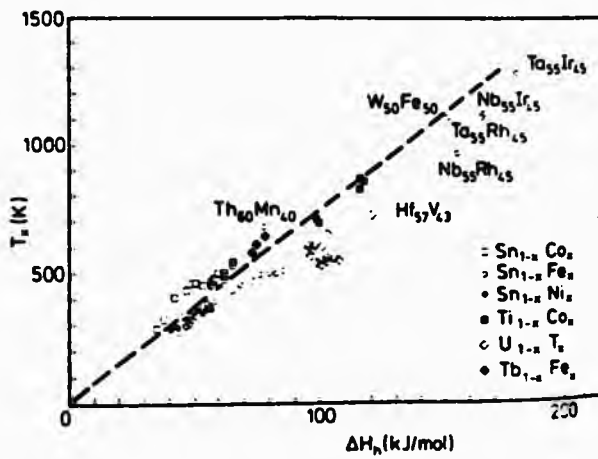


Fig. 14 Correlation of measured crystallisation temperature with calculated enthalpy of formation of holes in binary amorphous alloys.

amorphous alloys, see Fig.14. The implication is that the higher the crystallisation temperature the lower the equilibrium concentration of 'holes' and therefore the lower the diffusivity of the solute species. Akhtar et al.[74] have compared the diffusivities of Pb, Pt and Au in Ni-Zr glass and more recently [75] compared the diffusivities of Pb, Ag and Al in Ni-Nb glass. Diffusivities decrease in the order cited in the first series which is also the order of the melting points but not the order of atomic radius. In the second series Al is out of order.

2.7 DIFFUSION BARRIERS

2.7.1 Introduction

The development of diffusion barriers for Pb-Sn overlayed bearings has largely been based on empirical knowledge. The reason is that the information on properties of materials necessary for a systematic approach to the problem of interdiffusion is difficult to obtain. Hence it is essential to draw inferences from the concepts used in other branches of technology. To some extent, parallels can be drawn from the most detailed investigations carried out on semiconducting devices, which also suffer from similar problems of diffusion controlled interfacial reaction of silicon with other metals.

To stop or reduce interdiffusion, the most practical method is to interpose a diffusion barrier [92]. To be effective a diffusion barrier must have a slow permeation rate with respect to the diffusing species; this constitutes a kinetic barrier. Additionally, the barrier must not react at either of the adjoining interfaces; this constitutes a thermodynamic barrier.

The use of a partially oxidised refractory metal film, a thin conductive oxide film, a nitride phase, or a metallic amorphous phase with high crystallisation temperature has been noted. These barriers will slow down interdiffusion kinetically; thus they are kinetic barriers meaning that the barrier and its neighbouring constituents are generally not in thermodynamic equilibrium.

The requirements demanded from diffusion barriers for bearings are somewhat stringent. They are expected to be kinetically and thermodynamically stable as well as possess suitable mechanical and at least emergency bearing properties. The method of barrier fabrication to date has been limited to electrodeposition since it is the cheapest, although a German bearing manufacturer [93] is currently evaluating a physical vapour deposition technique. Hence, the choice of materials and the design of diffusion barrier are also limited.

Diffusion barriers can broadly be classified into the following different types:

2.7.2 Elemental Barriers

One obvious choice for the material of the barrier X is the metal which does not react chemically with A and

B on either side of it and has negligible mutual solid solubility with both A and B. Of course there is no assurance that such a material can be found but, even if it exists, it may not behave as a diffusion barrier if grain boundaries or other extended defects are present.

Campisano et al [94] have demonstrated the nature of the problem in a study of bilayer films of Cu and Pb. The two metals are immiscible in their solid bulk phases and do not form compounds. Both films were polycrystalline. The average grain size for Cu was of the order of 10 nm and that for the Pb was much larger, about 200nm. After annealing it was found that Pb had penetrated throughout the Cu but that of Cu in Pb was not detected. This was due to the much larger number of grain boundaries in Cu than in the Pb film. Since the bulk solubilities are nil, the intermixing resulted from structural defects such as grain boundaries. In a second experiment the ratio of average grain size was inverted; the predominant moving species was also found to be changed from Pb to Cu.

The grain size of polycrystalline film is thus of primary significance in determining the atomic transport properties. The size of grains, other structural characteristics such as defects, the texture and stress generally depend on the method of fabrication. Similar effects to the above example were also observed by

Baglin and d'Heurle [95] who investigated Cr/Cu and Bi/Cu thin films. These two pairs of metals have very low mutual solid solubilities; intermixing was nevertheless observed. Other examples of this kind are found in the Ti/Mo/Au metallisation systems [96] and in magnetic bubble memories. The mutual bulk solid solubilities of Mo and Au are exceedingly low below 800°C and the two metals do not form intermetallic phases. However since the melting point of Mo is much higher (2620°C) than that of Au, the Mo film is the finer grained of the two, so that Au diffuses preferentially into the Mo film. Thus, thin film Mo does not constitute a diffusion barrier for Au. This was further confirmed by Nowicki and Wang [97].

Most diffusion barriers for bearings appear to have been based on this concept, for example Ni, Ag and Co [13,12] of which Ni is most widely used. Although these barriers prevent the interdiffusion of Cu they fail to curtail the interdiffusion of Sn. Indeed they all react with Sn to form compounds [12]. Fe however, approximates closely to a passive barrier, with the lowest rate of compound growth. This may be due to partial oxidation of Fe during the plating process.

2.7.3 Single Crystal Barriers

The way to eliminate fast diffusion paths such as grain boundaries and dislocations is to use single crystal films. The solution is not practical for normal applications but investigations have been carried out which show that, in principle, such films do indeed constitute effective passive diffusion barriers.

Tu and Rosenberg [98] produced thin film couples of 200 nm Pd and 70 nm Au separated by an intermediate layer of Ag about 300 nm thick. In one specimen the Ag layer was single crystalline as was the underlying Au film. In the other specimen the Ag barrier layer and the Au layer underneath were both polycrystalline and had an average grain size of 35 nm. Au forms solid solution with Ag and forms compounds with Pb but Ag and Pb do not react and have low mutual solid solubility. Regardless of this, Tu and Rosenberg found that after vacuum annealing for 48h at 200°C, the single crystal layer of Ag was essentially impermeable to Au and Pb. In contrast, the polycrystalline layer of Ag did not prevent the formation of PbAu compound at the Pb-Au interface after only 24h at 200°C.

A second experiment with a polycrystalline Ag layer was performed with Pd instead of Au. Metallurgically,

Pd and Au behave similarly with respect to Ag and Pb but Pd and Ag are sufficiently dissimilar for Pd to alter the lattice parameter of Ag noticeably if a sufficient amount of the diffusing Pd goes into solid solution with the Ag grains. The lattice parameter of Ag was found to be unchanged even when the amount of Pd transported was substantial compared with the amount of Ag layer. This result indicates that Pd is confined to grain boundaries and does not penetrate the grains.

Kirsch et al [99] also investigated the interdiffusion of Au/Ag thin film couples in the single crystal and polycrystalline state. In contrast to the previous experiment, their thin film couples were self supporting and the Pb layer was absent. The absence of the Pb film was significant. When the single crystal couple was vacuum annealed at 150°C for 40min the films underwent no detectable change. When the polycrystalline film was similarly treated, Au was seen to diffuse into the Ag layer and Ag was also seen to diffuse into the Au layer. The presence of Pb acts as a sink for Au (or Pd) atoms and the Au (or Pd) does not alloy with Ag, but forms compounds with Pb, the rate of reaction with Pb being much faster than the process of diffusion into the Ag grains.

The presence of a sink at the boundary of a film which contains rapidly diffusing impurity atoms

constitutes a strong driving force in thin film couples. A demonstration of this is provided by thin evaporated films of Au or Ag on Si single crystal substrate [100-102]. Si and Au are mutually insoluble. Because the Si substrate is single crystalline, no significant diffusion of Au into Si occurs but fast diffusion of Si into Au is indeed observed. In an oxidising atmosphere (O_2 , air, steam) SiO_2 will grow rapidly on top of the Au film at temperatures as low as 100°C.

Another demonstration of the effect a sink can have on the behaviour of thin metal layers is offered by the Ge/Au/Ni system [103]. Bulk Au and Ge form a single eutectic, Au and Ni form a solid solution and Ge and Ni form compounds. If the Ge layer and the Ni layer are separated by a layer of Au, all the Ge diffuses through the Au layer and combines with the Ni during the heat treatment. Au and Ni do not interact much during this process. The condition which must be satisfied is that the atomic percentage of Ni exceeds that of Ge. This guarantees that all the Ge can be bound in the form of NiGe compound. If there is not sufficient Ni to bind all the Ge all three elements become mixed in laterally non-uniform aggregate. The results are similar if Pt is substituted for Ni [104].

2.7.4 Amorphous Diffusion Barriers

A significant recent development is the use of amorphous alloy films as interlayer diffusion barriers for metal-semiconductor contacts. Wiley and co-workers were the first to recognise the potential of amorphous alloys as diffusion barriers [105].

If extended defects present rapid diffusion paths, one way to eliminate them is to use amorphous materials also known as metallic glasses. These glasses can be produced from a large variety of different alloys, presenting a scale of different properties [106]. One important parameter is the glass transition temperature T_g . A high value of T_g for the amorphous phase results in a greater resistance to crystalline transformation [71]. Refractory metals such as Nb, Hf or W in combination with transition metals such as Fe or Ni or metalloid such P, B or Si often form metallic glasses[107] with T_g high enough to withstand service and process temperatures for semiconductor devices.

Amorphous thin film diffusion couples have been shown to have diffusivities of 10^{-22} cm²s⁻¹ and hence diffusivities in some amorphous films are many orders of magnitude smaller than those in polycrystalline metals[108,109]. Generally, diffusivity in amorphous

alloys are intermediate to those of defect free single crystals and of polycrystalline materials [21,70]. The main reason for this observation has been the elimination of the grain boundary component to diffusion. Anderson et al [110] have observed no interdiffusion of Au or GaAs after 16h anneal at 400°C in the Au/amorphous W-Si/GaAs system and that for Au/amorphous W-Si/InP, no interdiffusion was observed after 8h at 450°C. The results were a significant improvement over previous polycrystalline barriers (e.g. TiPt) which degrade after 1h at 350°C. Similar improvements have been demonstrated by Suni and Nicolet[111] for the Fe-W barrier, Thomas et al.[112] for the Ni-Nb barrier and by Zhu et al.[113] for the Ni-N-W barrier.

2.7.5 Stable Diffusion Barriers

A stable barrier layer must have a positive free energy of reaction with the material of the films on both sides of the barrier. The solution is to seek a material with a large negative energy of formation.

Compounds have the advantage of being numerous. By selecting strongly bonded materials, chemical stability with respect to materials on both sides of the barrier can be achieved. A good example of such a barrier is TiN, but nearly all nitrides, borides and carbides of early transition metals are attractive candidates for stable compound barriers [114]. These compounds are characterised by high melting points, chemical inertness and extreme hardness, and are formed by sputtering of sintered compound targets or reactively sputtering of elemental target.

An application of this idea has been described by Fournier [115] for the gate metallisation of transistors where TiN is used as a barrier between Ti and Pt layers. A layer of Ti only 10 nm thin provides adequate protection against diffusion of Pt during a heat treatment for 30 min at 450°C. Reactively sputtered TiN and TaN have been successfully used for Ni metallisation of PtSi layers on a Si substrate [116]. A 75 nm thick TiN was found to be adequate for a heat

treatment of 90 min at 600°C. In the absence of the barrier, the Ni and PtSi layers strongly intermix [117]. These barriers are also used in Ti/Pd/Ag [118] and Cr/Ni [116] metallisation schemes.

It is possible that reactively sputtered films behave as "stuffed" barriers (set.2.7.8), but overall these compounds behave as a fair approximation to the ideal case of a passive barrier.

2.7.6 Partially Stable Barriers

An attractive feature of the compound diffusion barrier is that it can be thermodynamically stable, i.e. with the barrier X in a state of lower free energy with respect to a reaction with adjoining materials A and B. Although this stability does not ensure low diffusivity of A and B in the barrier, it does ensure that the barrier itself will not react with A and B.

An example of this kind has been investigated by Tu and Chance [119] in which a polycrystalline layer of Ag deposited on Pb was shown not to prevent diffusion of Au atoms and the subsequent formation of Pb₃Au. However, if Au alloys with Ag rather than react with Pb the molar free energy of Au is reduced with respect to its pure state since the alloy has a negative free energy of

formation. The next step is to bind the Au chemically (i.e. to lower the molar free energy) so that the reaction with Pb becomes energetically unfavourable. By calculation and experimentation, Tu and Chance show that Pb ceases to react with Au if the Au-Ag solid solution contains more than 70 at/o Ag. For Pd this limit is in the vicinity of 99 at/o.

This stability condition still leaves out of consideration the second interface of the barrier layer against the Au film. As long as such a layer is present, the Au (or Pd) concentration in the compound layer cannot be maintained at a fixed value but will necessarily change with time. To ensure complete chemical stability of a compound barrier layer, it is necessary in general to reach a state of stability against both A and B simultaneously.

Another thin film couple which is claimed to be stable is $Ti,W_{1-x}/Au$. This metallisation system has been introduced by Cunningham et al [120]. The stability of Ti,W_{1-x} against Au has been deduced from electrical measurements after annealing of the thin film couple at 450°C for 600h. A thermodynamic calculation to support the claim is not given. However, Harris et al.[121] have shown experimentally that Ti,W_{1-x} film is not stable against Si but forms a ternary compound with it. The reaction with Si sets in only at

elevated temperatures. At lower temperatures the alloy is metastable against Si, it should serve as an acceptable barrier between Au and Si if neither are fast diffusers through the Ti_3W_{14} layer.

A general kind of partially stable barrier is provided by silicide contacts. $PtSi$ and Pd_3Si are used as the first contacting material. Usually this first layer is then covered by a second metal such as Ti. The free energy of the whole system can thus be lowered if Ti reacts with the Si. Whether $PtSi$ is dissociated in the process and reforms elsewhere or whether the titanium silicide is directly formed by diffusion of Ti or Si across the Pd_3Si is a question of kinetics. At the temperatures and times usually encountered, Ti reacts slowly with $PtSi$; this is the reason why the system can be applied successfully in practice.

Alloy and multilayered barriers have the advantage of being numerous, though, for bearing applications, only Ni-Fe [9], Cu-Zn [9] and Ni-Sn [122] have been reported, none of which arrest interdiffusion of Sn. Recently, Hodes et al [123] have reported the use of Cu-(30-70w/o)Sn alloy in combination with an additional layer of Sn or Zn. It is not clear whether any or all of these alloys were designed to be thermodynamically stable against Sn by free energy considerations. The

use of multilayered barriers are not common to bearing industry, although two examples can be cited, the work of Hodes et al [123], and that of Glyco Metalwerke [124] in which a two-layered barrier construction is described. One layer consists of Ni and the other was Ni-(30-90w/o)Sn alloy deposited on top.

2.7.7 Sacrificial Barriers

Sacrificial barriers exploit the fact that the adjacent films that react and form compounds often do so in a laterally very uniform fashion. A barrier layer X that reacts uniformly with the material A and B on either side of it then effectively maintains a separation between A and B as long as the barrier layer is not fully consumed by these reactions.

One of the first applications of a sacrificial barrier was proposed by Bower who investigated the role of Ti as a diffusion barrier in the Si/Ti/Al metallisation system [125]. A recent patent describes the use of a sputtered film of the intermetallic compound TaAl₃ as a barrier between Al and Ta on a Si substrate [126]. A Ta film does not react with Si below 650°C, but it does react with superimposed Al film to form TaAl₃ interfacial layer.

All of the practical barriers developed for bearing applications tend to fall into this category, not by design but by the ensuing interaction of the barrier material with either Sn or In from the overlay. Ni and Fe effectively separates Cu and Sn or In but permits the formation of compounds with Sn or In whose rate of growth is lower than that of Cu-Sn or Cu-In compounds.

2.7.8 Stuffed Barriers

Stuffed barriers are those whose low atomic diffusivities are attributable to the inhibiting effects of impurity segregation along the fast diffusion paths. The pronounced improvement of the diffusion barrier properties of Mo and Ti_3W_2 films in the presence of impurities such as O or N confirms this. Impurity concentrations of the order of 0.1 at.pct or less are usually taken as indicative of this type of barrier.

To unambiguously establish the role of an impurity in a particular case is difficult, but there are many instances where stuffed barriers are likely. For example the presence of oxygen impurity in Cr improves its effectiveness as a barrier against Al [127] and that of Ni against Pt [128]. In another instance, the presence of 10-15 ppm of S in Cu is known to inhibit

the growth of Cu-Si compounds to quite elevated temperatures [129].

Stuffed diffusion barriers can be quite effective, but their use is treacherous when the essential role of a particular impurity is not recognised, a prime example of which is the work of Kalubowila [4,5,6], whose Cu-P and Cu-B barriers appear to be based on this concept.

2.8 Electroplating Processes for Plain Bearings

There are three main areas of application of electrodeposits in the bearing industry;

- (a) overlay plates;
- (b) diffusion barriers and bonding layers between the bearing alloy and the overlay, eg. Ni plate; and
- (c) protective coatings for steel backed bearings.

With the exception of Ni as a diffusion barrier and Sn or Cu as protective coatings for steel backings the majority of electrodeposits are alloy based.

Brenner [146] describes the following four main types of alloy plating;

(i) Regular and Irregular Co-deposition

In this type of process the composition of the deposit is governed by the rate of diffusion of a particular species of metallic ion in the cathode double layer. Thus an increase in the concentration of a particular type of ion in the double layer caused by forced convection or elevated temperature leads to increased composition of the alloy deposit. This is

most likely to occur in the baths in which equilibrium potentials of species are far apart.

In irregular co-deposition the process is not totally dependent on diffusion phenomena and the effects of plating variables on the composition of the deposit are less. Irregular co-deposition occurs in systems in which equilibrium potentials are closer.

(ii) Equilibrium Co-deposition

Examples of equilibrium co-deposition are Cu-Bi and Pb-Sn alloys in which the ratio of metals deposited are the same as that of the metal ions in the plating solution at low to intermediate current densities.

(iii) Anomalous and Induced Co-deposition

Anomalous co-deposition is rare and only recognised for some of the iron group of metals. In this system the less noble metal is deposited in preference to the more noble one under certain plating conditions.

Induced co-deposition takes place when metals such as Mo, W and Ge are induced to be deposited in small quantities with Fe, Co and Ni which are otherwise not plateable in elemental form. The effect of plating variables on alloy composition are not clearly established.

2.8.1 Electrodeposition of Lead-Tin Alloys

The most widely used overlay deposits are Pb-Sn and Pb-In. However, there are certain customary preferences for their use; in the USA Pb-In is preferred despite the higher cost of indium. The manufacture of Pb-In overlayed bearings involves additional costly processes since Pb and In are deposited as separate layers and subsequently diffusion heat treated to form a homogeneous alloy. A recent review by Walsh and Gabe [147] indicates that future developments for Pb-In electrodeposits are likely to be based on tartrate or sulphamate solutions.

In the UK and Europe, Pb-Sn based overlays are preferred. Fluosilicate solution were first used for the electrodeposition of Pb and Sn in the refining industry. However, since the mid-1950's the use of fluoborate solutions for Pb-Sn alloy plating has come into prominence. This plating system belongs to the regular type of solutions in which metallic ions are introduced in the form of concentrated Pb and Sn fluoborates. The ratio of metallic ions in the solution is the same as that desired in the deposit [146].

The boric acid content of the bath is not critical; however, a certain minimum quantity is necessary to prevent the hydrolysis of lead fluoborate otherwise lead

fluoride precipitates. Free fluoboric acid is also added to prevent the hydrolysis of stannous fluoborate. The presence of addition agents as glue in the bath is a requisite as it promotes lateral growth and improves adhesion and surface roughness. The addition agents also enhance the Sn content of the deposit and are generally one or a combination of two of the following; gelatin, resocinol, or beta-naphthol. Glue is generally used up during the operation of the bath through inclusion in the deposit, precipitation, or decomposition. Glue content of the bath is maintained on the daily basis to retain control of the deposits.

The International Tin Research Institute [148] recommends a current density of 3 Adm^{-2} for still vat plating and 6 Adm^{-2} for barrel plating. The composition of the anodes is the same as the desired composition of the deposits. The operating temperature of the bath is usually maintained between 25 and 30°C.

2.8.2 Electrodeposition of Amorphous Alloys

Generally, the electrochemical techniques for preparation of amorphous alloys have preceded as techniques of metal finishing for corrosion resistance, wear resistance etc.; consequently there are relatively few reported studies about their preparation and

physical properties by this method. The amorphous metals and alloys prepared by plating techniques are listed in Table 1 [130].

The amorphous metals or alloys have the following properties:

(1) Bi-S [131], Bi-Se [132], Cd-Te [133], Cd-S, Cd-S-Se and Cd-Se [134], Si [135] and Si-C-F [136] alloys show the characteristics of n-type or p-type semiconductors, developed as materials for solar cells.

(2) Cr and Cr alloys [137] and Ni-, Co-, Fe-based alloys [138] including W, Re and Mo are highly resistant to corrosion and have good thermal stability.

(3) The structural transformation from a crystalline one to an amorphous one for the Ni and Co alloys [139] takes place continuously with an increase in concentration of S, P, or B

(4) Ni-Mo-P and Ni-W-P [140] and Co-Ni-P are recognised for good electrical insulation and magnetic properties.

The cathodic reactions for both the electroless and electrodeposition of P- or B-based amorphous alloys are similar and believed to consist of direct and indirect processes. The direct reactions are simply nickel and

Electroplating		Electroless Plating
Pb - S	Ni - W	Ni - B
Pb - Se	Co - W	Co - B
Co - Te	Co - Re	Co - P
Mo-S-Co	Co - V	Ni - P
Ni	Fe - W	Fe - Co - B
Co - Cu	Fe - Mo	Ni - Fe - P
Ni - P	Cu	Ni - Mo - P
Cu - P	Cr - W	Ni - Co - P
Cr - P	Cr - Mo	Ni - W - P
Co-Ni-P	Cr - Fe	

Table II. Amorphous alloys deposited by plating methods.

hydrogen reduction. The indirect reactions are discussed by Scholder et al.[141] who showed that in the presence of phosphine (PH_3) and Ni ions, Ni-P alloys could be formed spontaneously. Because this reaction most probably occurs on the surface, elemental P is incorporated in the Ni lattice by chemisorption and prevents normal crystal growth. The greater this inhibition the lower the nucleation energy. As a consequence the nucleation rate is high and the lateral growth is low [142], resulting in a fine grained or even an amorphous alloy if sufficient P is present.

In general it has been established that if the amount of P dissolved in Ni exceeds about 12 at.pct. then the structure of Ni-P alloy becomes amorphous. In the case of Ni-B alloy approximately 16 at.pct. B is required. The upper limits, are respectively, 25 and 35 pct. The concentration of P in the alloy is reported to increase with the decrease in the current density [144] while its distribution varies with its thickness [145].

The deposition processes for the amorphous alloys remains poorly understood, but some variations in the alloy types occur. These include at least two different amorphous phases: layered or homogeneous in the case of Ni-P [144]. The different amorphous phases [143] depend on the deposition conditions. As a result of pH

oscillations in the cathode region, a layered structure is formed for alloys deposited under conditions of natural convection. The layered structure is composition modulated with regards to P content [144] and can be reduced or eliminated by reducing the thickness of the cathode diffusion layer by pulse plating or by forced convection.

3. EXPERIMENTAL PROCEDURE

3.1 Introduction

The experimental section of this thesis was originally designed to be complementary to the work of Kalubowila et al [4,5,6]. As such it falls into two main categories. A detailed investigation into the deposition and performance of Cu-P and Cu-B diffusion barriers on actual bearings for commercial exploitation of patented processes together with concurrent investigation into the possibility of co-deposition of P or B with Pb-Sn alloy on the basis of previous work. Having established the invalidity of this previous work, efforts were channelled into the development of alternative diffusion barriers based on amorphous Cr-C and amorphous Ni-P alloys of which Ni-P was investigated extensively.

Generally, there are three aspects to testing of bearings for commercial viability. One concerns the rate of chemical interaction among the bearing materials and, therefore, the rate of growth of intermetallic compounds. The other two concerns the corrosion resistance and the tribological properties of bearing alloys. The use of test rigs enables these properties to be investigated simultaneously under dynamic conditions.

A number different types of bearing test rigs are described in the literature [16]. Generally, these are of two main types; fatigue test rigs and wear test rigs. The former apply to hydrodynamically lubricated bearings in which dynamic loading is achieved by 'out of balance' weights on a rotating shaft. The latter apply to marginally lubricated bearings in which load is applied by means of 'dead weight'. The test rig intended for use in this project was of the latter type. This rig was designed to study the rates of corrosion of bearing overlays by weight-loss analysis. However, after extensive modifications of the test rig, significant wear of the bearing overlays was found to be persistent and therefore the true rate of corrosion of the overlays in the presence of diffusion barriers became difficult to assess. Consequently, corrosion testing, and heat treatment to assess compound formation were investigated separately.

In all cases preliminary studies of barrier deposition processes were carried out on plane Cu substrate. The behaviour of diffusion barriers during the heat treatment in non-oxidising silicon fluid was monitored by metallographic examination and the compound layer thickness was determined with the aid of optical/scanning electron microscopy. Concentration microprobe analysis and marker studies were also

conducted. The results were then used to determine the kinetic parameters of the diffusion processes involved.

3.2 Electrodeposition processes

Commercially pure (99.9 wt/o Cu, 0.03 wt/o oxygen; BS2870 C101) high conductivity cold rolled sheet Cu of 0.8 mm in thickness was used as the substrate in all plane sample experiments on barrier plating. The Cu sheet was cut into panels 5 cm x 7 cm for preparation.

There were three stages in the preparation of barriered samples; cleaning, electrodeposition of the barrier, and immediate electrodeposition of the overlay. The cleaning and preparation sequence was:

-
- i mechanical cleaning on wet paper - grit size 800
 - ii vapour degreasing in trichloroethylene
 - iii water rinse, acetone rinse, drying
 - iv masking uncritical areas with lacomite
 - v storage of masked samples
-

The following procedure was used immediately prior to plating:

-
- 1 cathodic degreasing - 41 g/l NaOH, 41 g/l Na₂PO₄
 - temperature: 80°C
 - current density: 1.5 Adm²
 - time: 20 s,
 - 2 anodic degreasing - " "
 - time 5 s,
 - 3 water rinsing,
 - 4 bright dip
 - H₂SO₄ 0.72 v/o
 - H₂O 0.12 v/o
 - HNO₃ 0.16 v/o
 - time 10 s,
 - 5 water rinsing
 - 6 commence barrier deposition - 'live entry',
 - 7 water rinsing,
 - 8 acid dip - HBF₄ 25 v/o,
 - 9 commence overlay deposition,
 - 10 water rinse, alcohol rinse, drying, and mechanical stripping of lacomite,
 - 11 storage
-

The same sequence of preparation was employed for electrodeposition on bearing shells.

However, mechanical cleaning and anodic degreasing were omitted. Acetone rinsing was replaced with alcohol and the bright dip replaced with 40 v/o HNO₃ acid dip.

In all cases, rinsing was by fresh mains water in a two stage tank with final rinse in distilled water. The cleaning sequence was carried out with minimum delay between treatments and, following the final rinse, the specimen was rapidly transferred to the plating bath.

The average plating thickness of the diffusion barriers were 5-6 μm and that for the overlay was 20-22 μm .

For the deposition of Cu-P and Cu-B barrier layers on bearing shells - type PT145/BEH 1011 (Glacier Metals Co) with Cu-22w/o Pb matrix, a technique commonly used in industry was employed. Bearing half shells were arranged so as to form a circular column with a rod anode suspended in the centre. Preliminary experiments led to loosely adherent 'burnt' deposits. Consequently, various anodes of different geometry were investigated in order to satisfy the requirement of cathode to anode area ratio of 1:1. Finally, a perforated tubular anode was adopted to yield satisfactory deposits.

The same anode configuration was used to deposit amorphous Ni-P diffusion barrier on bearing shells.

Smooth and adherent deposits of Pb-Sn overlay were readily obtained on bearing shells with an anode to cathode area ratio of 0.46. A cast anode of the same composition as that required in the deposit was used in the form of a solid rod.

3.2.1 Deposition processes for Cu-P and Cu-B barriers

The deposition processes for Cu-P and Cu-B diffusion barriers were previously developed by Kalubowila et al [4,5,6]. These barriers were deposited using cupric sulphate baths containing phosphoric and phosphorous acid as a source of phosphorus and boric acid as a source of boron.

The composition and conditions of the plating bath for Cu-P are given in Table 2. Barriers were also deposited from modified baths with the following variations.

(i) The CuSO_4 content of the plating bath in Table 2 was increased to retard porosity and improve the adhesion of the deposits. CuSO_4 concentration was increased from 30 to 60 and 90 g/dm³. Accordingly, barriers were also investigated in the extended range of current density (c.d.), i.e. from 0.5-1.5 Adm⁻² to

0.5-3.2 Adm^{-2} .

(ii) The phosphorous and phosphoric acid contents were doubled and tripled from that given in Table 2 to promote greater P content in the deposit.

(iii) The effect of periodic variation of the c.d. during barrier deposition was investigated in order to produce barriers with a P concentration gradient. The following variation in c.d. was made:

Current density (Adm^{-2})	0.4	0.6	0.8	0.6	0.4
Plating time (min)	0.5	3.0	20.0	3.0	0.5

The plating bath composition and conditions for Cu-B alloy deposition are given in Table 3. As in the case of Cu-P barriers, Cu-B barriers were also deposited from modified baths with increased CuSO_4 and boric acid content.

TABLE 2. Bath Composition and Operating Conditions for Electroplating Cu-P Alloy

Cupric Sulphate	30 gdm ⁻³
Phosphoric Acid	45 gdm ⁻³
Phosphorous Acid	12.5 gdm ⁻³
Temperature	40-45°C
pH at 25°C	0.5-1.0
Current Density	0.3-1.5 Adm ⁻²
Anode/Cathode Area Ratio	1:1
Anode	Cu

TABLE 3. Bath Composition and Operating Conditions for Electroplating Cu-B Alloy

Cupric Sulphate	30 gdm ⁻³
Boric Acid	40 gdm ⁻³
Temperature	20-25°C
Current Density	0.5-1.0 Adm ⁻²
Anode/Cathode Area Ratio	1:1
Anode	Cu

TABLE 4. Bath Composition and Operating Conditions for Electroplating Bi

Bismuth Trichloride	122 gdm ⁻³
Ammonium Hydroxide	144 gdm ⁻³
Hydrochloric Acid	517 gdm ⁻³
Gelatine	2 gdm ⁻³
pH at 20°C	0.4-0.5
Temperature	20-25°C
Current Density	0.4-1.5 Adm ⁻²
Anode/Cathode Area Ratio	1:1
Anode	Bi

3.2.2 Deposition processes for Bi, Pb-P and Pb-Sn-Ni alloys

The deposition of Bi is normally carried out from perchlorate baths. However, due to their hazardous nature, a chloride bath developed by Dingley et al [151] was investigated instead. Bi deposits from this bath were nearly always accompanied by a film of 'black mud'. Consequently, a modified composition given in Table 4 was developed to yield bright deposits. For good adhesion on Cu, the following pretreatment was necessary after degreasing:

- acid dip
 - 23 w/o HNO_3
 - 32 w/o acetic acid
 - 29 w/o phosphoric acid
 - balance H_2O
 - time 10-15 s

rinsing

- activation dip - 18 w/o HCl
 - BiCl_3 1gdm⁻³
 - time 15 s

Plating was initiated immediately, without intermittent rinsing.

In an attempt to deposit Pb-P alloy, a lead fluoborate bath containing sodium hypophosphite (20 gdm⁻³) as a

source of phosphorus was used. Plating conditions and composition of the bath were as given in Table 10 for deposition of lead.

Pb-Sn-Ni deposition was carried out from the Pb-Sn plating bath given in Table 8 to which 40 ml of nickel fluoborate containing 22 gdm³ of NiCO₃ was added. Similar plating conditions as those in Table 8 were used.

3.2.3 Deposition of Amorphous Cr-C and Amorphous Ni-P Alloys

The development of plating processes for amorphous alloys was not the subject of this investigation but established processes were used for the study of the effectiveness of amorphous alloys as diffusion barriers. Consequently, a process described by Hoshino et al [149] to deposit amorphous (amps) Cr-C and that described in a patent by Gamblin [150] for amps Ni₈₀-P₂₀ alloy were used.

The electrolytes used for conventional chromium deposition are based on chromic acid, sulphuric acid and proprietary brightening agents. For the deposition of amps bright chromium, formic acid as the only addition agent was used. The composition and conditions for this

process are given in Table 5. Barriers were deposited on high purity Cu sheet and therefore the same procedure of pretreatments as that described for Cu-P and Cu-B barrier deposition was employed. An insoluble Pb anode of commercial purity was used in cast sheet form of the same dimensions as the cathode. Barrier layers were deposited for 15 min giving an estimated thickness of 5 μm .

This process requires the electrodeposition to be carried out within 90 min of the preparation of the electrolyte so as to maintain an optimum concentration of formic acid, which otherwise decreases by chemical oxidation and results in the loss of the amorphous structure of the deposit [149].

The deposition of Pb-Sn overlay on amps Cr-C was performed sequentially with intermediate rinsing, acid dip in conc. HCl for 10s, rinsing, and acid dip in 25 v/o HBF₄. Although good overlay deposits were obtained on amps Cr-C, adhesion was poor. This became evident on quenching the samples in silicon fluid at 150 °C which led to extensive 'out gassing' and complete delamination of the overlay in the central portion of the panels but remained adherent in the peripheral regions. These areas with good adhesion between the overlay and the barrier were selectively cut from the rest of the panel and diffusion annealed.

In the method described by Gamblin [150] to electrodeposit amorphous transition metal alloys the preferred bath constituents are nickel chloride, nickel carbonate and phosphorous acid. A number of other additives are recommended which influence contact and corrosion resistance of the deposit. Typically, one or more of the following are added; boric acid hydroxy acetic acid, acetic acid, succinic acid, surfactants, and hexa-fluorides of Si, Ti, or Zr. The plating bath selected for the deposition of amorphous $\text{Ni}_{40}\text{P}_{60}$ alloy for subsequent investigation as a diffusion barrier was based on nickel chloride, nickel carbonate and phosphorous acid and was absent of any addition agents. The composition and operating conditions for this bath are given in Table 6.

The preparation and pretreatment of the substrate was substantially the same as that for Cu-P and Cu-B barrier deposition. However, for deposition on a Cu substrate, dilute HCl (50 v/o) dip was applied immediately prior to immersion in the plating bath. For the deposition on Cu-Pb based bearings dilute (40 v/o) HNO_3 dip was applied, followed by rinsing. This bath permits the use of both active and inert anodes. To minimise the maintenance of the electrolyte, rolled Ni (99.9 pct) sheet was used as an active anode. Plain and perforated tubular anodes were used for deposition on plane samples

and bearing shells respectively with anode to cathode area ratio of 1:1.

For the comparison of the performance of amps Ni-P diffusion barrier with that of conventional (crystalline) Ni barrier a Watt's nickel bath was used for the deposition of matt-nickel. The composition and operating conditions for this bath are given in Table 7. Substrate preparation and pretreatment were the same as that for amps Ni-P deposition.

TABLE 5. Bath Composition and Operating Conditions for Electroplating Amorphous Cr-C Alloy

Chromic Acid	100 gdm ⁻³
Sulphuric Acid	5 gdm ⁻³
Formic Acid - 85v/o Soln.	20 mldm ⁻³
Temperature	30°C
Current Density	40 Adm ⁻²
Anode/Cathode Area Ratio	1:1
Anode	Pb

TABLE 6. Bath Composition and Operating Conditions for Electroplating Amorphous Ni-P Alloy

Nickel Chloride	178 gdm ⁻³
Nickel Carbonate	30 gdm ⁻³
Phosphorous Acid	102 gdm ⁻³
Temperature	80°C
Current Density	150 mAdm ⁻²
Anode/Cathode Area Ratio	1:1
Anode	Ni

TABLE 7. Bath Composition and Operating Conditions for Electroplating Crystalline Ni

Nickel Sulphate	122 gdm ⁻³
Nickel Chloride	144 gdm ⁻³
Boric Acid	175 gdm ⁻³
pH at 20°C	4-5
Temperature	20-25°C
Current Density	0.4-1.5 mAdm ⁻²
Anode/Cathode Area Ratio	1:1
Anode	Ni

3.2.4 Deposition processes for Pb-Sn and Sn

Lead-tin overlays were deposited from fluoborate bath containing Sn and Pb together with free fluoboric acid, boric acid and gelatin as an addition agent. The composition of Pb-10w/o Sn alloy plating bath is given in Table 8. Cast anodes in rod form of the same composition as the deposit were used, with anodic to cathodic area ratio of 0.46. For plating on plane samples, rolled sheet anodes were used.

Pb-Sn plating baths were prepared from concentrated fluoborate solutions of Sn (300 gdm⁻³) and Pb (520 gdm⁻³). On each occasion the stannous content of the Sn-fluoborate was determined by iodate titration and test coupons were analysed by SEM-EDAX to determine the Sn content of the deposit. In all cases barriered samples were pretreated with a 5 s dip in 25 v/o fluoboric acid prior to overlay plating.

In order to make a detailed investigation of the reaction mechanisms between Ni and Sn and also Ni-P and Sn, barriered samples were also coated with Sn overlays from stannous fluoborate bath. The composition of this bath is given in Table 9. The sample preparation and pretreatment for Sn deposition was the same as that for Pb-Sn deposition.

TABLE 8. Bath Composition and Operating Conditions for Electroplating Pb-10w/oSn Alloy

Tin (as stannous fluoborate)	10 gdm ⁻³
Lead (as lead fluoborate)	90 gdm ⁻³
Fluoboric Acid (free)	100 gdm ⁻³
Boric Acid (free)	25 gdm ⁻³
Gelatine	0.5 gdm ⁻³
Temperature	25-30 °C
Current Density	3 Adm ⁻²
Anode/Cathode Area Ratio	1:1
Anode	Pb-10w/oSn

TABLE 9. Bath Composition and Operating Conditions for Electroplating Sn

Tin (as stannous fluoborate)	80 gdm ⁻³
Fluoboric Acid (free)	90 gdm ⁻³
Gelatine	6 gdm ⁻³
Temperature	25-30°C
Current Density	2.2 Adm ⁻²
Anode/Cathode Area Ratio	1:1
Anode	Sn

TABLE 10. Bath Composition and Operating Conditions for Electroplating Pb

Lead (as lead fluoborate)	120 gdm ⁻³
Fluoboric Acid (free)	30 gdm ⁻³
Gelatine	1 gdm ⁻³
Temperature	30-35°C
Current Density	3 Adm ⁻²
Anode/Cathode Area Ratio	1:1
Anode	Pb

3.3 Corrosion tests and Heat treatment

Accelerated corrosion tests were performed in hot medicinal white oil (MWO). Since MWO is not inhibited, unlike commercial engine lubricants, these tests are taken as the norm for assessing the corrosion resistance of bearing overlays. Plane Cu samples coated with Pb in the presence and absence of Cu-P barriers were suspended in MWO maintained at 150°C. Prior to immersion each set of samples were weighed and their respective areas recorded. Periodically one sample was removed from each set, carefully washed in white spirit and reweighed. The loss in weight per unit area was then recorded as corrosion rate in mgcm^{-2} .

Similarly, heat treatment to assess nucleation and growth of intermetallic compounds in barriered samples were carried out in non-corrosive silicon fluid. Oil baths used for corrosion tests and heat treatment consisted of insulated one litre beakers seated on independent hot plates. Motor driven propellers in each beaker were used to keep the temperature fluctuation to $\pm 1^\circ$ by careful adjustment of the propeller speed and temperature controller. Cut samples were suspended from hooks on a glass rack which facilitated easy immersion and removal of the samples.

3.4 Metallography

Samples prepared for metallographic and analytical examination were in most cases cold mounted to obtain a normal cross section. In some cases it was necessary to mount samples obliquely (appx 5° to horizontal) for magnification of X10 of the compound layer thickness. This was achieved by using a special die in a two stage hot mounting process. The resulting mount was then turned on a lathe until the edge of the sample was exposed. Thereafter the sample was ground and polished.

A great deal of care had to be exercised in grinding and polishing the samples. The soft overlay tended to wear out preferentially, and in particular the brittle compound layers were found to fracture and lodge in the overlay. Consequently, microblocks were sectioned using a circular disc saw and coarse to fine grinding performed on silicon carbide paper (120-1000) by hand.

Attempts to polish the samples in a normal manner were futile. Therefore polishing was carried out directly after pregrinding on a selvyte cloth (stationary wheel) using 'Silvo' silver polish. To minimise the fracturing of the compound layers, the direction of the pregrinding and polishing was maintained at appx. 15° to the plane of the sample. The desired final polish and the conspicuity of the compound

layers were achieved by alternate polishing and etching.

The thickness of the compound layers were quite conspicuous for the Cu-based diffusion barriers, particularly after etching in freshly prepared NH_4OH solution with 10v/o of 20 vol H_2O_2 . For the Ni-based barriers, various combinations of etching solutions were tried; finally, a solution of 1 part nitric acid to 1 part acetic acid was used for deep etching. The deep etching dissolved away the Ni and Sn matrices, and left the compound layers unreacted. This etchant also enabled the phase boundaries between different compound layers to be observed.

In most cases, the measurement of compound layer thickness was performed using an optical microscope with the aid of an optical filler gauge. Because of the irregularity of the compound thickness, at least 25 random measurements were taken in order to obtain reproducible average of compound thickness per sample.

3.4.1 Marker Experiments

In order to determine the relative mobilities of Ni and Sn in the Ni-Sn intermetallic compounds, marker experiments were performed on Sn overlayed samples with

crystalline and amorphous Ni barriers. The use of artificial markers such as W or Mo wires or Alumina particles sandwiched between the barrier and the overlay was not possible. Attempts to interdeposit a thin layer of Cr led to difficulties in overlay deposition. Consequently, barriered samples were mounted obliquely and polished as described above. Markers were then fixed as 'knoop' micro-indentations on or near the original interface and photographed prior to heat treatment. Periodically samples were removed from the oil bath and lightly polished in 'silvo' and photographed again before re-immersion in the oil heat treatment bath. In this way a record of marker drift during the heat treatment was obtained.

3.5 SEM and X-Ray Analysis

Qualitative analysis were performed on the SEM and the Joel type JXA-3A x-ray microprobe analyser. Quantitative analysis of some of the barriered bearings was carried out on a Joel 733 microprobe analyser. SEM in conjunction with Princeton EDAX analyser was used for assessing the initial Sn content of the overlay and the composition of the intermetallic compounds. Specimens prepared for the quantitative analysis were in the unetched condition. In all cases, Quantitative analysis was performed using pure Cu, Sn, Pb-10 w/o Sn

-115-

(homogenized for 30 min at 150 °C), and GaP, Ni and Ni-Sn alloys as comparative standards.

4.0 RESULTS

4.1 Introduction

The scheme of presentation of results is in accordance with the course of this investigation which generally progressed in two separate directions but with the same aim of developing superior diffusion barriers.

Firstly, reports on the results of previously developed Cu-P and Cu-B diffusion barriers [4,5,6] are presented of which the Cu-P diffusion barrier was extensively investigated. This was primarily due to the difficulties encountered in depositing Cu-B barrier of good quality. Furthermore, based upon previous presumptions that P played a beneficial role in retarding the diffusion of Sn, fluoborate and chloride plating baths in conjunction with various complexants were also investigated concurrently but failed to yield Pb-Sn-P alloy deposits.

Failure to substantiate previous claims for Cu-P and Cu-B barriers led to the second phase of the investigation which was concerned with the study of amorphous Ni-P barrier. Results are presented on the effectiveness of amorphous barriers in the form of metallographic examination, compound growth morphology,

-117-

and approximate interdiffusion coefficients. Comparisons are also made with the conventional Ni-crystalline barriers, widely used in bearing industry.

4.2 Investigation of Pb-Sn Overlayed Cu-P and Cu-B Diffusion Barriers

4.2.1 Electrodeposition of Cu-P and Cu-B Diffusion Barriers

In the first instance Cu-P and Cu-B barriers were deposited on Cu-Pb based bearing shells in accordance with the original plating bath composition and conditions as described in Tables 2 and 3 (Sectn. 3.2.1). It was found that the Cu-P barrier plated at a c.d. of 1 Ampdm² which, according to [4] is the condition intermediate to those producing the best and worst deposits. However, Cu-B barriers plated at similar intermediate conditions, ie at c.d. of 0.75 Ampdm² were burnt, semi-adherent and powdery.

Examination of the Cu-P barrier under the scanning electron microscope revealed that the deposits were micro-porous. Furthermore, Pb phases in the Cu-Pb bearing substrate became passivated due to the pre-plating acid dip (bright dip). Heat treatment of such Cu-P barriered bearings overlayed with Pb-Sn led to Cu-Sn compound formation, contrary to the work of Kalubowila [4] in which the Cu-P barrier was investigated on Cu substrate only. Micro-Probe analysis of barriered bearings showed that P was extensively diffusing into the Cu-Pb substrate and not into the Pb Sn overlay as would be required according to

Kalubowila [4]. It was also thought that the porosity in the barrier itself may be responsible in-part for the loss of P into the Cu-Pb matrix.

Generally, porosity in electrodeposits results from a low metal content of the plating bath and also from the presence of substances which may inhibit the deposition process. It was found that the rate of mass deposition of the Cu-P barrier decreased as the P content of the plating bath was increased. In addition, the increased P content of the bath also decreased the range of c.d. for good deposits. Despite this, the need to increase the P content of the barrier in order to counteract the loss of P into the substrate entailed the investigation of a range of plating baths, which included up to three times the P and/or Cu content from that given in Table 2.

4.2.2. Metallography and Analysis

Qualitative micro-probe analysis of barriered bearings together with their SEM photomicrographs are shown in Figs 15, 16 and 17. These barriers were deposited in the c.d. range of 1.6-2.8 Ampdm² from plating baths containing twice as much Cu and three times as much P. These samples were heat treated at 150°C for 168h. The photomicrograph in Fig 15 shows the

Phosphorus and Tin concentration profiles of modified CuP barriered bearings heat treated for 168h at 150°C. Barriers deposited in accordance with Table 2 with increased phosphorus (135 gdm⁻³ H₃PO₄ and 37.5 gdm⁻³ H₃PO₃) and copper (60 gdm⁻³ CuSO₄·5H₂O) content. Fig 15 - Plating current density of 1.0 Adm⁻², Fig 16 - 1.5 Adm⁻², Fig 17 - 2.0 Adm⁻².

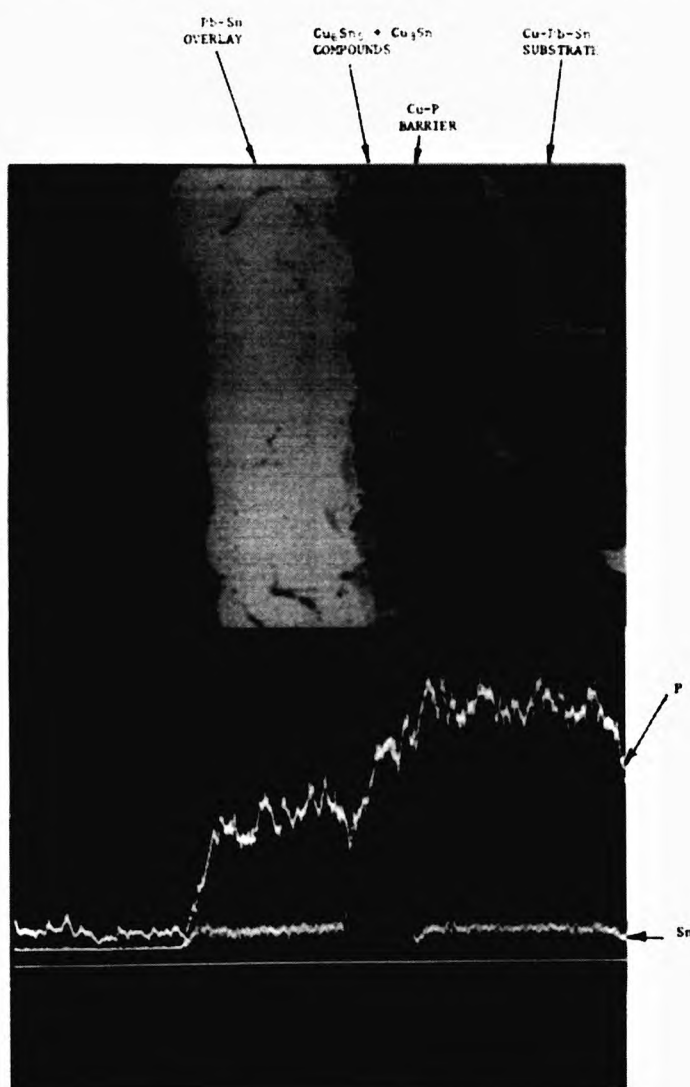


Fig 15

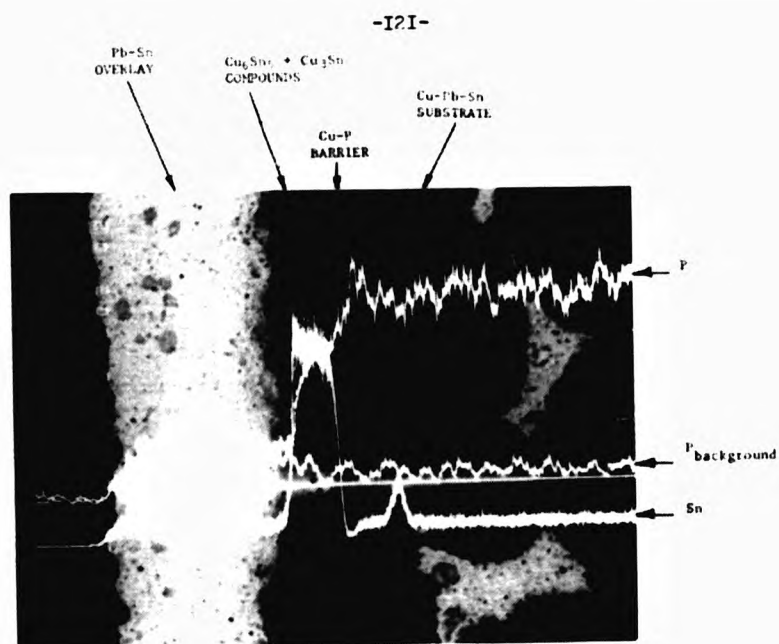
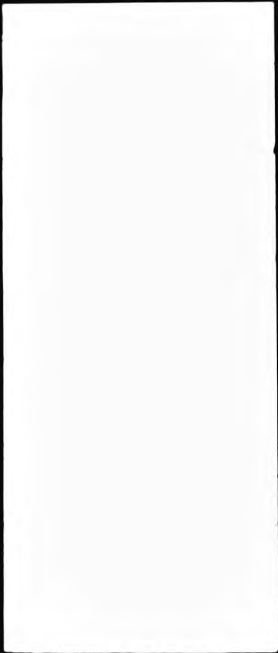


Fig16

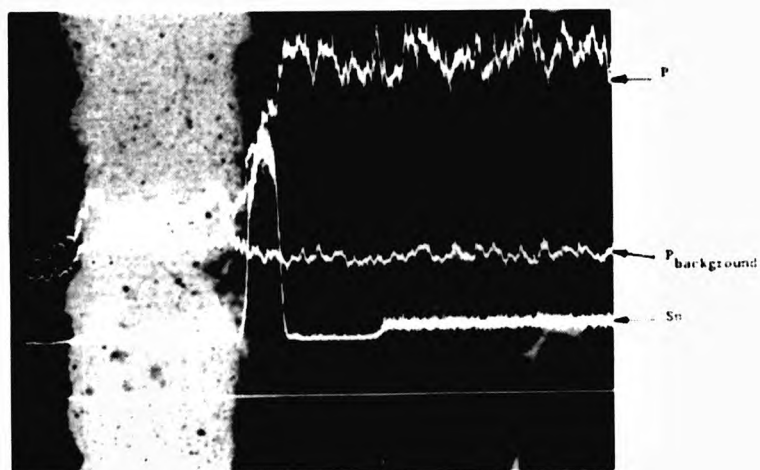


Fig17

existence of Cu_3Sn compound lying adjacent to the barrier which has transformed from Cu_6Sn_5 compound which forms first and lies adjacent to Pb-Sn overlay. The presence of duplex compound may be confirmed by the occurrence of two peaks in the Sn line scan. However, since the line scan is qualitative only, it is not a definitive proof of duplex compounds. On the other hand in Figs 16 and 17 the presence of only one compound, Cu_3Sn , is evident. The difference between P-line scan and P-background line scans in Figs 16 and 17 gives an appx. indication of P distribution from which it is evident that the majority of P resides in the substrate and only a negligible amount diffuses into the overlay. Comparison cannot be made for the P distribution in the substrate with that in the barrier layer except for the sample shown in Fig 17, where the P content of the much thicker barrier layer appears to be the same as that in the substrate.

Typical quantitative concentration profiles of some of the Cu-P barriered bearings are shown in Figs 18 - 21. These barriers were plated in the c.d. range of 1.6 - 2.8 Ampdm² from a bath containing twice as much Cu and were heat treated for 1000h at 140°C. By comparing P concentration profiles in these Figs it is seen that P diffuses readily out of the barrier and has greater preference to reside in the substrate than the barrier itself. At first glance, P appears to be

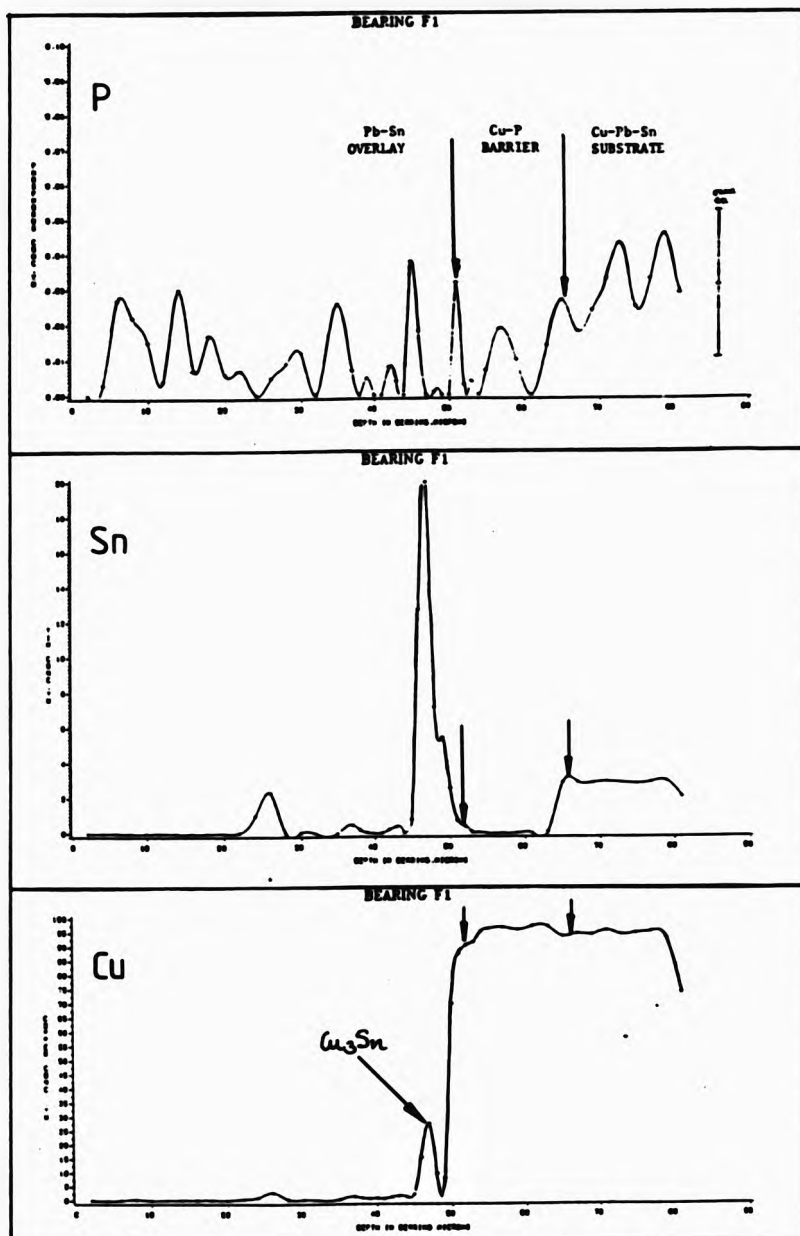


Fig 18

Concentration profiles of Phosphorus, Tin, and Copper of modified Cu-P barriered bearings heat treated for 1000h at 150°C. Barriers deposited in accordance with Table 2 with increased copper content (60 gdm^{-3} of $\text{CuSO}_4 \cdot 5\text{H}_2\text{O}$). Fig18 - Plating current density of 1.6 Adm^{-2} , Fig19 - 2.0 Adm^{-2} , Fig20 - 2.4 Adm^{-2} , Fig21 - 2.8 Adm^{-2} .

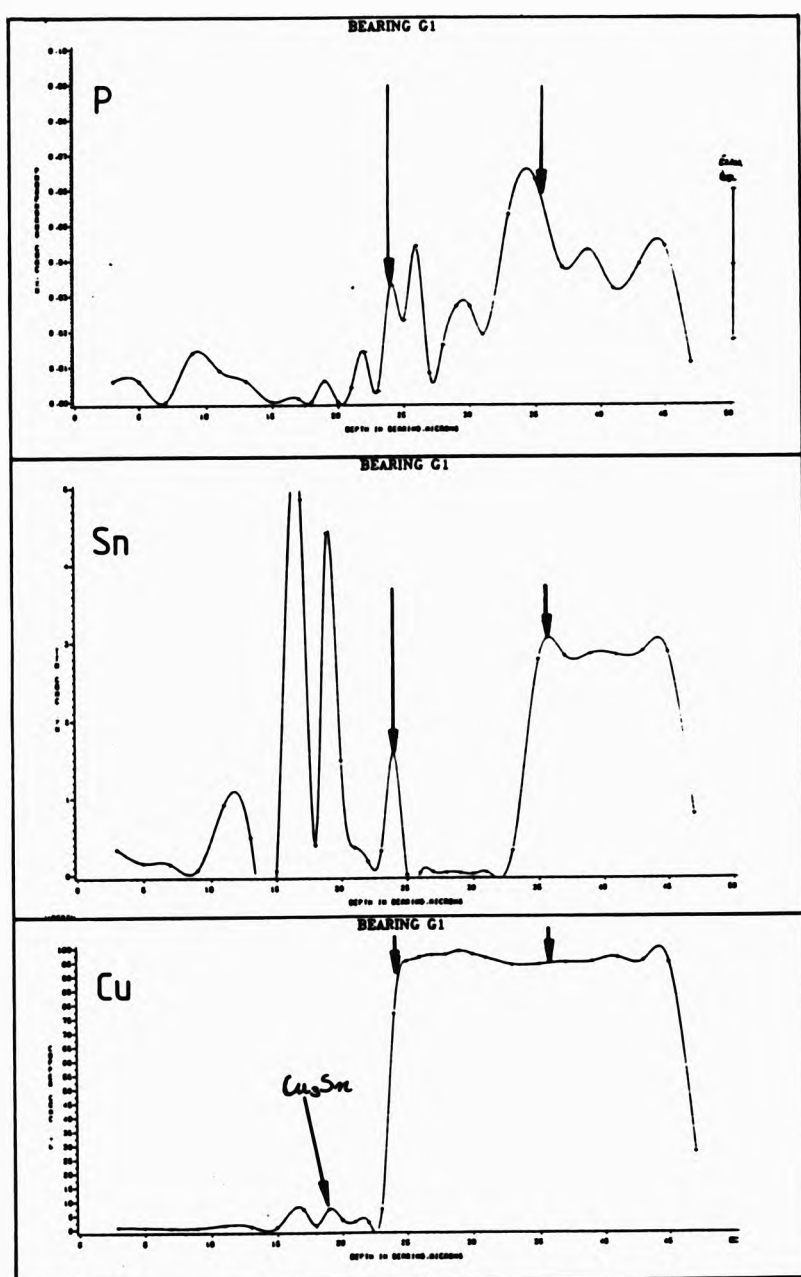


Fig19

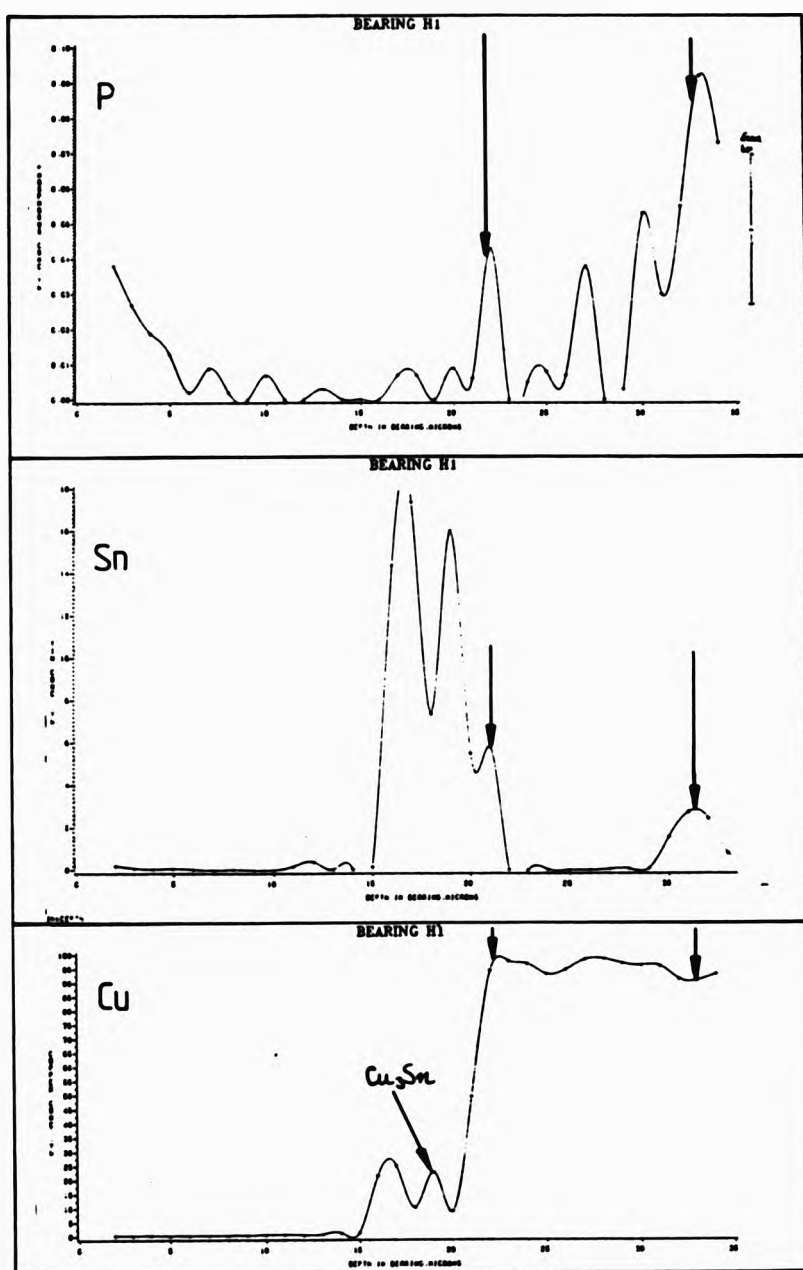


Fig20

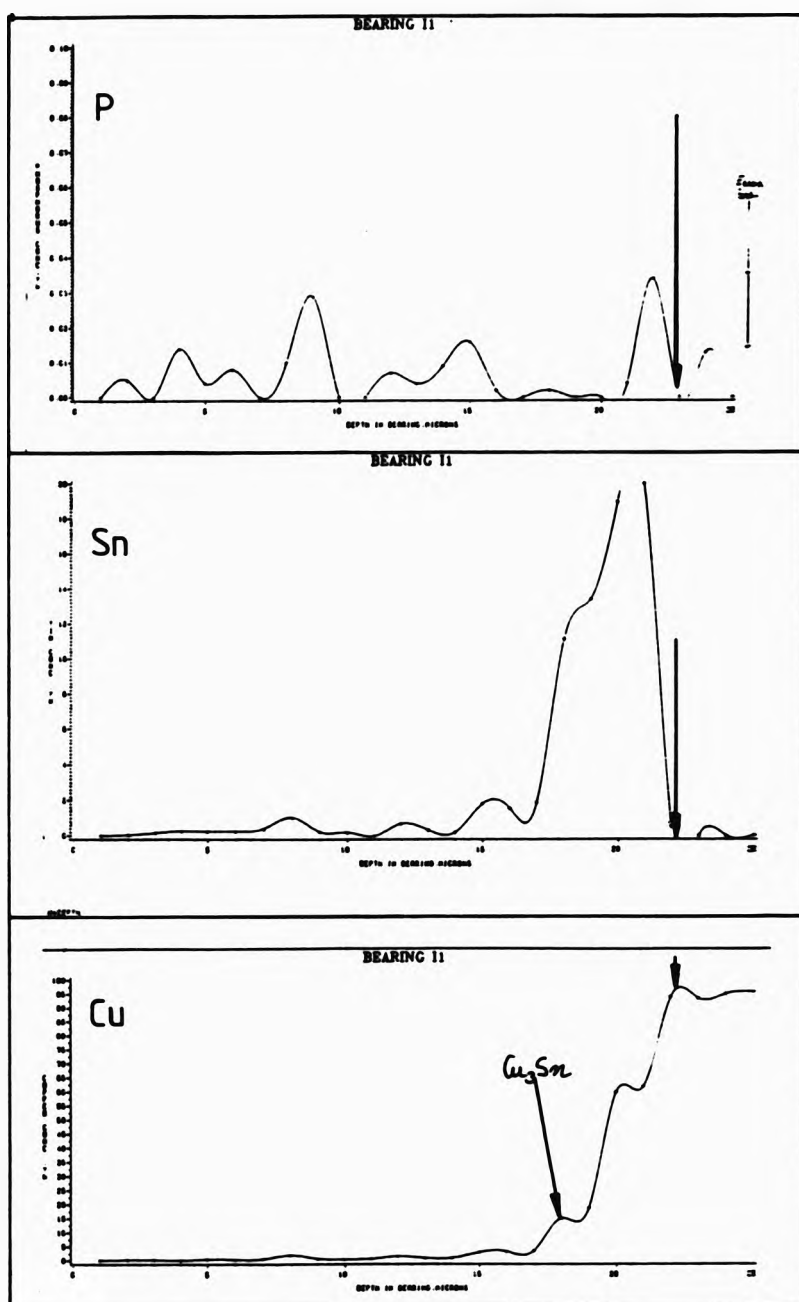


Fig21

randomly distributed in the Pb-Sn overlay, however, comparing P profiles with those of Sn it is found that P peaks do not coincide with the Sn peaks of the Sn rich Pb phase. This is particularly evident in Figs 18 - 21.

A striking feature of Figs 18 - 21 is that Sn acquires a concentration gradient at the barrier/overlay interface and to some extent diffuses into the barrier as seen from the position and the magnitude of the peaks. The occurrence of secondary Cu peaks in the overlay is indicative of Cu diffusion in Pb-Sn, in fact the coincidence of Cu and Sn peaks is indicative of Cu₃Sn compound formation.

The quantitative concentration profiles in Figs 22 - 24 are those of Cu-P barriered samples from previous work [4]. Barriers in these samples were deposited by the previous investigator from an unmodified bath (Table 2) in the c.d. range of 0.5 - 1.2 Ampdm² onto plane Cu sheet substrates which were subsequently annealed at 140°C for 960h.

The P distribution in Figs 22 - 24 is comparable to those in Figs 18 - 21, except that there is no loss into the Cu substrate. In comparing the Sn and P profiles, similar observations to Figs 18 - 21 can be made, ie P and Sn peaks do not coincide. However, the Sn profiles are markedly different to those in Figs 18 - 21. The

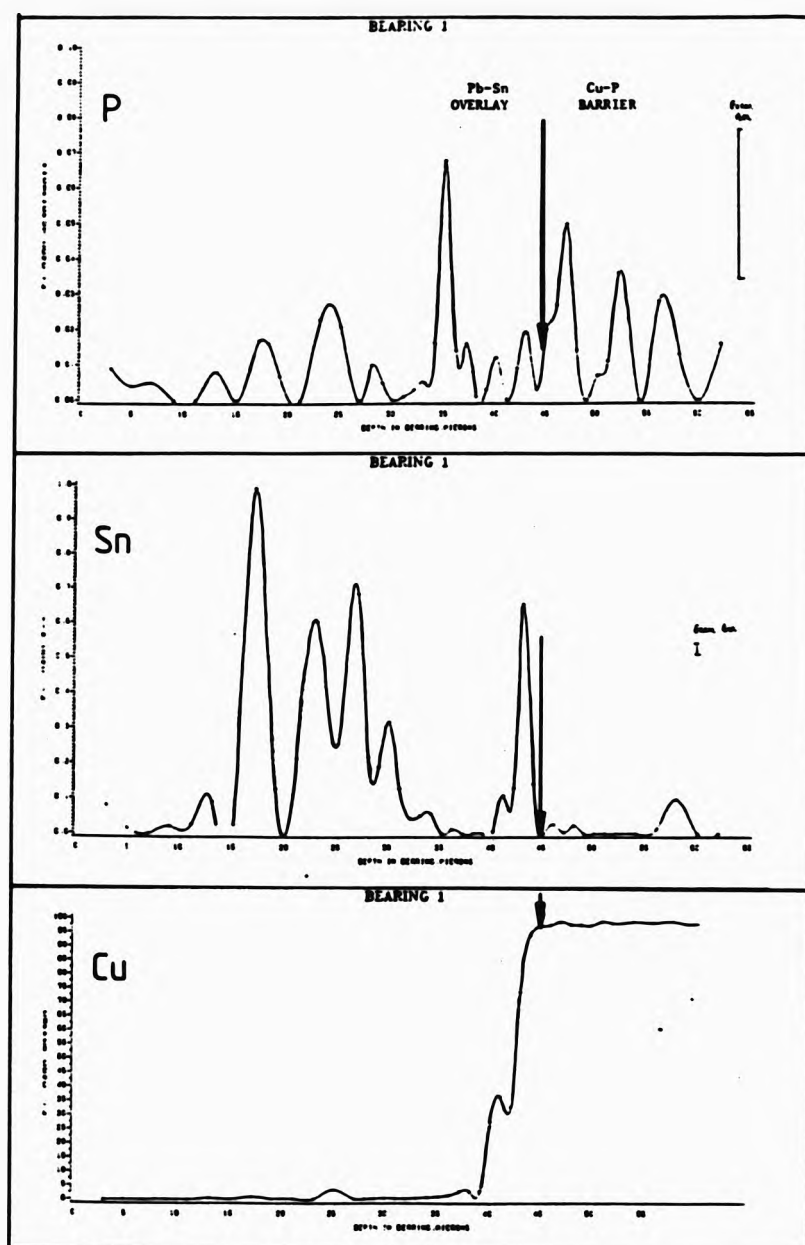


Fig22

Concentration profiles of Phosphorus, Tin and Copper of Cu-P barriered samples from previous work heat treated for 960h at 140°C. Barrier deposited in accordance with Table2. Fig22 - Plating current density of 0.5 Adm^{-2} , Fig23 - 1.0 Adm^{-2} , Fig24 - 1.2 Adm^{-2} .

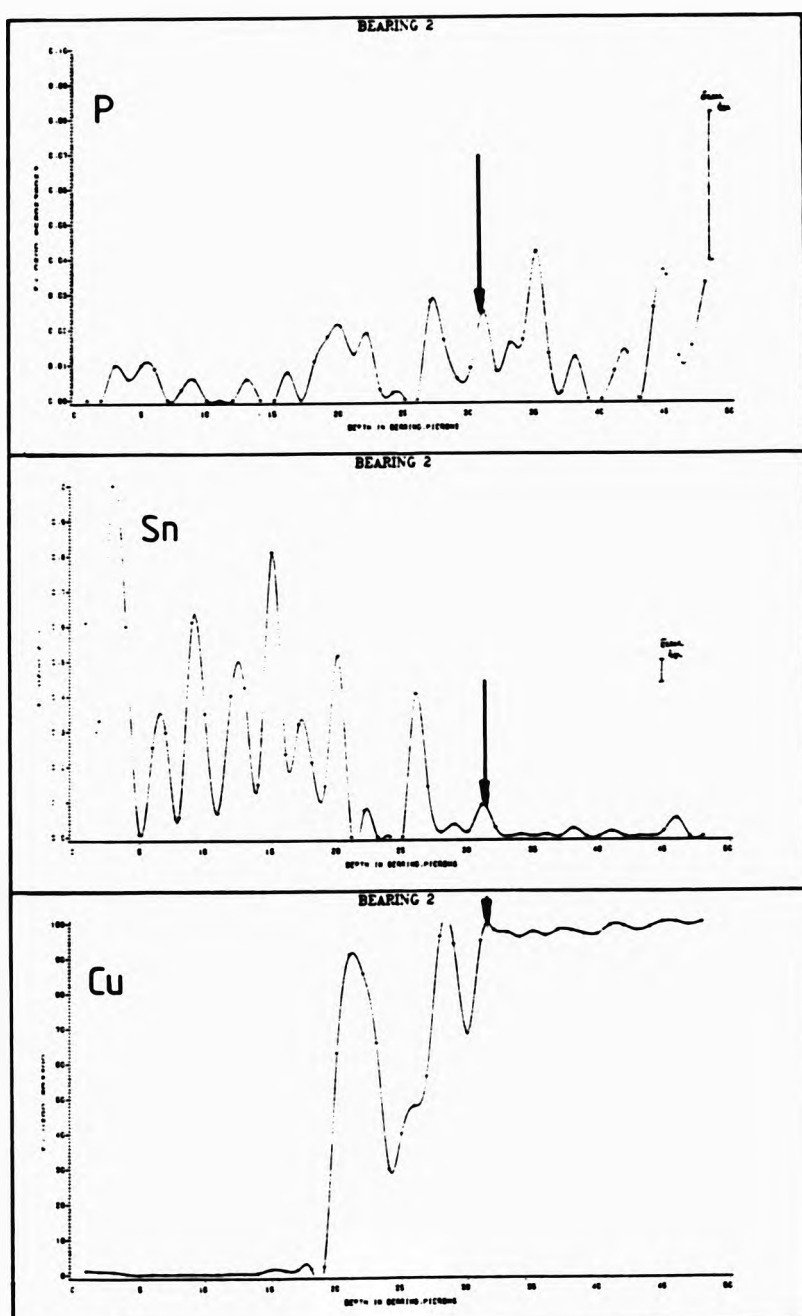


Fig23

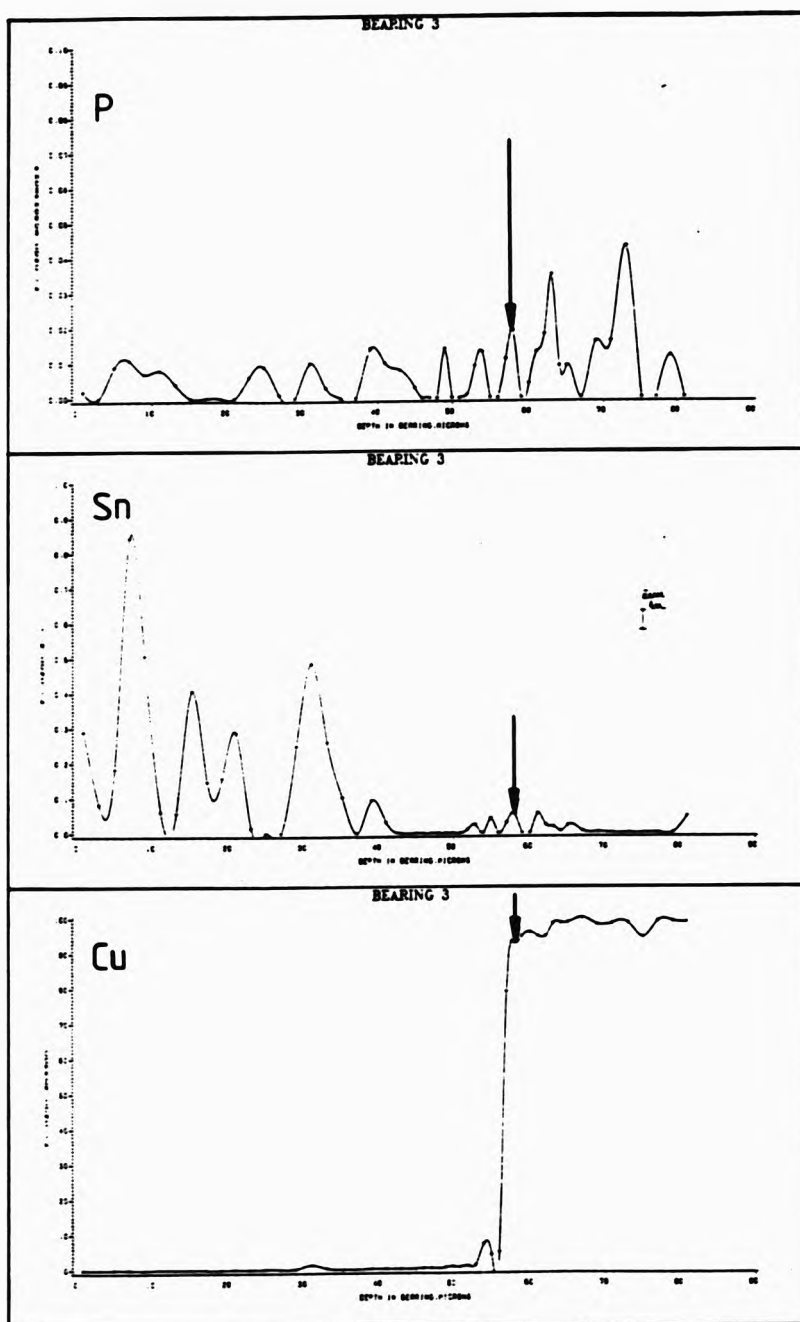
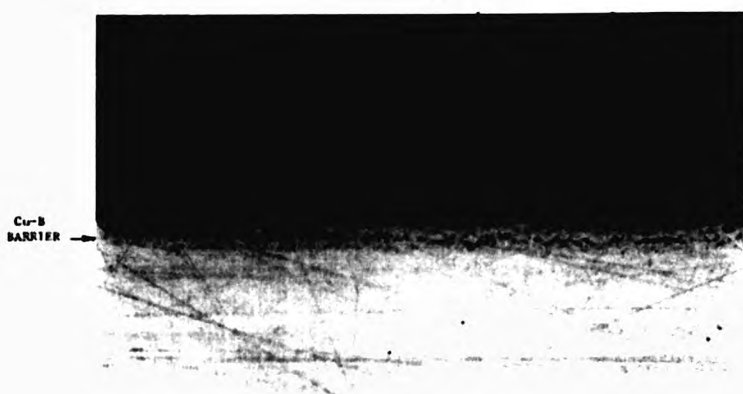
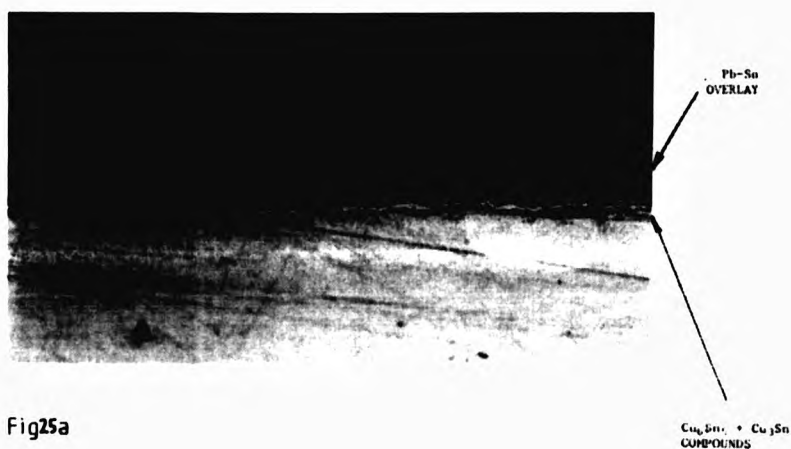


Fig24

largest Sn profile registered in Figs 22 - 24 is only of the order of 1 wt/o compared to 20 wt/o in Figs 18 - 21. In fact the average Sn content of the samples in Figs 22 - 24 was found to be 0.2, 0.4, 0.15 wt/o respectively. Furthermore, it is seen from the relative positions of the Sn profiles that Sn in Figs 22 - 24 does not acquire a concentration gradient adjacent to the barrier but towards the outer surface of the overlay. The coincidence of Sn and Cu peaks in Fig 22 is indicative of the existence of a compound at the barrier overlay interface, however, its compositional ratio does not confer with any of the compounds in the phase diagrams. Two secondary Cu peaks for the overlay seen in Fig 23 is due to fractured Cu-P particles from the barrier - embedded into the overlay during sample preparation.

The deposition of the Cu-B diffusion barrier according to the process described in Table 2 resulted in burnt deposits which were unavoidable. Nevertheless, this barrier was investigated on plane Cu samples. Growth rates for this barrier were not obtained but metallographic examinations have revealed that compound formation was not arrested. Figs 25a and 25b shows the micrographs of Cu-B barriered samples with 0.8 and 4.9 wt/o Sn in the overlay, heat treated at 150°C for 148h. Even with 0.8 wt/o Sn in the overlay compound formation is evident.

Compound growth on Cu-B barrier after 148h heat treatment at 150°C.
Fig25 (a) - with Pb-0.87Sn and Fig25 (b) - with Pb-4.9%Sn in the overlay.



4.2.3. Growth Kinetics of Copper-Tin Diffusion Compounds

The combined growth rates for the sum of Cu_3Sn_2 and Cu_5Sn compounds for Pb-10 wt/o Sn overlayed barriers deposited on a Cu substrate from the bath composition given in Table 2 are shown in Fig 26. In Fig 27, the total compound growth rates from the same bath containing twice the amount of P are shown whereas Fig 28 shows the effect of halving the Sn content of the overlay. Figs 26 - 28 also shows the growth rate of unbarriered samples heat treated at the same temperature of 150 °C. Thus, by comparing the barriered and the unbarriered samples it is evident that a Cu-P diffusion barrier has no effect in combating the Cu-Sn compound formation.

The parabolic form of compound growth rates in Figs 26-28 are shown in Figs 29 and 30. It is seen that the compound thickness extrapolates to about 2.35 and 1.48 μm for the 10 and appx. 5 wt/o Sn in the overlay.

It is also evident from Figs 29 and 30 that the parabolic rate law $x^2 = 2kt$ is followed reasonably well. Where,

x = compound thickness,

t = time and

k = growth constant.

However, according to Einstein-Smoluchowski [165],

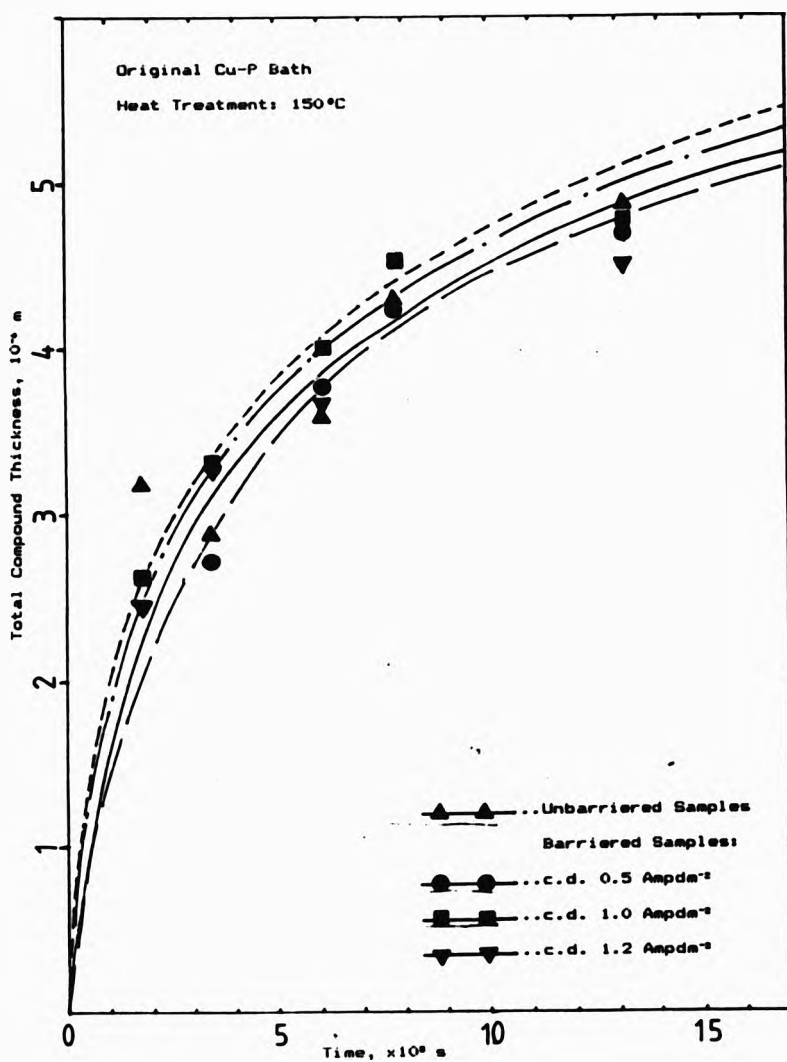


Fig26

Total ($\text{Cu}_3\text{Sn}_2 + \text{Cu}_2\text{Sn}$) compound growth rate on Cu-P barriered (Table 1) and unbarriered Cu substrate with Pb-10 wt/pct Sn overlay heat treated at 150°C.

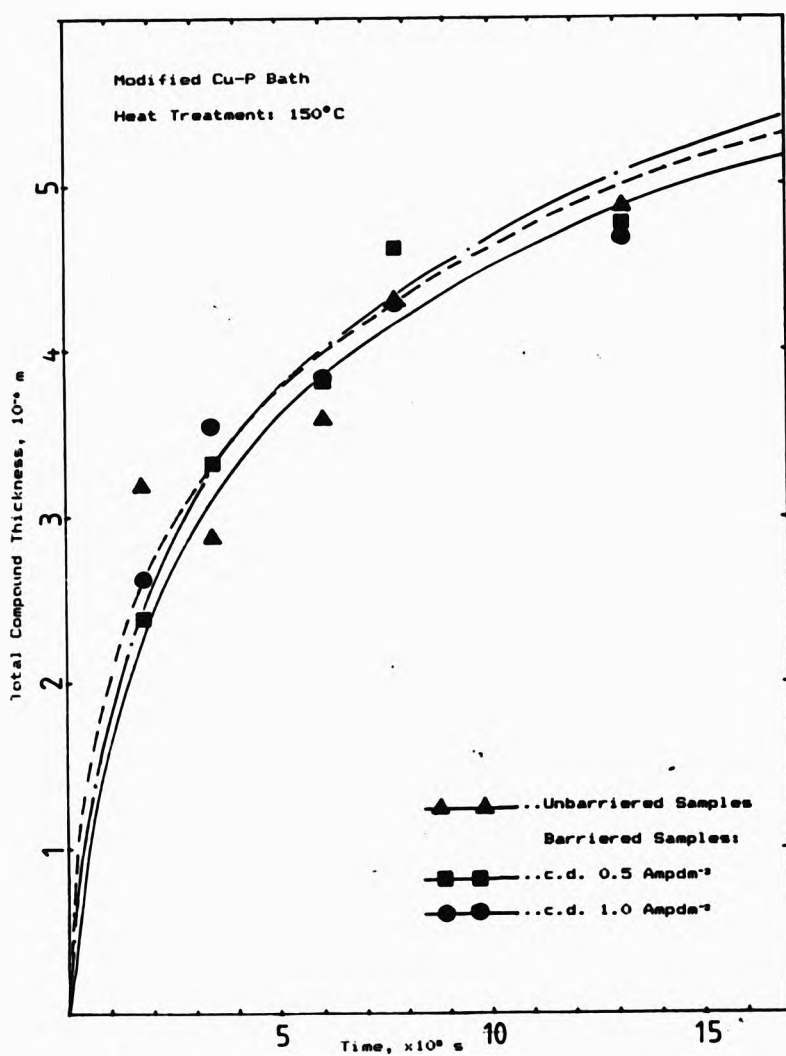


Fig27

Total ($\text{Cu}_2\text{Sn}_2 + \text{Cu}_3\text{Sn}$) compound growth rate on modified Cu-P barrier (Table 1, 90 gdm $^{-3}$ H_3PO_4 and 25 gdm $^{-3}$ H_2PO_4) with Pb-10 wt/pct Sn overlay, heat treated at 150°C.

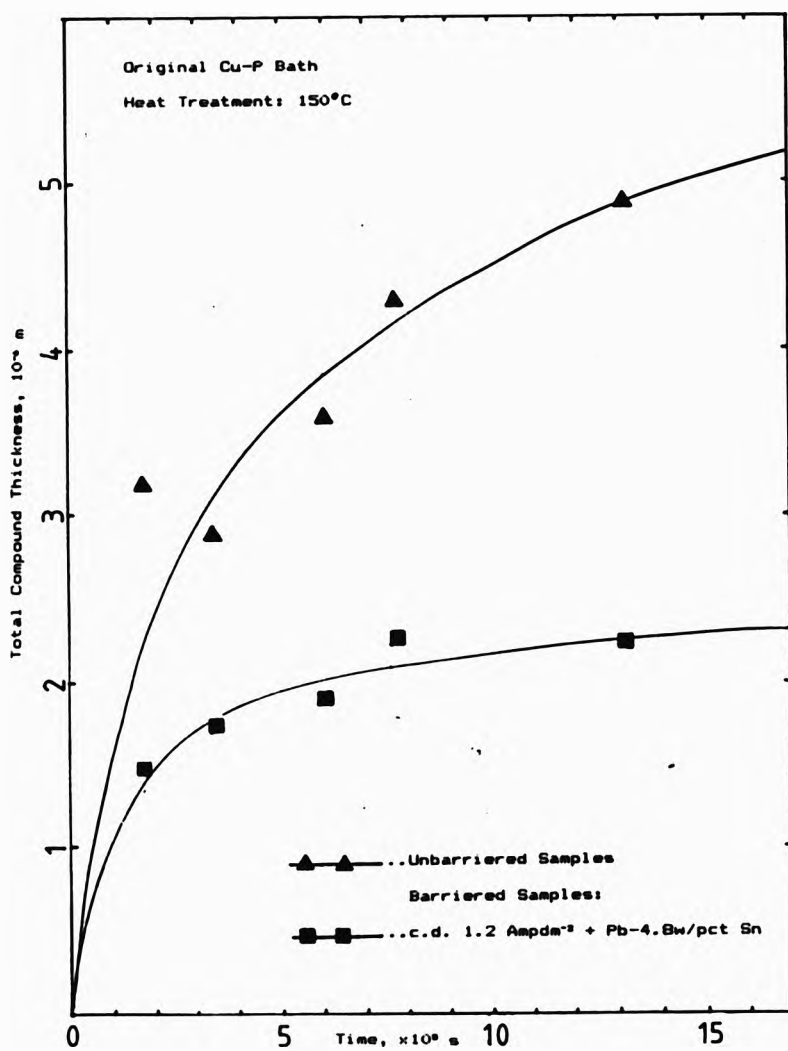


Fig28

Total Cu-Sn compound growth rate Cu-P barriered (Table 1) substrate with Pb-4.8wt/pct Sn overlay, heat treated at 150°C.

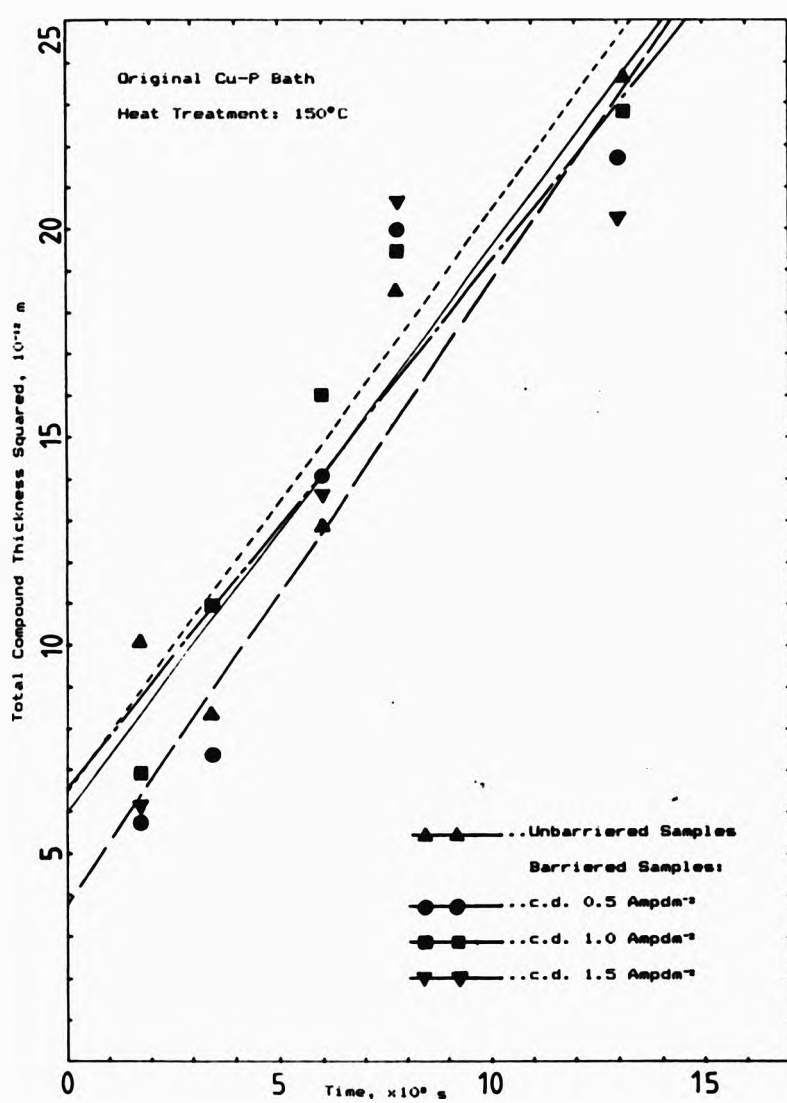


Fig29

Parabolic plot of total compound growth rate on unmodified Cu-P barrier.

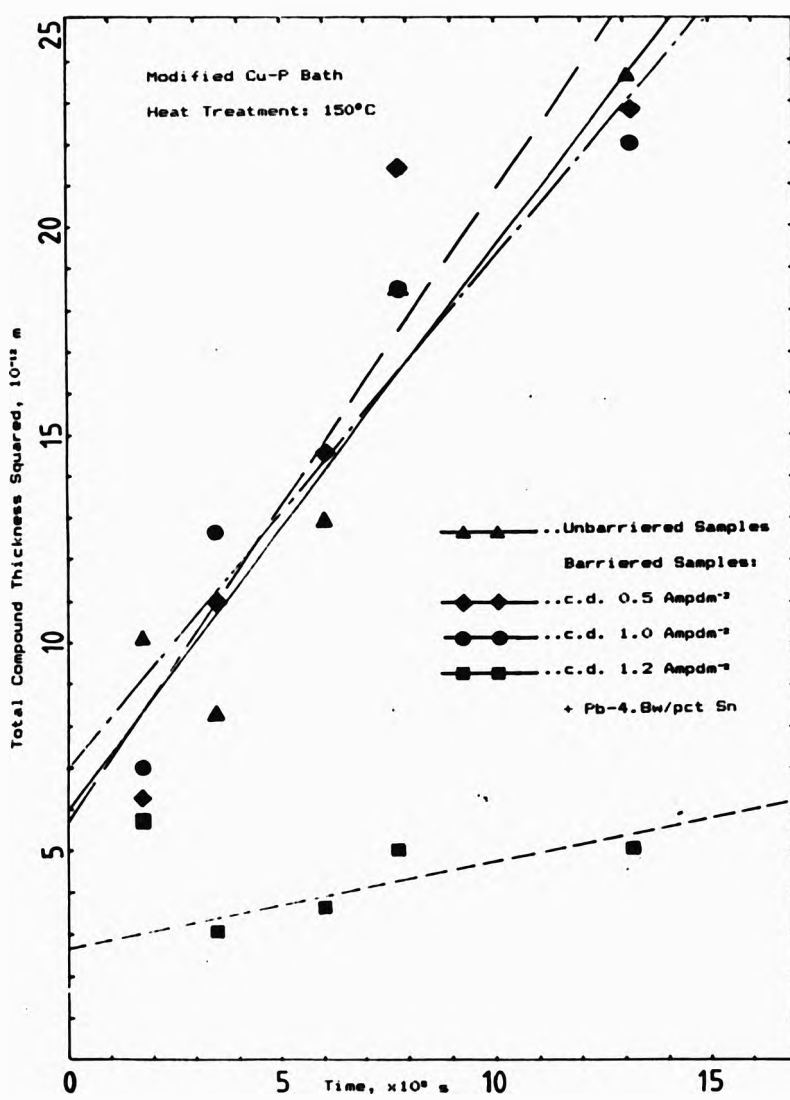


Fig30

Parabolic plot of total compound growth rate on modified Cu-P barrier.

k is appx. interdiffusion coefficient. Accordingly, the interdiffusion coefficients estimated from Figs 29 and 30 for Cu and Cu-P barriers overlaid with Pb-10 wt/o Sn were found to be in the range $6.55 - 7.55 \times 10^{-18} \text{ m}^2\text{s}^{-1}$ and those for the 4.8 and 4.9 wt/o Sn in the overlay were $1.04 - 1.18 \times 10^{-18} \text{ m}^2\text{s}^{-1}$.

4.2.4 Corrosion of Pb Overlay in the presence of Cu-P Barrier

Fig 31 shows the rate of corrosion of electrodeposited Pb in the presence and absence of Cu-P barriers. The barriers were plated from an unmodified bath (Table 2) at c.d. of 0.5 and 1.0 Amp dm^{-2} . It is apparent from Fig 31 that the Cu-P barrier does not impart any influence on the corrosion resistance of Pb. For the duration of the experiment, the rate of corrosion increases slowly up to 50 - 60h but thereafter it increases at a greater rate.

4.3 Investigation of Pb-P and Bi Barriers and Pb-Sn-Ni Overlay

Attempts to deposit Pb-Sn-P alloys were fruitless. However, it was found that impurity co-deposition of P, up to appx 0.05 wt/o with Pb was possible. Fig 32a shows the Pb-P barrier with a Pb-Sn overlay in the as-deposited condition. The presence of P is denoted by

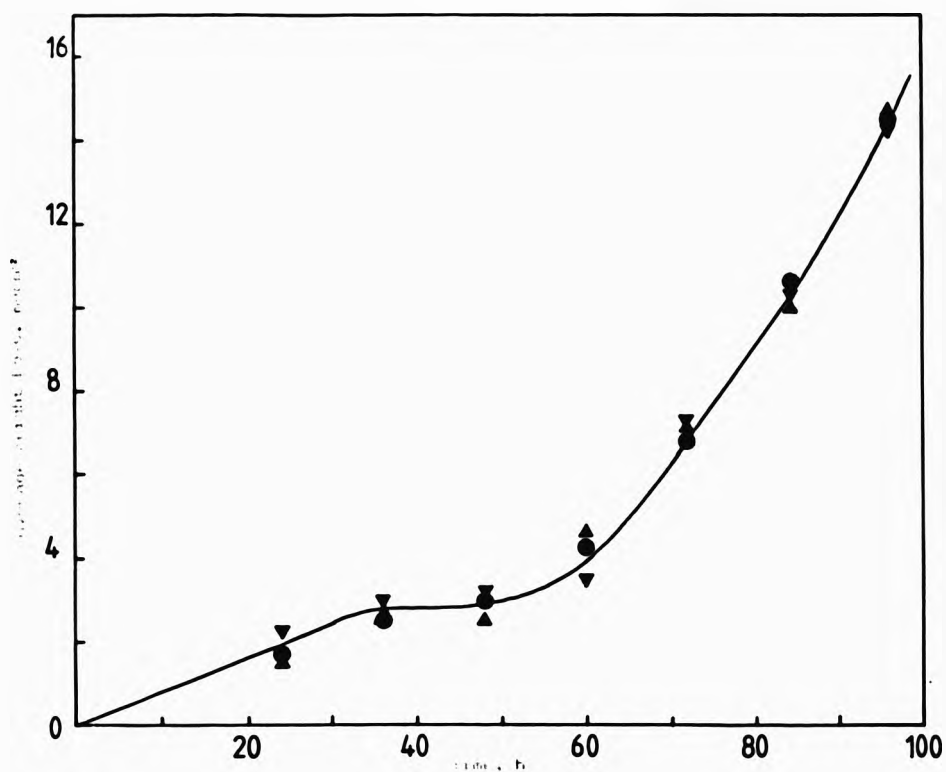
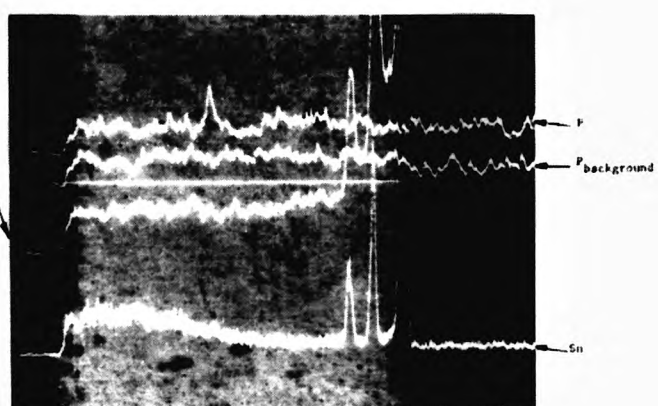
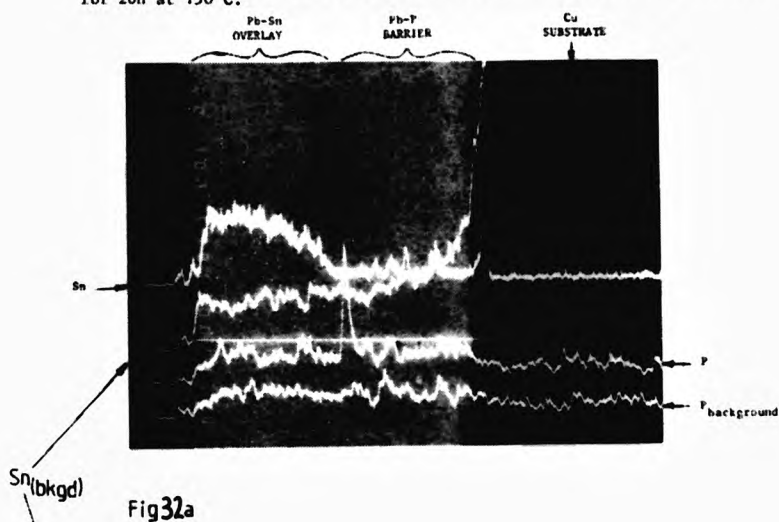


Fig 31 Corrosion of Pb overlay in medicinal white oil at 150%, in presence of unmodified Cu-Pb barrier, ▲ plated at 0.5 adcm², ▼ plated at 1.0 adcm² and ● in absence of Cu-Pb barrier.

Phosphorus, Tin and Copper concentration profiles of Pb-P barriered samples. Fig32(a) - Unheat treated condition - Fig32(b) heat treated for 20h at 150°C.



the sharp peak in the profile at the barrier/overlay interface.

The effect of heat treating for 20h at 150°C is evident in Fig 32b, where Sn has diffused through the Pb-P barrier and has acquired a concentration gradient at the barrier/substrate interface. At the same time P has partially diffused into the overlay. As a result of this, further investigations on Pb-P barrier were discontinued.

Although Bi barriers were successfully plated on Cu, exhaustive efforts to improve adhesion between Bi and Pb-Sn overlay failed. In the cases where 'seal tape' adhesion tests were successful, insertion in a hot Si fluid heat treatment bath led to overlay delamination by blistering. Consequently, further investigations were ceased.

A limited number of Cu samples with Pb-Sn-Ni overlay were investigated. The Ni impurity content of the overlay was not quantifiable, however it was found that heat treatment at 150°C led to compound formation.

4.4 Investigation of Pb-Sn and Sn Overlaved Ni and Amorphous Ni-P Diffusion Barriers

4.4.1 Metallography and Analysis

In the early course of this investigation amorphous Ni-P barrier was examined on Pb-20 wt/o Sn. Fig 33a shows a micrograph of such a barrier after heat treatment at 150°C for 141h. A two layer structure is seen at the barrier/overlay interface of which a uniform layer of Ni₃Sn₄ compound lies adjacent to the overlay. The other layer has grown within the barrier and was not identified as one of the Ni-Sn compounds, but was found to contain a greater amount of P than the rest of the barrier. The same micrograph is shown in Fig 33b after 'deep' etching in 1:1 in nitric and acetic acids. Again the zone of rejected P within the barrier is clearly visible. The columnar structure of the Ni₃Sn₄ compound is also apparent after etching.

Figs 34-37 shows optical micrographs using Normaski phase interference contrast. The combination of such an optical technique with 'deep' etching to reveal phase boundaries was found to be well suited for the study of Ni-Sn compounds. Detailed examination under SEM was not possible as it necessarily required more exotic techniques e.g. TiO and Zn-Se film phase contrasting.

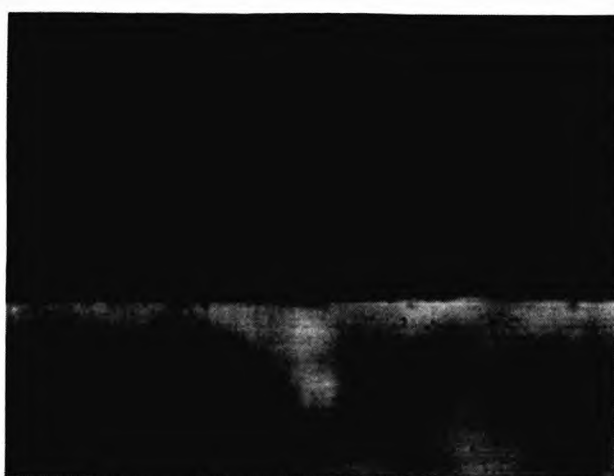


Fig33a



Fig33b

Photomicrographs amorphous Ni-P barrier with Pb-20 wt pct Sn overlay after heat treatment at 150°C for 141h: (a) before and (b) after etching.



Fig 34a

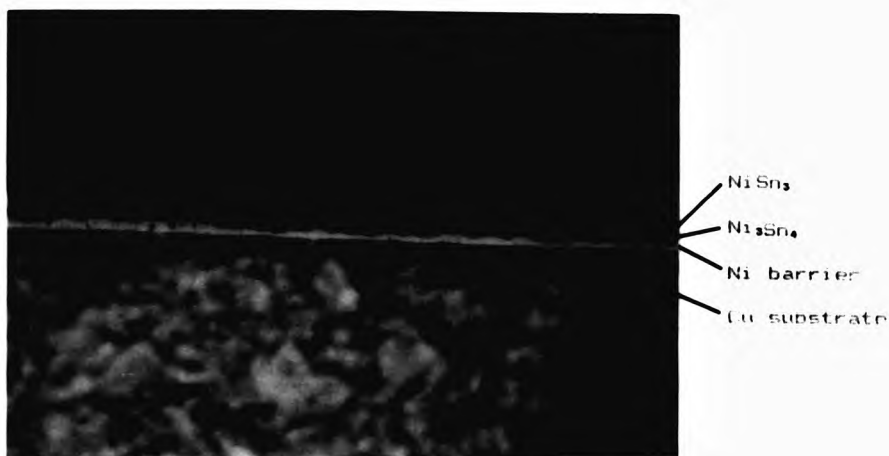


Fig 34b

Crystalline Ni barrier overlayed with Sn after 2500h heat treatment at 150°C. Fig 34a - lightly etched in 1 pct Nital, Fig 34b - deeply etched in 1:1 nitric and acetic acid.

-146-

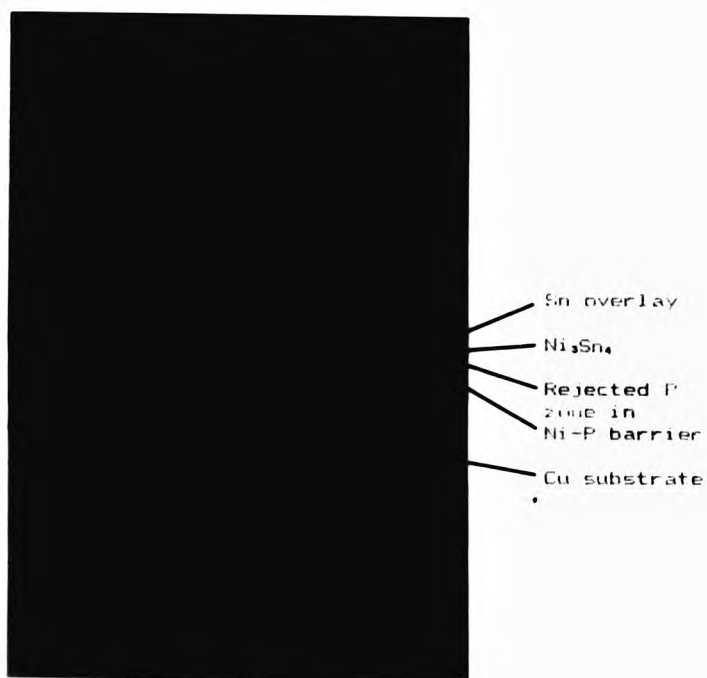
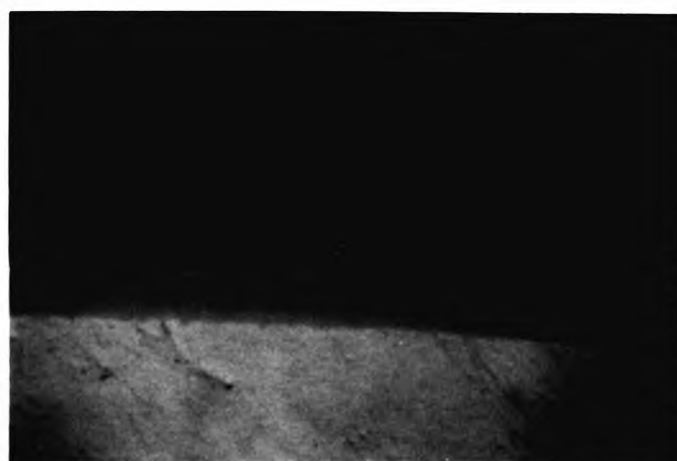


Fig 35 Amorphous Ni-P barrier overlayed with Sn after 2504h heat treatment at 150°C - deeply etched in 1:1 nitric and acetic acid.



NiSn₃
Fig. 36
Ni barrier
Cu substrate

Fig 36



Sn overlay
Ni₃Sn₄
Rejected P
zone in
Ni-P barrier
Cu substrate

Fig 37

Barriers overlayed with Sn after 4592h of heat treatment at 150°C. Fig 36 - crystalline Ni barrier, Fig 37 amorphous Ni-P barrier.

Fig 34a shows a micrograph of a conventional Ni barrier overlayed with Sn after heat treating for the extended time of 2504h at 150 °C. This sample was 'lightly' etched in 1% Nital which preferentially contrasts the Ni_3Sn_4 compound. Fig 34b shows the same sample after deep etching which reveals the duplex nature of the Ni-Sn compounds. The NiSn_2 compound which forms below 100°C and occurs only in electroplated Ni-Sn couples is seen as the outermost compound with a plate-like structure. The high temperature Ni_3Sn_4 compound is seen between the NiSn_2 and the remaining Ni barrier with a more uniform but columnar structure.

The micrograph shown in Fig 35 was taken after heat treating amorphous Ni-P barrier overlayed with Sn for 2504h at 150°C. After deep etching the existence of only Ni_3Sn_4 compound is evident and, compared to the micrographs in Fig 34, the structure consists of coarse grains with irregular outwardly growth. Again, the P precipitated zone in the barrier is clearly evident.

After prolonged heat treatment of the Ni and amorphous Ni-P barriers for 4592h at 150°C only the Ni_3Sn_4 compound is evident (Fig 37) for the amorphous Ni-P barriered sample as described above. However, a four layered structure is seen for the Ni barriered

sample (Fig 36). The Sn overlay has been completely consumed by the formation of NiSn_2 and Ni_3Sn_4 compounds. Although a part of the original Ni barrier still remains, Sn has also diffused through it to form Cu_3Sn compound with the underlying Cu substrate.

4.4.2 Marker Studies

Marker experiments were performed on Ni and amorphous Ni-P barriers overlayed with Sn only. Unheat treated samples were mounted obliquely to give a barrier/overlay interface distortion ratio of 1:10. Fig 38a shows three micrographs of samples with the amorphous Ni-P barrier prior to a diffusion anneal at 180, 170 and 150 °C respectively. At this stage it is seen that in all three samples crystallisation of the Ni-P barrier has commenced at preferential sites near the barrier/overlay interface. However, compound formation is not observed at this stage. In comparing with the corresponding micrographs for specimens heat treated for 33.67 h (Fig 38b) it can be seen that lateral spread of crystallites has occurred in the barrier at 180°C. However, at 150°C no further growth of the larger crystals is evident, but formation of a fairly thin and continuous layer of crystals at the interface is evident.

Fig 38a

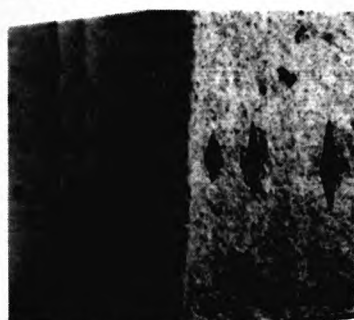


As mounted: Sn overlay on amorphous Ni-P barrier.

Fig 38b



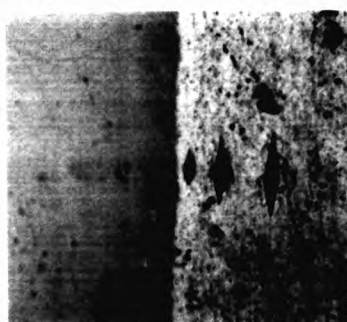
Heat Treatment 180°C/33h+40min



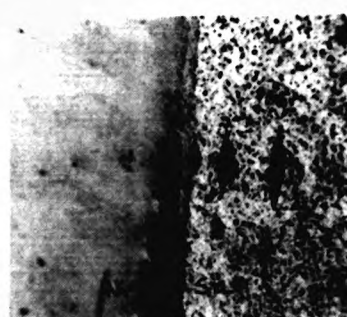
As mounted: Sn overlay on amorphous Ni-P barrier.



Heat Treatment 170°C/33h+40min

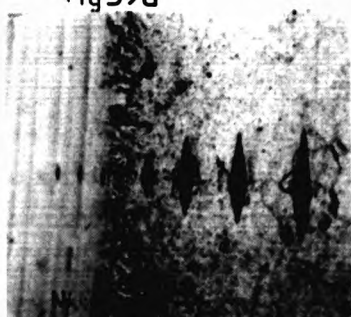


As mounted: Sn overlay on amorphous Ni-P barrier.



Heat Treatment 150°C/33h+40min

Fig 39a



As mounted: Sn overlay on
amorphous Ni barrier.

Fig 39b



Heat Treatment 180°C/33h+40min



As mounted: Sn overlay on
amorphous Ni barrier.



Heat Treatment 170°C/33h+40min



As mounted: Sn overlay on
amorphous Ni barrier.



Heat Treatment 150°C/33h+40min

Fig 38b also shows the onset of a continuous compound-like layer which grows in the Sn overlay. Compositional analysis of this layer revealed that it does not constitute a Ni-Sn compound but it is in fact a zone of intermixing. Figs 39a and 39b show micrographs of Ni barriered samples before and after heat treatment. In Fig 39a what appears to be extensive compound formation at the barrier/overlay interface is in fact the Ni barrier itself and is a manifestation of exaggerated ($\times 10$) surface roughness of the barrier; it gives the erroneous appearance of a highly irregular 'compound-like' growth front in the Sn overlay. The effect of the same heat treatment as that for the amorphous Ni-P barrier is clearly evident in Fig 39b where the zone of intermixing in the Sn overlay is found to be more extensive than that for the Ni-P barrier (Fig 38b). It was also found that Sn was diffusing in the barriers. But, unlike the diffusion of Ni in the overlay, no optical evidence of this was found. As a result, the original aim of the marker study which was to elucidate the dominant diffusant as well as the direction of growth front could not be achieved and therefore further marker studies were suspended.

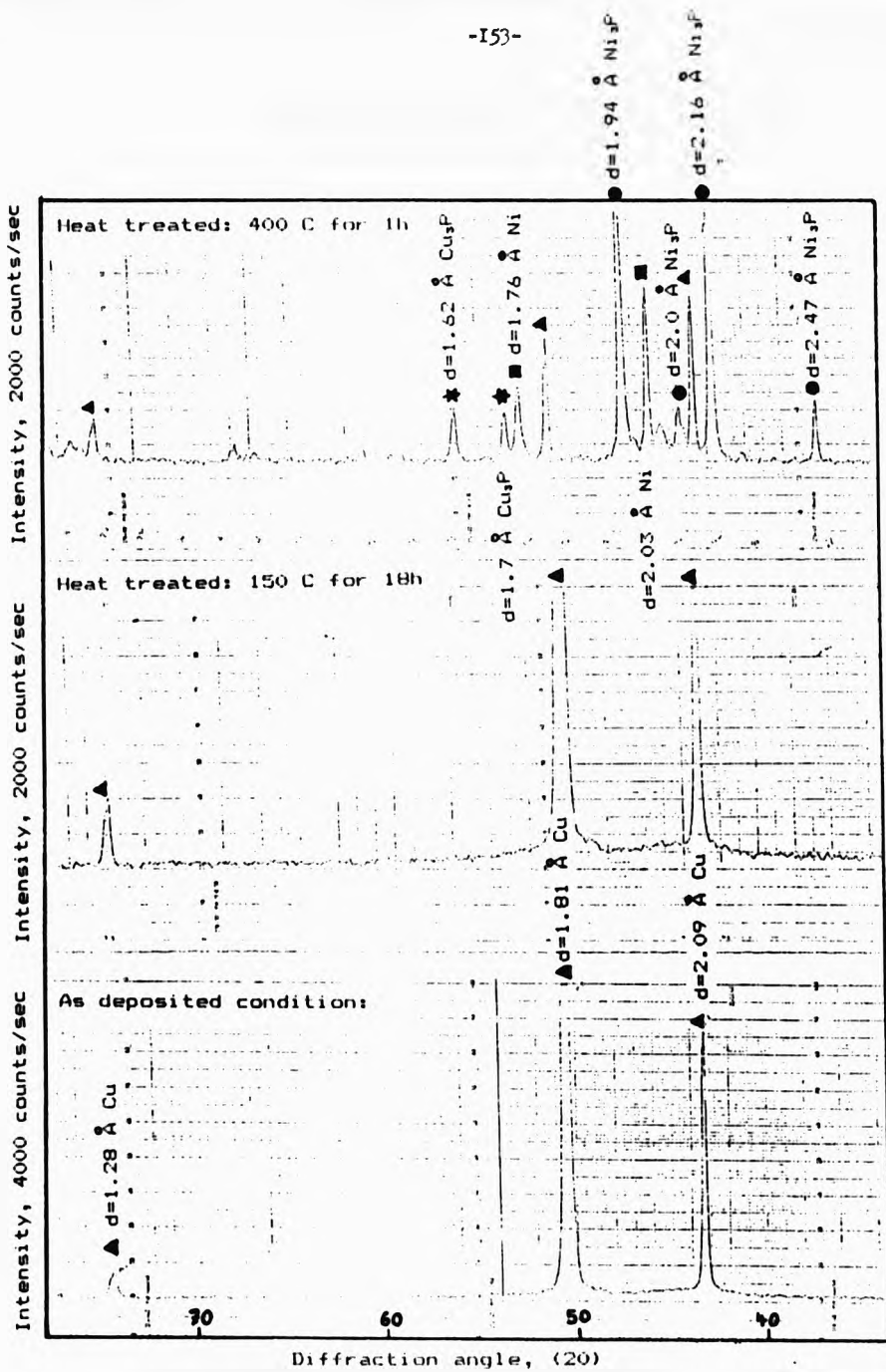


Fig40 X-Ray diffraction profiles of amorphous Ni-P barrier in - as deposited and heat treted condition.

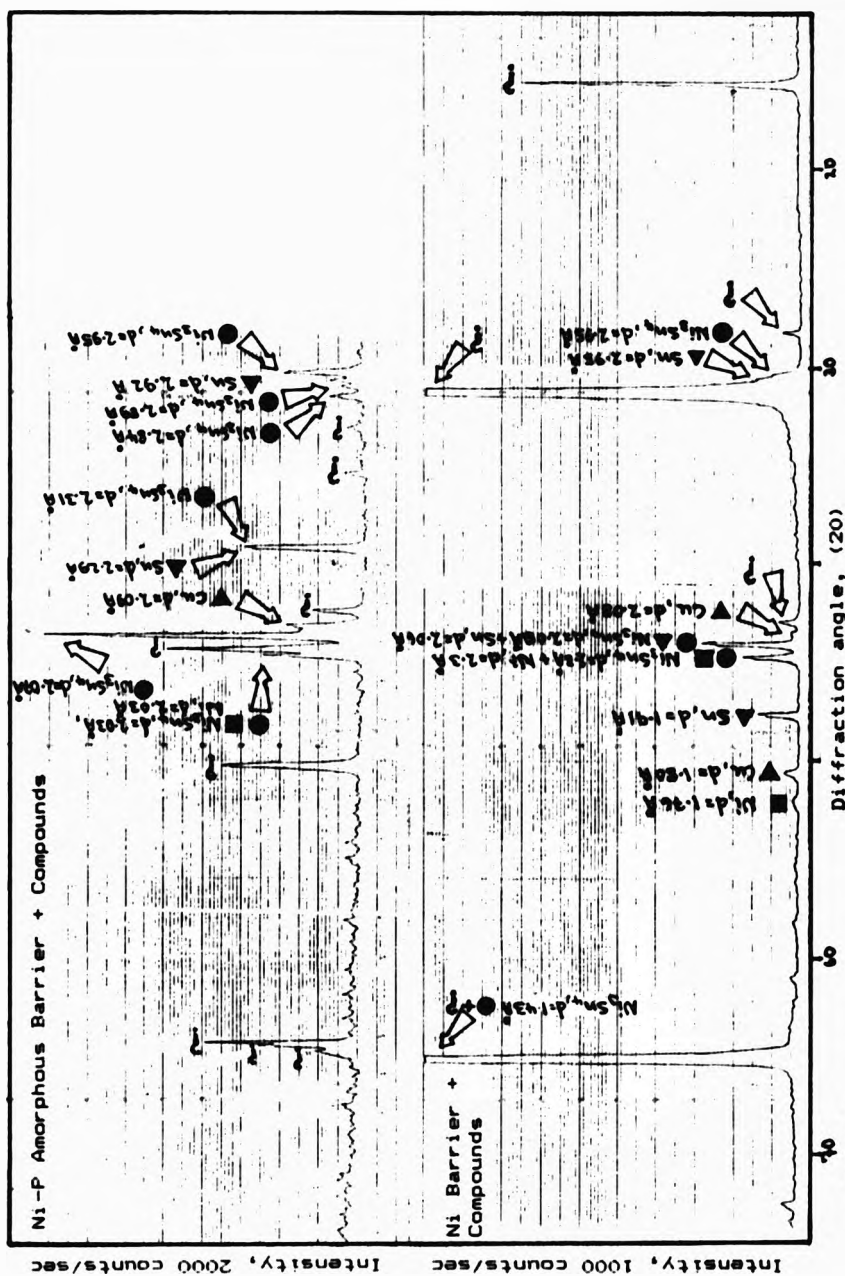


Fig41
X-Ray diffraction profiles of Ni-Sn intermetallic compounds after heat treatment of 2504 h at 150 °C.

4.4.3 Analysis of Ni and Amorphous Ni-P Diffusion Barriers

The analysis of Ni-based barriers together with Ni-Sn intermetallic compounds was performed by X-ray diffractometry and EDAX compositional point analysis across the layered samples.

4.4.3.1 X-Ray diffraction studies

Fig 40 shows three X-ray diffraction profiles of amorphous Ni-P barrier on a Cu substrate. In the as-deposited condition, Ni and Ni_3P peaks are absent and only those major peaks of the underlying Cu are present. The high level of the back-ground trace is a further indication of the amorphous nature of the Ni-P barrier in the as-deposited condition. A heat treatment of 18h at 150°C produces no change in the state of the deposit. However, a 1h heat treatment at 400°C leads to crystallisation of the amorphous Ni-P barrier into Ni and Ni_3P . A possible interaction with Cu in the form of Cu_3P is also evident.

Ni and Ni-P barriered samples heat treated for 2504h at 150°C after which the remaining Sn overlay was stirpped and x-ray diffraction profiles produced are shown in Fig 41. In both cases Cu, Ni, Sn and Ni_3Sn ,

compound were identified, though some peaks remain unidentified. In comparing the profile for the Ni-P barrier annealed for 2504h with that of crystallised Ni-P barrier after annealing for 1h at 400 °C (Fig 40), the absence of Ni₃P peaks confirms that the Ni-P barrier after 2504h of anneal does not undergo complete crystallisation. For the Ni barrier, however, the existence of the second compound NiSn₂ could not be confirmed from the X-ray profiles as the data is not cited in the ASTM card index [166]. Furthermore, for the identification of Ni₃Sn₄, a correlation with the d-spacing of peaks was obtained but not that of the intensity ratio given in the ASTM card index.

4.4.3.2 Compositional analysis of Ni/Sn and Ni-P/Sn diffusion couples

Figs 42 and 43 shows the EDAX compositional analysis across Ni and the Ni-P barrier/Sn overlay interface respectively. They are accompanied by SEM micrographs depicting the interface morphology and 'knoop' hardness 'markers' placed on either side of the original interface. As stated previously, (Sect.4.4.2) the Ni barrier/Sn overlay interface gives an impression of a dendritic type Ni-Sn compound, however, this is the manifestation of surface roughness of the Ni barrier. As for the Ni-P barrier/Sn overlay interface, partial

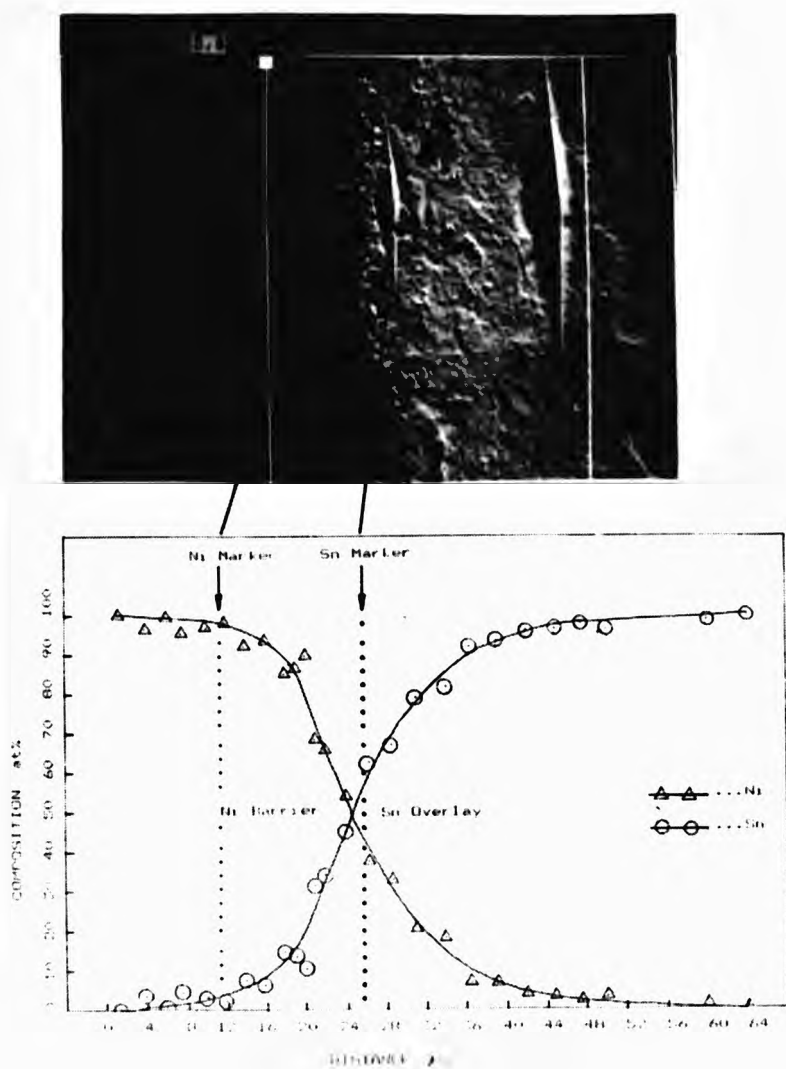


Fig42 Photomicrograph and concentration profiles of Ni barrier overlayed with Sn after 12h of heat treatment at 150°C.

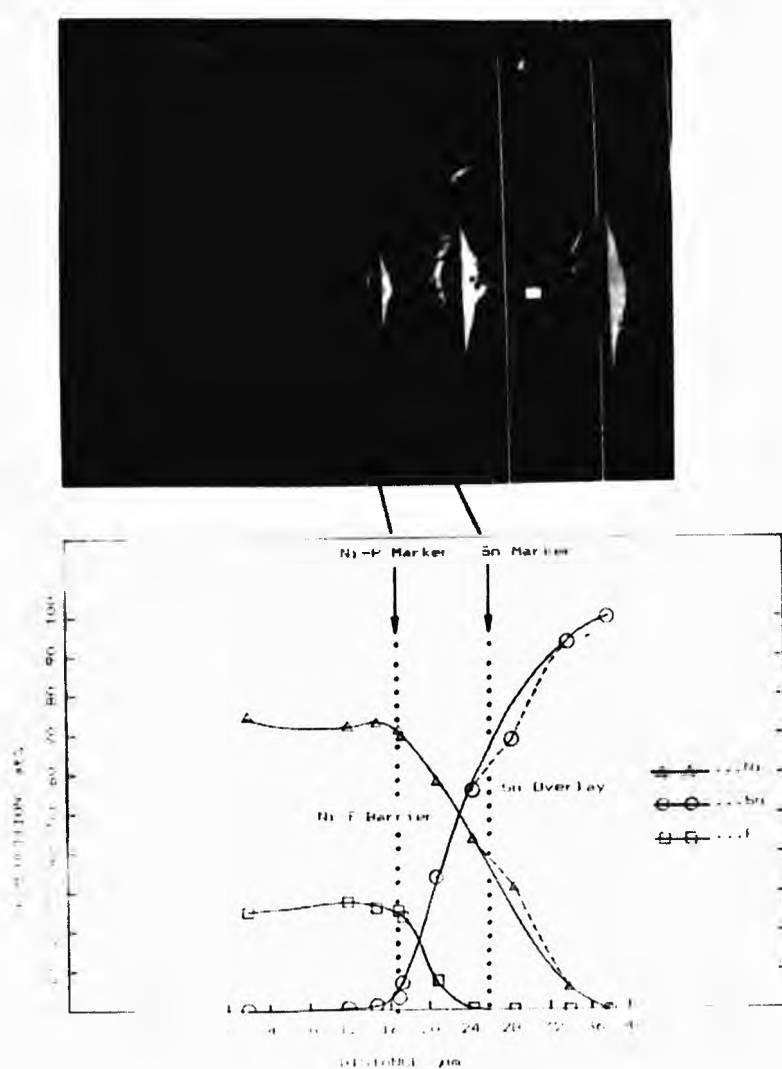


Fig43 Photomicrograph and concentration profiles of amorphous Ni-P barrier overlaid with Sn after 12h of heat treatment at 150°C.

crystallisation of the barrier at the interface occurs in the form of protrusions and a discontinuous layer.

From these Figs it is seen that a 17h heat treatment at 150°C is insufficient (within the limit of distance between the successive point of analysis) for the observation of Ni-Sn compounds, if any. For the Ni-P barrier, Fig 43, broken-lines shows a deflection in the Ni and Sn composition profiles. The solid-lines show the assumed profiles accounting for the limit of accuracy (1-2 at/o). A 17h heat treatment appears to be a prerequisite stage for the occurrence of Ni-Sn compounds, in which extensive interdiffusion takes place for the Ni barrier. Where the depth of penetration of Ni into the Sn overlay is greater than that of Sn into the Ni barrier. For the Ni-P barrier, (Fig 43) the extent of interdiffusion is less compared to the Ni/Sn system (Fig 42) although Ni is the dominant diffusant. P also diffuses to a limited extent in the Sn overlay and forms a region of ternary Ni-Sn-P solid solution enclosed by Ni-P and Sn markers; some of it precipitates within the barrier as seen from the slight (2 at/o) build-up in the P concentration profile.

Figs 44 and 45 shows micrographs and concentration profiles of the same samples as in Figs 42 and 43 after an extended heat treatment of 143h. In both systems the presence of Ni₃Sn₄ compound corresponding to 42-43

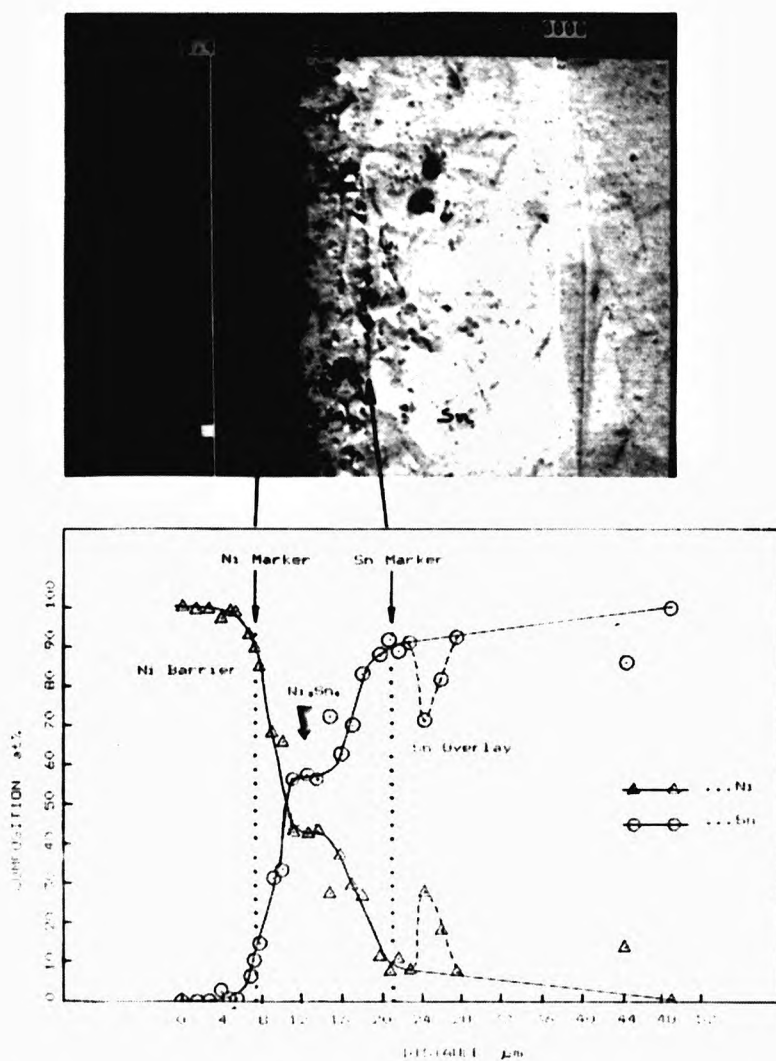


Fig44 Photomicrograph and concentration profiles of Ni barrier overlayed with Sn after 143h of heat treatment at 150°C.

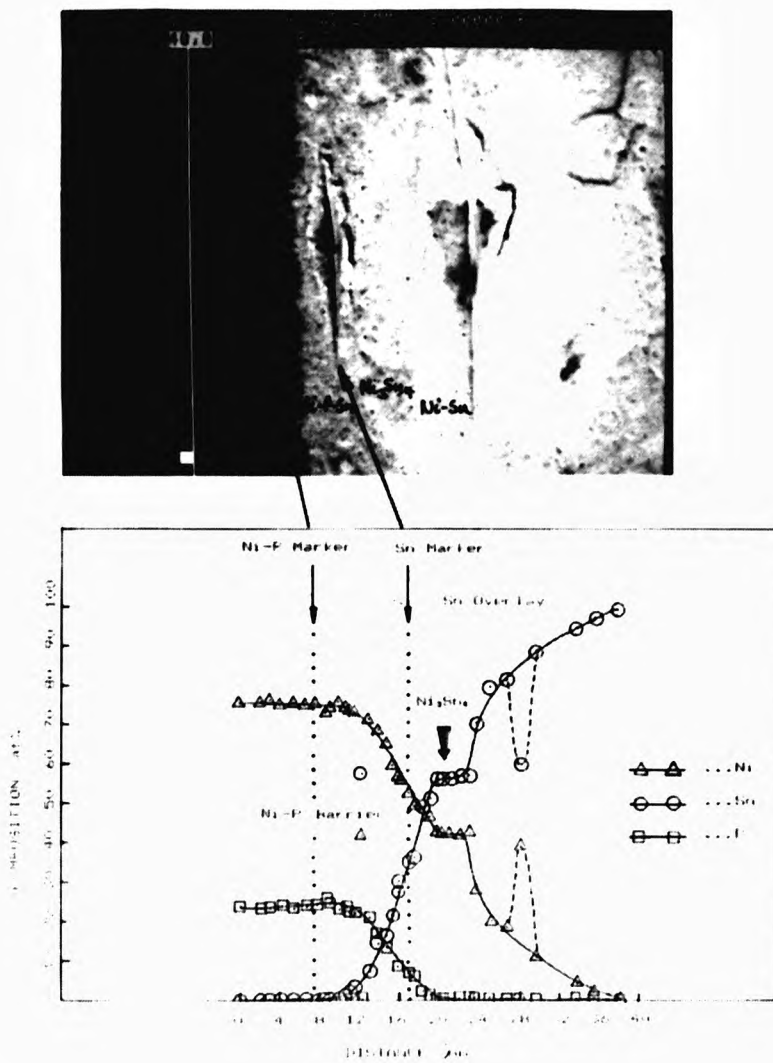


Fig45 Photomicrograph and concentration profiles of amorphous Ni-P barrier overlaid with Sn after 14.5h of heat treatment at 150°C.

at pct Ni was confirmed by good agreement with the published phase diagram (42.8-43.7 at/o Ni) [167]. Again, compositional discontinuities (broken line) are observed for Ni in the Sn overlay. For the Ni barrier (Fig 44), the peak of the discontinuity in the Ni profile occurs at 28 at/o Ni which is appx. 3 at/o in excess of the Ni_3Sn_4 compound. On the other hand, in the case of the Ni-P barrier, (Fig 45) the peak of Ni discontinuity corresponds to 40 at/o, which is appx. 2-3 at/o deficient in the composition of Ni_3Sn_4 compound. These compositional discontinuities may be explained in terms of excess Ni from Ni saturated Sn.

Photo-micrographs and compositional analysis of Ni and Ni-P barrier samples after 2504h of heat treatment at 150°C are presented in Figs 46 and 47. Fig 46 clearly indicates the presence of duplex Ni-Sn compounds on the Ni barrier. The average composition of Ni_3Sn_4 compound was found to be 40 at/o Ni which is deficient by 2-3 at/o [167] whereas that of Ni_3Sn_2 is 25 at/o Ni in good agreement with 24.5 at/o Ni found by Kay and Mackay [12]. Only the Ni_3Sn_4 compound was observed on the Ni-P barrier with average Ni content of 41.5 at/o though with a greater (40-43 at/o) range of homogeneity.

Once again, P accumulates in the Ni-P barrier by as much as 4 at/o. In both systems, the prolonged heat treatment induces the diffusion of Cu through the

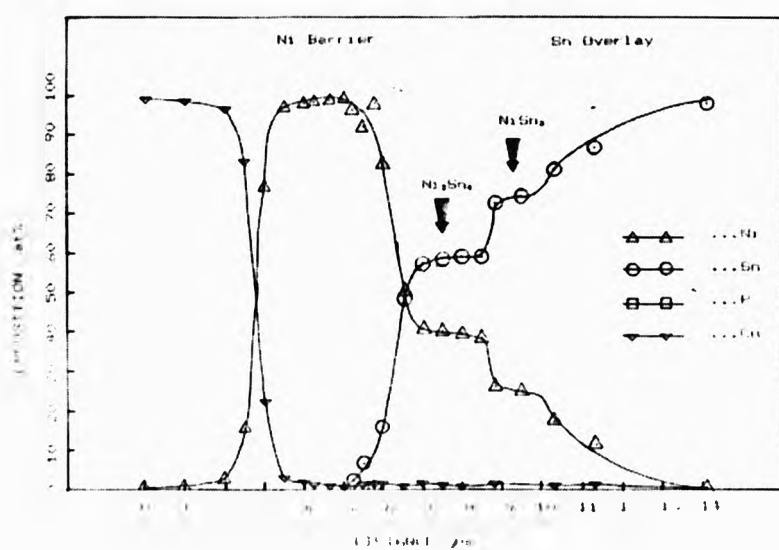


Fig46 Photomicrograph and concentration profiles of Ni barrier overlaid with Sn after 2504h of heat treatment at 150°C.

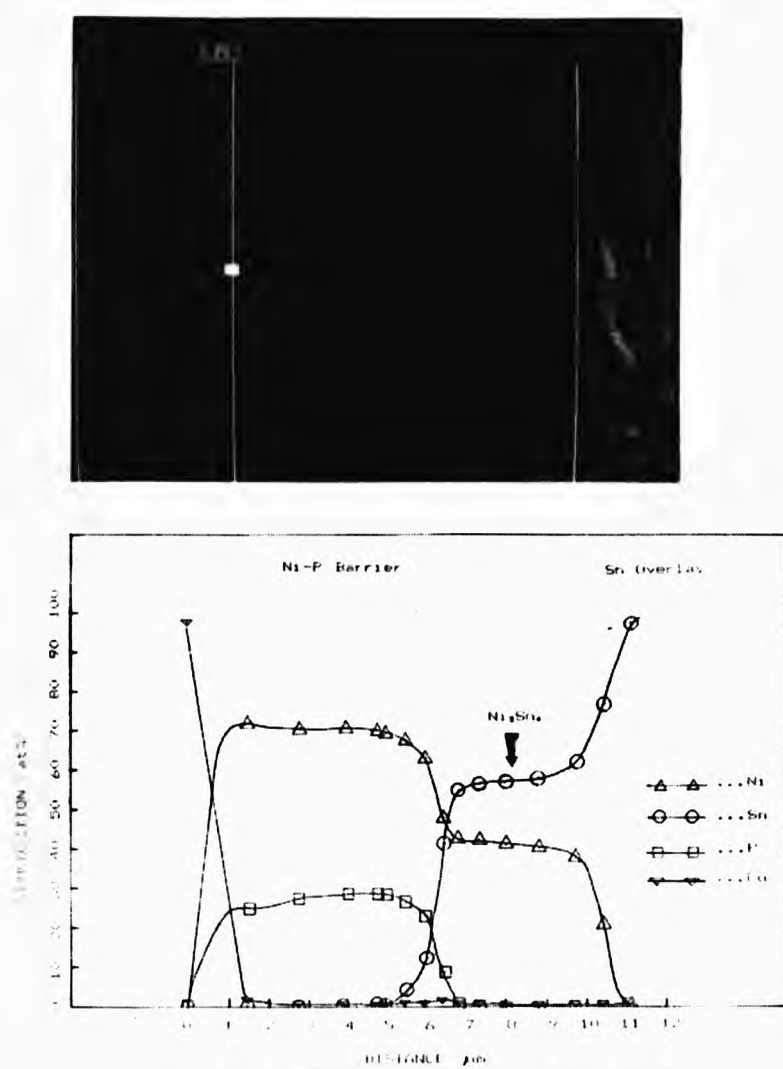


Fig 47 Photomicrograph and concentration profiles of amorphous Ni-P barrier overlaid with Sn after 2504h of heat treatment at 150 °C.

barrier and into the Sn overlay. Although the quantity of diffusing Cu is within the limit of detection, a greater amount was found to diffuse through the Ni barrier than the Ni-P barrier.

4.3.3 Compositional analysis of Ni-P/Pb-Sn diffusion couples

Figs 48 and 49 shows the EDAX compositional analysis of Ni-P barrier overlayed with Pb-20 wt/o Sn alloy after 33.67h and 236h anneal at 150 °C, respectively. It is seen (Fig 48) that for the shorter heat treatment(33.67h), Sn acquires a concentration gradient of appx 40 at/o at the barrier/overlay interface and that its diffusion into the barrier is considerably less compared to that in the Ni/Sn and Ni-P/Sn systems. In fact, similar conclusions can be drawn for the diffusion of Ni into the Sn overlay. It is of interest to note that a peak in the P profile is absent for the barrier/overlay interface. Also, P appears to penetrate the overlay to the same extent as that in the Ni-P/Sn system, however its average concentration is only appx 4 at/o. Furthermore, from the SEM photomicrograph no evidence of partial crystallisation of the barrier was found.

After extended annealing of 236h (Fig 49), Ni₃Sn₄ compound has grown between the barrier and overlay, its

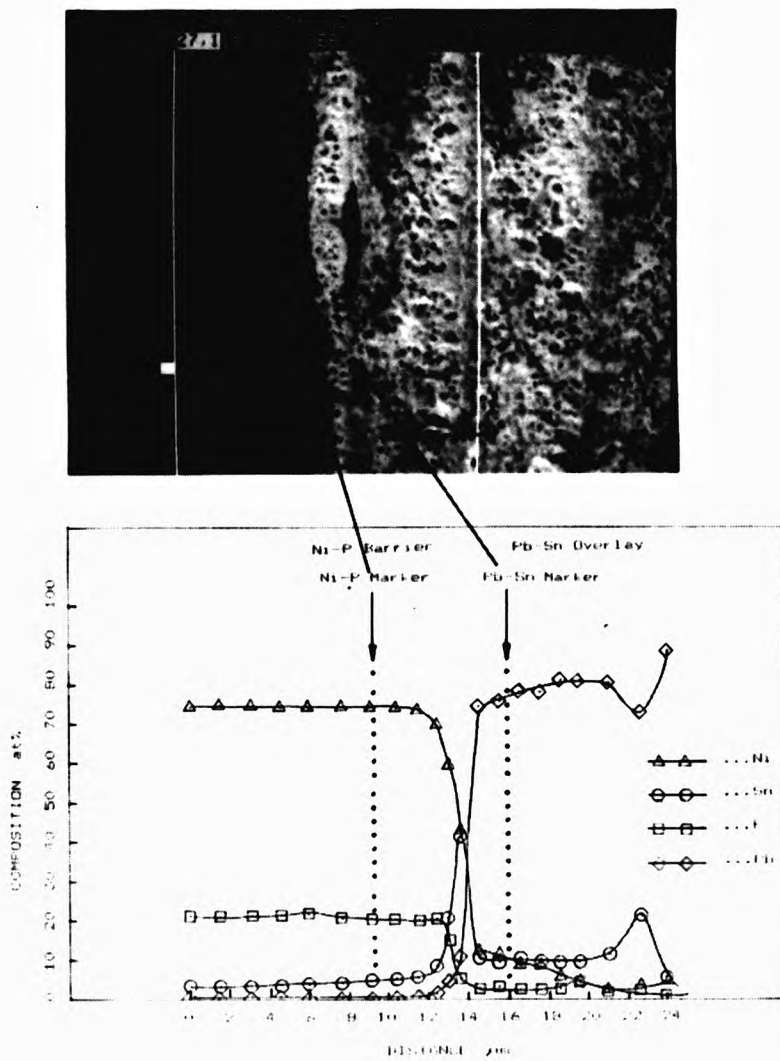


Fig48 Photomicrograph and concentration profiles of amorphous Ni-P barrier overlaid with Pb-20 wt pct Sn after 33+40min heat treatment at 150°C.

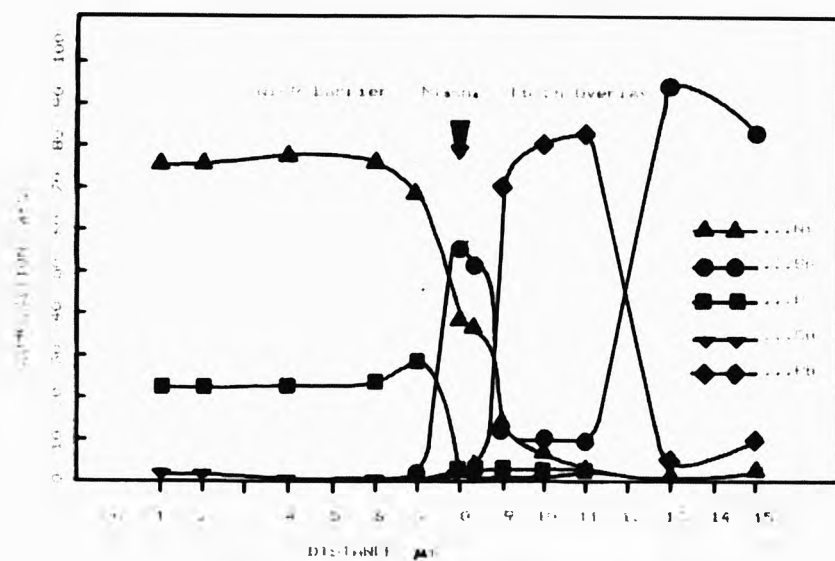


Fig 49 Effect of distance on the percentage of various components in the tissue. The tissue was sectioned and stained with H&E. The percentage of each component was determined by counting the number of cells in each category and dividing by the total number of cells. The results are shown in the graph above.

composition at the barrier/compound interface approximately corresponds to that given in the Ni-Sn phase diagram, but deviates by 5 at/o at the compound/overlay interface. It seems that Ni_3Sn_4 compound grows out of and around the Pb-rich phase. The build up of rejected P is also evident in the barrier. From the SEM photomicrograph the partial crystallisation of the barrier is not evident.

4.4.4 Growth Kinetics of Ni-Sn Compounds

The growth rates of the Ni_3Sn_4 compound on an amorphous Ni-P barrier and Ni_3Sn_4 + NiSn_3 compounds on a Ni barrier are shown in Fig 50. The average thickness of these compound layers were determined using a deep etching technique which relied on a preferential attack of Ni and Sn in order to highlight the compounds for optical measurement. Thus, it is possible that the measurement of compound thickness may have incurred constant errors. However, Fig 50 demonstrates the advantage of the Ni-P barrier over the Ni barrier in restricting the average compound thickness to appx. one third for the same duration of heat treatment.

The growth rates shown in Fig 50 are plotted on parabolic axes in Fig 51. The broken lines show that for the Ni barrier the early portion of the growth is non-parabolic whilst the later may be parabolic.

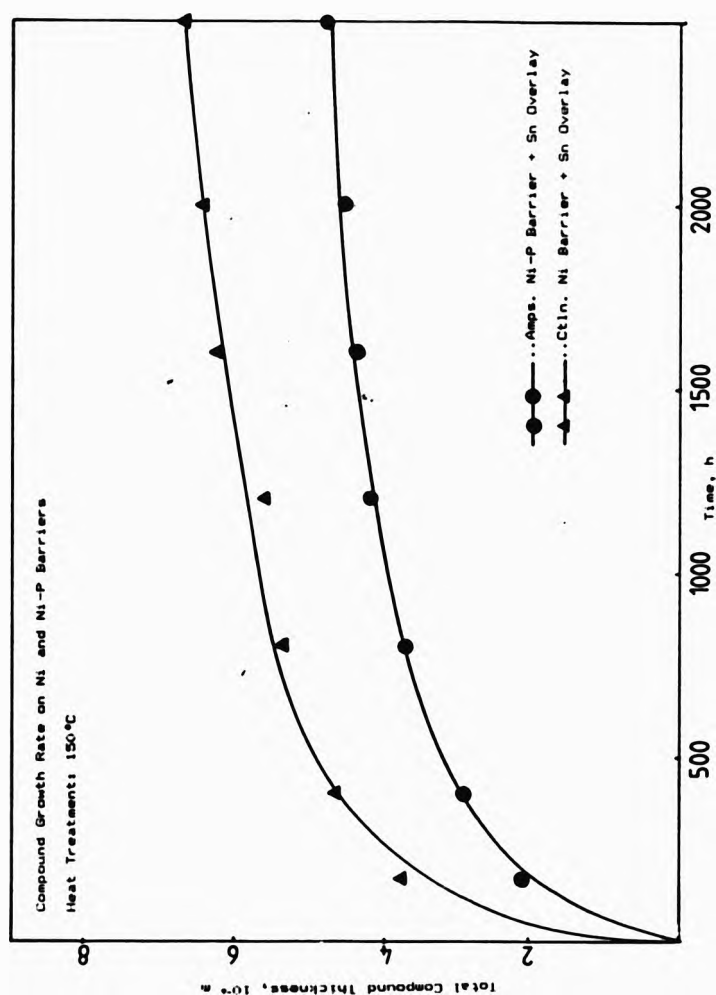


Fig50 Total compound growth rate on Ni (Ni_3Sn_2 + NiSn_3) and amorphous Ni-P (Ni_3Sn_2) barriers heat treated at 150 °C.

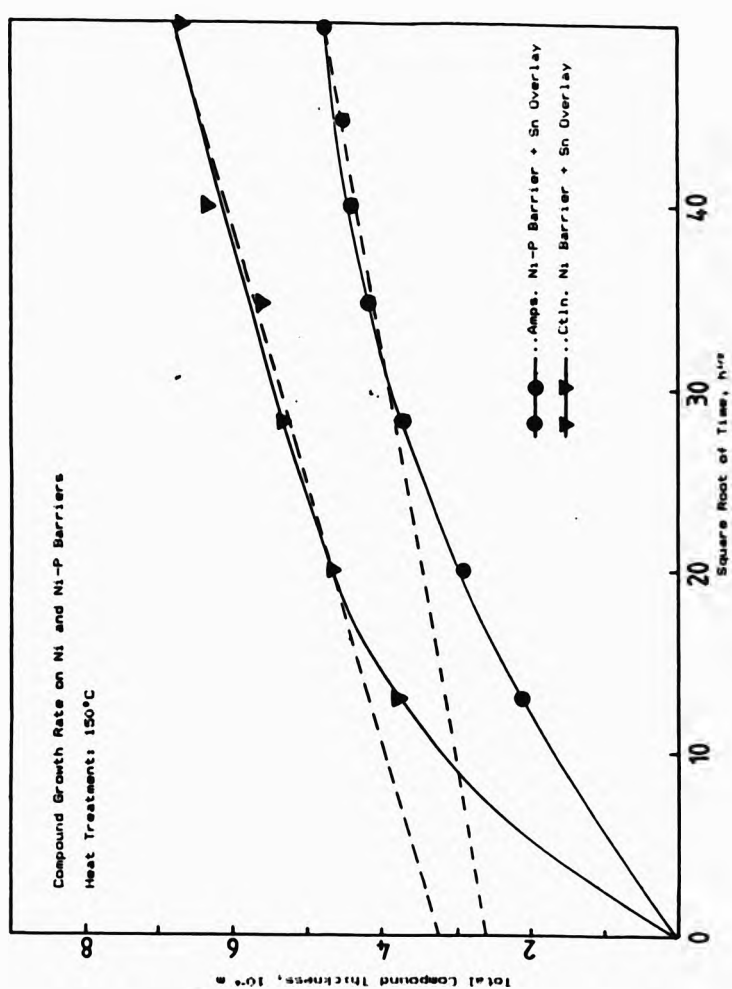


Fig 51 Parabolic plot of total compound growth rate on Ni and amorphous Ni-P barriers.

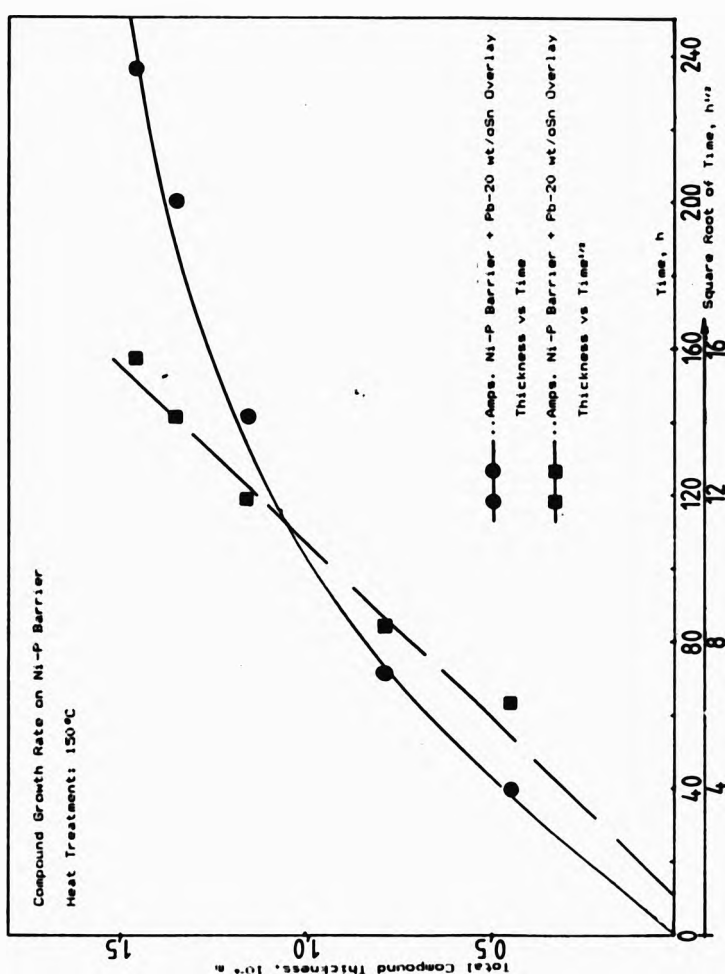


Fig52 Linear and parabolic plots of Ni₃Sn₄ compound growth rate on amorphous Ni-P barrier with Pb-20wt/pct Sn overlay, heat treated at 150 °C.

Similar considerations apply for the growth rates from the Ni-P barrier, but the on-set of parabolic growth occurs at a later stage.

Fig 52 shows linear and parabolic growth rates from Ni-P barriered samples with Pb-20 wt/o Sn overlay. The rate of growth for the Ni-P/Pb-Sn system is lower than that of the Ni-P/Sn and was found to be parabolic. The intercept of the broken line on the \sqrt{t} time axis suggests an incubation period of approx 1h whereas that for the Ni-P/Sn system (Fig 38) a growth of 2.5 μm at zero time is indicated assuming parabolic growth.

4.5 Determination of interdiffusion coefficients in intermetallic compounds

It was shown in the literature review that there are two methods which are amenable to the determination of interdiffusion coefficients in intermetallic compounds. These are, the Wagner's and the Boltzmann-Matano-Haumann method, of which the former was used since the latter method also requires the integrals represented by the shaded areas in Figs 53a and 53b to be evaluated.

The penetration profiles shown in Figs 53a and 53b are representative of the Sn concentration after annealing the Ni-P/Sn and Ni/Sn diffusion couples for 2504h at 150 °C. In these figures, the first subscript

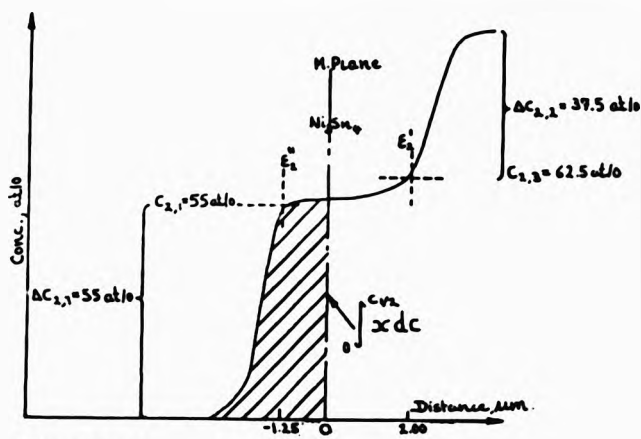


Fig 53a

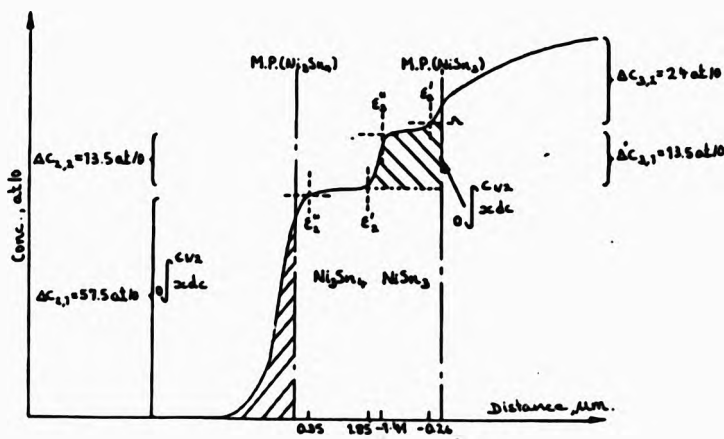


Fig 53b

Concentration penetration profiles illustrating the application of Boltzmann-Matano-Heuman and Wagners solution for the determination of D in intermetallic compounds. (a) Ni-Sn compound on amorphous Ni-P barrier. (b) Ni-Sn compounds on Ni barrier.

2 to the ΔC term refers to Ni_3Sn_4 compound, whereas the first subscript 3 refers to NiSn_3 . The second subscripts 1 and 2 refers to the lower and higher concentration gaps respectively.

Substitution of the values for relative concentration gaps as well as the respective distance of the compound boundaries from the Matano plane in the Wagner formula (Eq 18) leads to the determination of the interdiffusion coefficient.

$$\frac{\Delta C_{2,1}}{\Delta C_{2,2}} \times \frac{C'}{C''} = \exp \left[\frac{C' - C''}{4Dt} \right] \quad (18)$$

It must be emphasised that there are numerous sources of errors. Generally, these stem from the accuracy of the determination of concentration profiles and estimation of the Matano plane. The theory also assumes linear concentration distribution within the compound and that it grows from single phase parent materials. Thus, the values of interdiffusion coefficients presented below are likely to incorporate errors.

The values of interdiffusion coefficients for the Ni_3Sn_4 compounds from both Ni-P/Sn and Ni/Sn systems were found to be in good agreement. These were, 1.51×10^{-11} and $1.93 \times 10^{-11} \text{ cm}^2\text{s}^{-1}$ respectively. That for the NiSn_3 compound was found to be one order of magnitude lower, i.e. $2.86 \times 10^{-12} \text{ cm}^2\text{s}^{-1}$.

5.0 DISCUSSION

5.1 Introduction

It has been demonstrated in the foregoing results that the claims made in a previous investigation on the ability of Cu-P and Cu-B diffusion barriers to prevent the nucleation of Cu-Sn compounds are unfounded. Indeed, it is shown that by critical consideration of the literature on diffusion phenomena and impurity segregation effects that the postulation of such barriers for bearing application would have been futile from the onset.

Consequently, a need to identify more efficient diffusion barriers was recognised. Amorphous diffusion barriers in the field of semi-conducting device fabrication has recently acquired greater application, but as yet remains unreported for bearing applications where the primary aim is not only to minimise interdiffusion but also to curtail the extent of compound formation.

Results on the application of amorphous Ni-P barriers to Sn overlay has demonstrated that Ni-Sn compound formation may be reduced by up to one third compared to the Ni crystalline barrier. Furthermore, the

conventional Ni crystalline barrier on Sn leads to duplex compound formation whereas the amorphous barrier leads to single compound formation. The interdiffusion and in particular the interaction between compound forming amorphous and crystalline couples remains one of the least understood subjects. Nevertheless, the collective information in the literature and the results of this thesis are used to describe a model for the phase suppression of NiSn_3 compound in the amorphous Ni-P/Sn couples. The results of the preliminary investigation on the interaction between amorphous Ni-P barrier and Pb-Sn overlay are complex and too few to fully unravel its mechanistic aspects. Even so, an attempt is made to include this system in the discussion.

Finally, a section is presented which relates to the technological significance of the experimental results obtained.

5.2 Investigation of Cu-P and Cu-B barriers

In essence this early part of the project became a repetition of previous work performed by Kalubowila [4,5,6]. In part, this constituted investigative work to elucidate experimental factors which may have been responsible for the failure of barriers on actual bearing shells. At the same time, efforts were expended in the development of alternative barriers and overlays based on previous reports that these barriers suppress Cu-Sn compound formation altogether.

Examination of Cu-P barriered bearings after heat treatment showed that Cu_3Sn compound formation persisted. This was thought to be due to preferential diffusion of P in the Cu-Pb bearing substrate and not in the overlay. This phenomena was then recognised as a possible source for the failure of this barrier since Kalubowila [4] postulates its success on the preferential diffusion of P in the Pb-Sn overlay which binds with vacancies in the overlay and thereby immobilises the diffusion of Sn. Hence, the need to optimise the barrier deposition processes on actual bearings was recognised in order that the P content and its distribution in the barrier and overlay be maximised, whilst at the same time the inherent porosity (due to the low metal content of the plating bath) be

minimised. Despite this, the compound formation was not alleviated even though the P content of the barrier and overlay were enhanced (Fig 15, 16 and 17). Furthermore, barriers were also investigated on plane Cu sheet substrates (as in [4]) in order to eliminate the effects of any prevailing electrochemical differences during the barrier deposition on actual bearings.

Comparison of compound growth rates on plane substrates (Fig 26 to 30) in the presence of both modified and unmodified Cu-P barriers led to the revelation that the Cu-P barrier and therefore, P does not impart any beneficial effect on compound growth rate, let alone prevent its nucleation. In fact, only by reducing the Sn content of the overlay was there any notable decrease in compound growth rate. Similar conclusions can be drawn for the interdiffusivities.

The compound growth rates of predominantly Cu_3Sn are not untypical of those observed by Unsworth and Mackay [13] who also found the initial stage of growth to be reaction controlled with almost linear growth followed by transition to parabolic control. They [13] too reported a decrease in the growth rate by reducing the Sn content of the overlay. Finally, the predominance of Cu_3Sn compound at temperatures above 60-100 °C is also in agreement with Tu and Rosenbug [64] who investigated Cu/Sn diffusion couples. Thus, if P imparts any

influence at all let alone prevent the growth of Cu-Sn compounds it would have been evident from the study of growth rates. Clearly then the ultimate possibility of there being no or very little Sn in the samples prepared in the previous [4] investigation emerged as a strong contender.

Indeed, quantitative analysis of the Cu-P barriered samples heat treated for 960h at 140°C taken from previous work [4] (Figs 22, 23 and 24) shows an average Sn content in the overlay to be less than 0.5 wt/o, whereas in Cu-P barriered bearings similarly heat treated most of the 10 wt/o Sn had reacted to form compounds (Figs 18 to 21 and Tab. 11). Qualitative analysis of Cu-B barriered samples also taken from the previous study led to the same conclusions.

It is important to briefly discuss the origins of the erroneous conclusions reported in the previous investigation;

i) Quantitative analysis of the Sn content of the overlay was not performed. It was inherently assumed from qualitative micro-probe analysis without ZAF correction or taking into account the sensitivity scale that a Sn profile from a sample produced during the earlier course of the investigation was automatically representative of the Sn content in the overlaid

Sample	Cu/Sn intermetallic	Average Sn content in Pb overlay, excluding intermetallics, %w	Average P content in Pb overlay, %w
F1	Yes	0.23	0.01
G1	"	1.0	0.005
H1	"	0.09	0.01
I1	"	0.55	0.01
1	No	0.2	0.01
2	"	0.4	0.005
3	"	0.15	0.004

Minimum detectable levels P \approx 0.02%w
Sn \approx 0.03%w

Table 11. Summary of observations from quantitative profiles of Cu-Pb barriered samples. Samples F1 - I1 were produced and evaluated in this investigation whereas, samples 1, 2 and 3 were produced and annealed by previous investigator [4].

samples subsequently prepared.

ii) The stannous Sn^{2+} ions in the Pb-Sn plating solution progressively oxidises to stannic ions. The concentration of stannous ions in the solution dictates the Sn content of the overlay during its deposition. It seems that the previous investigator was unaware of these facts.

Finally, a brief discussion on the mechanistic aspects of the Cu-P and Cu-B barriers is warranted. It is shown in this investigation that Cu-P and Cu-B barriers do not impart any influence on the nucleation and the growth of Cu-Sn compounds. The postulation that P and B impurities plays a beneficial role in retarding the diffusion of Sn is incongruous. Where such effects are reported [153], these are only valid for the very dilute alloys, and not for concentrated alloys with 10 w/o solute. It may be that P and B segregates at grain boundaries in the Pb-Sn overlay and if so it may retard grain boundary diffusion of Sn. However, at the prevailing heat treatment temperature of 150 °C lattice diffusion of Sn dominates and not grain boundary diffusion. Alternatively, the nucleation and growth of compounds may be perturbed if P or B strongly interacts with Cu or segregates at the barrier/overlay interface. This is not the case since P and B diffuses readily out of the barrier and into the substrate and

the overlay. Thus the Cu-P and Cu-B barriers were mis-conceived from the onset, regardless of their mode of operation.

5.3 On the nucleation and growth of Ni-Sn compounds:

Crystalline Ni vs amorphous Ni-P barrier.

In the present study of bulk diffusion couples as opposed to thin film studies, little information exists on the criterion for the nucleation of the first compound. However, it is generally accepted that the compound which exhibits largest interdiffusivity (D) nucleates first. Recently, Bene' [154] has proposed a model for solid-state silicide nucleation which also accounts for the rate of free energy (ΔG) degradation and, therefore, assigns $-D\Delta G$ product as the governing parameter which enables the selection of a particular compound among others as the one to nucleate first. Bene' [155] has also formulated first nucleation rules for low temperature metal-metal thin film systems based on the review of existing literature. In the majority of such systems the first phase to nucleate is the one adjacent to the low temperature eutectic in the binary phase diagram.

In thin evaporated film couples of Ni and Sn, Ni_3Sn_4 has been reported as the first compound to

nucleate at room temperature [156], yet other authors [157] found NiSn compound. From the study of thin electroplated Sn film on rolled Ni sheet, NiSn [158] and Ni₃Sn₄ [159] compounds were reported whereas, NiSn₃ was found [12,159] in the study of thick film couples where both Ni and Sn films were produced by electrodeposition.

It must be emphasised that the aforementioned studies relates to the initial interaction between Ni and Sn at room temperature and that the first compound to nucleate also depends on the method of fabrication which dictates the defect concentration as well as the mode of diffusional transport.

The present investigation is concerned with the study of bulk diffusion compound(s) in which an incubation period in excess of 17h was observed resulting in an interphase consisting of Ni and Sn and Ni, Sn and P solid solutions for the Ni and Ni-P barriers respectively. It is most likely that as a precursor to this interphase formation, that during the course of Sn deposition on the barriers and in the initial stages of the heat treatment a first interface layer develops, perhaps a few atomic layers thick consisting of an intermetallic compound with the lowest free energy. However, as the heat treatment progresses, the need to maximise the rate of energy degradation ($-\Delta G$)

leads to extensive intermixing (ΔH for Ni-Sn is -ve) and the growth of a bulk interphase or solid solution. Thereafter, at a critical composition an opportunity may present itself for the nucleation and growth of the first bulk compound (Ni_3Sn_4) which not only has a larger $-\Delta G$ compared to the mixed state but the rate of energy degradation is also expected to be greater during its growth.

The situation for the amorphous Ni-P/ crystalline Sn system is more complex and not directly comparable with the above description of the Ni/Sn system. Since an amorphous structure is highly energetic in comparison with a crystalline one a competition is expected to be encountered between the rates of energy degradation due to crystallisation of the barrier and that due to intermixing. Self diffusion in most amorphous alloys is known to be greater than in its crystalline equivalent but interdiffusion is known to be much less. Thus, a need to maximise energy degradation by intermixing requires structural changes in the amorphous barrier. Amorphous Ni-P alloys are known to crystallise by precipitation of Ni-rich phases surrounded by Ni_3P matrix [164]. The crystallisation temperature of a Ni-P alloy increases with P content up to 20 at/o and decreases with P content greater than 25 at/o [164]. Furthermore, the effect of ternary alloying in amorphous/crystalline diffusion couples is also known to

reduce the crystallisation temperature [112] depending on the nature of the third alloying element.

By consideration of these factors, it is highly probable that in order to sustain intermixing crystallisation of the Ni-P barrier must take place. The key question is whether the crystallisation of the barrier precedes intermixing. In this investigation partial crystallisation was found to occur prior to diffusion annealing (Fig 36a) and, thereafter, interalloying was observed after 17h of heat treatment. Thus, crystallisation precedes intermixing and as a result, (Fig 43) interphase formation can proceed at a greater rate after crystallisation since the newly formed grain boundaries can then act as fast diffusion paths.

In comparison with a crystalline Ni barrier, the extent of interphase development is much less since the partial crystallisation of the Ni-P barrier at the Sn interface leads to a 'self limiting' system ie, Ni is effectively 'locked up' as precipitated pools; some Ni is also bound in the form of Ni₃P matrix surrounding the Ni pools and only the excess is available for interphase and/or compound formation. Finally, a situation similar to the crystalline Ni/Sn system is acquired, where the rate of energy degradation by continued growth of the interphase and

crystallisation of the barrier would be less than that due to nucleation and growth of the first (Ni_3Sn_4) bulk compound.

5.3.1 The growth of Ni-Sn compounds.

In the preceding section it was stated that Ni_3Sn_4 was the first bulk compound observed in both the Ni-P/Sn and the Ni/Sn systems at 150 °C. However, for the Ni barrier NiSn_2 also forms as a second compound. From the x-ray diffraction profiles the existence of NiSn_2 could not be elucidated as the relevant data is not listed in the ASTM powder diffraction data files. Neither is the compound predicted in the Ni-Sn phase diagram (Fig 54). But, the existence of such compound is cited [12, 160] and is unique to electroplated structures. Therefore, its identification is based on compositional analysis only. However, information concerning the rate of growth of NiSn_2 is not reported.

The crystal structure and the morphology of the compounds that form depend on the type of electrolytic processes used for the preparation of diffusion couples and the time and temperature of diffusion. For the Ni barrier, a continuous layer of Ni_3Sn_4 with columnar type grains forms at the Ni interface whereas a discontinuous layer of NiSn_2 with plate-like structure

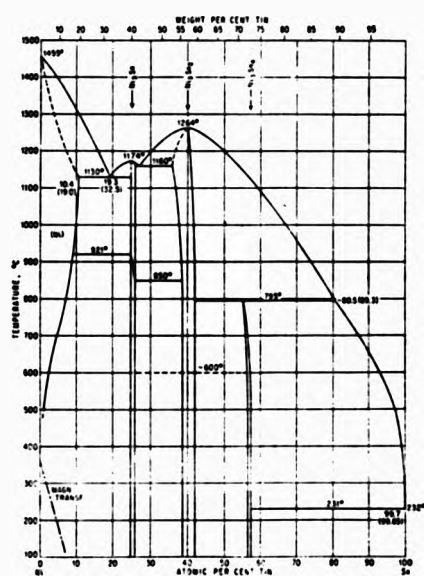
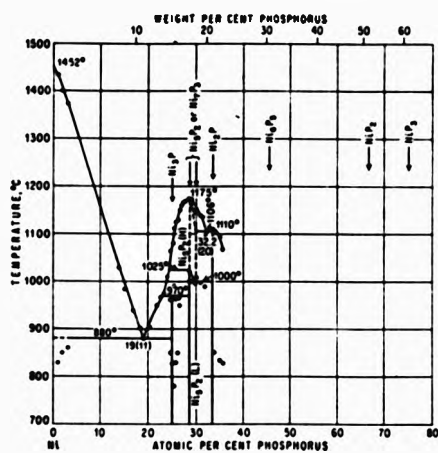


Fig54 Ni-P and Ni-Sn equilibrium diagrams

develops at the Sn interface (Fig 34b and 36). By contrast, Ni_3Sn_4 compound formed on a Ni-P barrier consists of much larger grains with a highly irregular compound/Sn interface. The reason for the difference in the morphology of Ni_3Sn_4 compounds growing from Ni and Ni-P barriers may be associated with the difference in the densities of the respective barrier layers. The densities of Sn, Ni_3Sn_4 , and Ni are 7.29, 8.42, and 8.90 respectively, and increases consistently from Sn to Ni. Therefore, Ni_3Sn_4 growing on a Ni barrier is likely to be under compression whereas the density of the Ni-P barrier is likely to be much lower than the Ni_3Sn_4 ; thus, the Ni_3Sn_4 compound is likely to experience tensile stress. In the cases where a compound experiences a large tensile stress the observation of intergranular pores within the compound layer have been reported. This point cannot be verified since detailed metallographic examination was not possible.

Alternatively, it may be that grain boundary diffusion within the compound makes a significant contribution to its growth which may lead to the irregular compound growth front. Again, lack of experimental evidence to confirm this effect implies that it only remains as one of the possibilities.

The intermetallic compound Ni_3Sn_4 is the only phase formed on amorphous Ni-P barrier whereas both Ni_3Sn_4

and NiSn_3 compounds are formed on crystalline Ni barriers. Parabolic growth rates of these compounds are shown in Fig 51 where the growth on a Ni barrier is the sum total of Ni_3Sn_4 and NiSn_3 . Comparing the two, the growth rate on the Ni barrier is appx. 1.5 times faster than that on a Ni-P barrier. The combined growth of duplex Ni-Sn compounds follows the parabolic kinetic rate law reasonably well (broken line in Fig 51) between 400 and 2504h of heat treatment. However, during the first 100h it follows an almost linear relationship. Bearing in mind that the exact time for nucleation and growth of the second compound (NiSn_3) is not known, it is reasonable to assume that this must occur at around 400h of heat treatment, beyond which both compounds are growing parabolically and are, therefore, under diffusion control. Below 400h of heat treatment, the growth of Ni_3Sn_4 compound follows a near-linear relationship (Fig 50) and is therefore growing under reaction control. Kay and Mackay [12] and Tomlinson and Rhodes [161] have reported parabolic growth of Ni_3Sn_4 compound on electroplated Ni and polished Ni sheet after heat treatment at 170 and 180°C respectively. In both cases the compound growth rate was found to pass through the origin. However, the growth of Ni_3Sn_4 on electroless Ni deposits with appx 17 at/o P was also found to be parabolic [161] with a thickness of 1 μm at zero time and was attributed to surface roughness. In the present study the initial rapid growth under

reaction control can be attributed to the same effect (see Figs 39a and 39b). However, if parabolic growth is assumed throughout the course of heat treatment then a compound thickness of $3.25 \mu\text{m}$ results at zero time, clearly this cannot be the case since an incubation period between 17 and 143h was observed.

In contrast to the initially linear growth reverting to parabolic form after 400h for the Ni barrier, the growth of Ni_3Sn_4 on the Ni-P barrier assumes parabolic form after 900h of heat treatment. Prior to this, the growth is non-parabolic and which cannot be described in simple terms. The non-parabolic nature of compound growth rates is often attributed to some intervening metallurgical factors. For example, non-planar starting interface of the diffusion couple, ie surface roughness effects, dominating grain boundary diffusion process or other restrictive processes such as impurity segregation and oxidation of one of the starting interfaces have all been proposed. The surface roughness effects can be ruled out for the present work since the surface of the Ni-P barrier in the as-deposited condition is smooth and bright. The most likely explanation is that the compound growth relies on grain boundary diffusion since the lattice diffusion of Ni from the partially crystallised barrier is restricted. Therefore, grain boundary diffusion dominates.

Finally, the incubation period observed prior to the growth of compounds is not reported for the Ni-Sn system in the literature. The fact that the incubation period was found for both the Ni and Ni-P barriers implies that the cause is inherent in the fabrication process, in which case either impurities are co-deposited or the barrier surface is oxidised during preparation.

5.3.2 Growth of Ni-Sn compound on amorphous Ni-P barrier overlaid with Pb-20 w/o Sn alloy.

In the given time constraint it has not been possible to study the Ni-P/Pb-Sn system in detail. Despite this, the observations made are sufficiently significant to warrant a brief discussion.

In the early stage of heat treatment significant penetration of Sn into the barrier was observed. At the same time both P and Ni were found to penetrate the overlay. The extent of interdiffusion is markedly less (Fig 48) compared to the Ni-P/Sn system heat treated at the same temperature for half the time (Fig 43). Furthermore, the barrier remains amorphous since crystallites in the vicinity of the interface were not observed. This implies that interdiffusion is limited as long as the barrier remains integral. However, precipitation of excess Sn from the Pb-Sn overlay leads

to a concentration gradient (40 at/o) at the barrier/overlay interface which does not correspond to any of the Ni-Sn compounds. In comparison with Ni-P/Sn system, the extent of Ni diffusion in the overlay is restricted whereas, the diffusion of Sn in the overlay itself remains unperturbed.

After further heat treatment of up to 236h (Fig 49), the onset of barrier crystallisation is evidenced by the build up of P (from 23 to 29 at/o) at the barrier/compound interface. This is substantiated by Pittermann and Ripper [164] who observed a decrease in the crystallisation temperature with the P content greater than 26 at/o. However, this factor alone does not explain the cause of Ni-P crystallisation. It may be that during the initial heat treatment, the average concentration (20 at/o) of diffusing Sn at the barrier/overlay interface is insufficient for the onset of crystallisation. During the ensuing heat treatment, this Sn content is likely to rise to the extent that the barrier begins to crystallise. Thereafter, the increase in the P content may provide further impetus for crystallisation. Even so, the increase in P results in part from its inability to diffuse in Sn as found in the Ni-P/Sn system and also from its inability to diffuse in Ni_3Sn_4 compound.

In both Ni-P/Sn and Ni-P/Pb-Sn systems, diffusion of

Sn in the barrier may be responsible for the onset of crystallisation and this stage precedes the nucleation and growth of Ni_3Sn_4 compound. The pertinent question is to what extent the partial crystallisation of the barrier influences the growth of Ni_3Sn_4 compound? The answer might be that, compared to the Ni barrier, a partially crystallised Ni-P barrier can still limit the supply of Ni. But in comparison with an amorphous barrier, a partially crystallised barrier can enhance interdiffusion via grain boundaries.

Marker studies for the Ni-P/Pb-Sn system was not conducted. Consequently, it is difficult to predict which of the two Ni_3Sn_4 interfaces contributes to its growth. If it is assumed that the Ni_3Sn_4 /Pb-Sn interface dictates growth then the growth at this interface is likely to be limited by the availability of Sn. Semlitsch [9] has investigated growth of Ni-Sn compounds at 170°C with overlays containing 12, 16, and 20 wt/o Sn. With 12 and 16 wt/o Sn, Ni_3Sn_4 grows, but for the 16 wt/o Sn this compound begins to transform to Ni_3Sn_6 after 300h of heat treatment. On the other hand, with 20 wt/o Sn, the transformation occurs after only 100h. This shows that the Sn content in the overlay not only dictates the growth of a compound but also the type of compound formed.

The growth rate of Ni_3Sn_4 from the Ni-P/Pb-Sn

system is shown in Fig 52. However, since the Ni/Pb-Sn system was not investigated the relative benefits of a Ni-P barrier over a Ni barrier cannot be discussed. Unlike the growth of Ni_3Sn_4 in Ni/Sn and Ni-P/Sn systems, Ni_3Sn_4 in the Ni-P/Pb-Sn system grows parabolically. The parabolic nature of Ni_3Sn_4 growth cannot be explained in any detail. Perhaps, one argument is that the compound once formed relies predominantly on the diffusion of Sn through the Pb-rich phase in the overlay.

5.4 Suppression of Ni_3Sn_4 intermediate phase in amorphous Ni-P/Sn diffusion couples

The kinetics of growth of intermediate phases in binary diffusion couples have been studied in several theoretical and experimental investigations. Williams et al [162] have presented a summary of earlier work. Recently, however, a model has been presented which establishes the criterion for the survival of a nucleated phase [163]. The model specifies a requirement of minimum flux through the intermediate phase in order that it acquires a stable thickness relative to its adjacent phases. Under conditions where the flux within the newly created phase is significantly less than that in its parent phases, the new phase

cannot acquire macroscopic dimensions and may even contract to satisfy the flux requirement.

In the following discussion the notions of the above model will be used to describe the absence of the Ni_3Sn_4 phase in Ni-P/Sn system with reference to a model which describes the formation of duplex Ni-Sn compounds in Ni/Sn system. However, since the above model is based purely on diffusional considerations a brief discussion on other impediments to the formation of intermediate phases will also be given.

5.4.1 Duplex Ni-Sn compounds on crystalline Ni barrier

Fig 55 shows the schematic representation of a Ni_3Sn_4 nucleus at a $\text{Ni}_3\text{Sn}_4/\text{Sn}$ interface after the Ni_3Sn_4 compound has acquired a critical thickness. The direction velocities of various interfaces are also shown together with their inequalities which describes the successful growth conditions for Ni_3Sn_4 compound in the crystalline Ni barrier/Sn overlay system.

The notion of critical thickness is well known; as the dominant phase grows, flux across it diminishes, the rate of migration of its boundaries decreases and conditions for successful growth of a subsequent phase are enhanced. Experimentally, this has been observed.

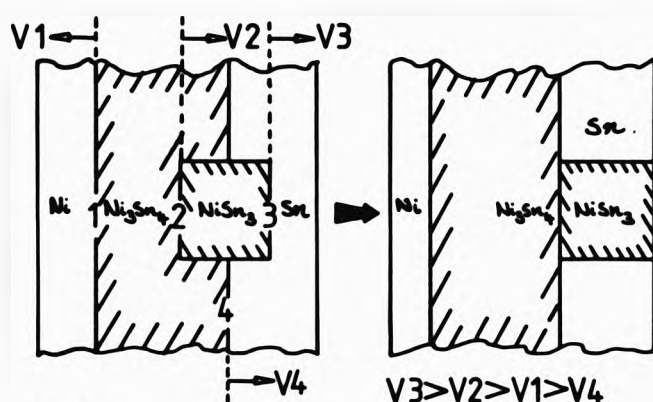


Fig55 Model for the growth of duplex ($\text{Ni}_3\text{Sn}_4 + \text{NiSn}_3$) compound on crystalline Ni barrier with Sn overlay.

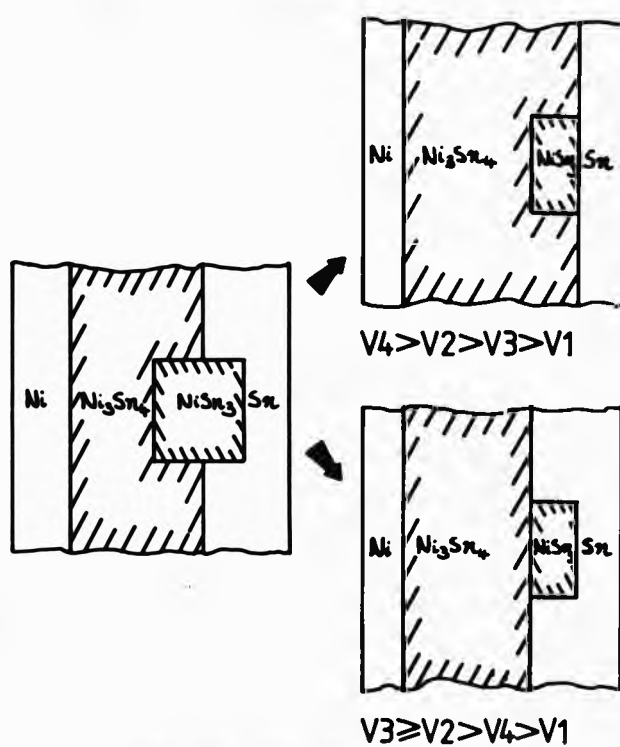


Fig56 Model for the growth of duplex ($\text{Ni}_3\text{Sn}_4 + \text{NiSn}_3$) compound on crystalline Ni barrier with Sn overlay.

With up to 143h of heat treatment the second compound was not detected however, for the samples heat treated up to 4592h, a substantial thickness of Ni_3Sn_4 compound was found. Initially, the growth velocity V_4 of Ni_3Sn_4 compound at interface 4 is expected to be greater than V_1 since Ni diffuses interstitially in Sn and the necessary composition and atomic rearrangement can be acquired relatively easily. However, as the compound layer approaches its critical thickness the Ni flux diminishes and V_4 decreases. Yet the compound is expected to continue its growth at interface 1 since Sn flux is thought to be greater than Ni flux through the compound. Thus, a part of the required inequality, that $V_1 > V_4$, is satisfied.

At the critical thickness of the Ni_3Sn_4 compound, Ni_3Sn_5 nucleates since the Ni flux through both compounds is greater than the critical value required to sustain Ni_3Sn_5 growth. This is evident from the excess Ni observed on the Sn side of the Ni_3Sn_4 compound (Fig 46) after 2504h of heat treatment. The continued growth of Ni_3Sn_5 nucleus depends on the relative order of magnitudes of interface velocities V_2 , V_3 , and V_4 . If it is assumed that V_4 is greater than both V_3 and V_2 then this leads to the condition that Ni_3Sn_4 out-grows the Ni_3Sn_5 nucleus. This cannot be the case, since a steady growth of Ni_3Sn_5 has been observed even up to 4592h of heat treatment. Furthermore, V_4 in

this model represents the velocity of the $\text{Ni}_3\text{Sn}_4/\text{Sn}$ interface at critical thickness in absence of NiSn_3 , which is expected to be very small since Ni flux is also expected to have fallen below the critical level. Hence, both V_3 and V_2 are greater than V_4 .

If NiSn_3 is to acquire macroscopic dimensions then it is clear that $V_3 > V_2$ and in the direction shown in Fig 55. This implies that V_3 , the growth rate of NiSn_3 , is greater than the rate of transformation at the $\text{Ni}_3\text{Sn}_4/\text{NiSn}_3$ interface. V_2 corresponds to either NiSn_3 transforming to Ni_3Sn_4 compound or vice versa. The latter case is unlikely since the higher temperature compound of the two is Ni_3Sn_4 , which cannot transform to the less stable, low temperature NiSn_3 compound. A direct proof of this was provided by Kay and Mackay [12] who found that NiSn_3 transforms to Ni_3Sn_4 compound at temperatures above 100°C . Finally, the growth front (V_3) of NiSn_3 in contact with Sn is expected to migrate at a much faster rate since only one Ni atom is required which readily diffuses in Sn and therefore easily facilitates the atomic rearrangement necessary for the growth of NiSn_3 .

Thus, the schematic of a model shown in Fig 55 describes the growth of duplex Ni-Sn compounds on a crystalline Ni barrier in terms of relative

interfacial velocities. It is postulated that for a successful growth of a second compound the interfacial velocities bear the following inequality:

$$V_3 > V_2 \quad V_1 \quad V_4$$

5.4.2 Single Ni-Sn compound on amorphous Ni-P barrier.

In the previous section the kinetic behaviour of a model system with two compounds growing on crystalline Ni barrier was considered. In the following the kinetic behaviour of the same model system will be investigated but with the view of postulating a set of possible conditions leading to the suppression of Ni₃Sn₂ compound on amorphous a Ni-P barrier.

As in the previous section, it is assumed that Ni₃Sn₂ nucleus has formed when the critical thickness of Ni₃Sn₂ compound is achieved. Two possibilities are considered; either the nucleus survives to the extent that it is not detectable within the limits of detectability during the concentration depth profiling or the nucleus once formed does not survive at all.

The schematic of the latter is shown in Fig 56 together with the necessary inequality of interfacial velocities. It is assumed that V₁ is practically zero.

This is justified by considering the concentration profiles in Figs 43 and 45 together with the marker motion, which indicates that Ni is the dominant diffusant and that the depth of penetration of Sn in the Ni-P barrier is substantially less than that in the crystalline Ni barrier. Furthermore, the interphase region bounded by Ni-P and Sn markers in Fig 43 is thought to be a crystallised Ni-P barrier consisting of Ni rich islands in Ni_3P matrix [164]. Thus it is highly possible that the growth of Ni_3Sn_4 at the Ni-P/ Ni_3Sn_4 interface is likely to encounter an even greater barrier in terms of atomic rearrangement and therefore $V_4 > V_1$.

For the model system shown in Fig 56, a situation is considered where the Ni_3Sn_4 nucleus is out-grown by Ni_3Sn_4 and undergoes dissolution by transformation to Ni_3Sn_4 . This requires the rate of growth of Ni_3Sn_4 to be much lower than its transformation to Ni_3Sn_4 , which in turn is lower than the growth of Ni_3Sn_4 at the Sn interface. This means that the Ni flux is high enough to sustain Ni_3Sn_4 growth but not high enough for Ni_3Sn_4 at the Sn interface. Such a possibility can arise if the Ni flux in Ni_3Sn_4 after the nucleation of Ni_3Sn_4 is such that the majority of Ni atoms arriving at the $\text{Ni}_3\text{Sn}_4/\text{Ni}_3\text{Sn}_4$ interface are consumed in the transformation to Ni_3Sn_4 . Yet, the rate of this transformation should be slower than the direct growth

of Ni_3Sn_4 at the Sn interface. Clearly, this cannot be the case and therefore the inequality

$$V_4 > V_2 > V_3 > V_1$$

is not satisfied.

An alternative scenario is presented in Fig 56 with the relevant inequality. It is postulated that the Ni_3Sn_4 nucleus once formed continues to grow at the Sn interface but at the same time undergoes transformation at the $\text{Ni}_3\text{Sn}_4/\text{Ni}_3\text{Sn}_4$ interface. The growth and transformation of Ni_3Sn_4 proceeds in such a manner that $V_3 \geq V_2$ so that the nucleus does not acquire macroscopic dimensions. This is possible since the Ni flux from the Ni-P barrier is less than that from the Ni barrier (compare Ni profiles in Fig 42 and Fig 43). Consequently, a smaller of Ni excess is observed on the Sn side of the Ni_3Sn_4 (Figs 45 and 47) which leads to the following implications:

(I) The critical thickness of Ni_3Sn_4 with the Ni-P barrier should be achieved much earlier than that with a Ni barrier.

(II) $V_2 \rightarrow V_3$ since the majority of the Ni is consumed in the transformation of Ni_3Sn_4 to Ni_3Sn_4 and only the remainder is available for Ni_3Sn_4 growth.

(III) V_2 is expected to be $> V_4$ on the basis that less Ni is required to undergo transformation at the $\text{Ni}_3\text{Sn}_4/\text{NiSn}_3$ interface than to maintain Ni_3Sn_4 growth at the Sn interface.

As a consequence of I, II, and III the NiSn_3 nucleus is expected to shrink to a finite thickness such that the Ni flux within it is maintained at a critical value so that its existence is continued. In a steady state condition, Ni_3Sn_4 is expected to grow at the expense of NiSn_3 at a somewhat greater rate than otherwise it would in the absence of NiSn_3 . This model also satisfies the requirements of the Ni-Sn phase diagram which predicts the presence of both Ni_3Sn_4 and NiSn_3 compounds at low temperatures if the following interfacial velocity conditions are fulfilled:

$$V_3 \gg V_2 > V_4 > V_1$$

However, the thickness of NiSn_3 may be such that its presence is not detected by EDAX spot analysis which was used to determine the concentration profiles. This is a possibility since the average distance between successive points of analysis was 0.5 μm .

Other means that may be offered for the missing

NiSn₃ phase are the nucleation barrier due to impurity segregation effects, or the rate of movement of the NiSn₃ interface being under reaction control. In the latter case the rate of migration could be slower than diffusion controlled migration. However, this is unlikely since the growth of NiSn₃ at the Sn interface is expected to be energetically more favourable and therefore does not pose a problem of reaction.

5.5 Technological importance of amorphous Ni-P barrier

Crystalline Ni is the most widely used diffusion barrier in the bearing industry. As recently as 1987, Tomlinson and Rhodes [161] have claimed to be the first to report the results of interaction between electroless Ni-P and Sn, which is primarily intended for application in the electronics industry. In the light of this, the results of this thesis concerning the interaction of amorphous Ni-P/Sn, Pb-Sn are novel. It is found that the amorphous Ni-P barrier with Sn overlay offers a significant advantage over the crystalline Ni barrier and this becomes apparent after 300-400 h of heat treatment. However, for bearing applications, Pb-Sn overlays are used and not Sn overlays. Nevertheless, an assumption that the amorphous Ni-P barrier is likely to offer similar advantages when used in conjunction with Pb-Sn overlay is not unjustified. A direct comparison of the Ni-P/Pb-Sn system with that of the Ni/Pb-Sn is not available but, it is found that with the Ni-P/Pb-Sn system the barrier remains amorphous for longer periods of heat treatment (33.67 - 236h) and that during this period interdiffusion and Ni_3Sn_4 nucleation is delayed.

The results presented in this thesis are from laboratory based experiments and require further investigation of the behaviour of the amorphous Ni-P barrier on bearings tested in actual engine test rigs. Two aspects to these tests requires elucidation:

i) The structural integrity of the Ni-P amorphous alloy in terms of rates of crystallisation and interdiffusion under extreme pressures.

ii) The fatigue behaviour of the amorphous Ni-P alloy.

5.6 CONCLUSIONS

1. Previous claims that Cu-P and Cu-B barriers based on Johnsons diffusional theory - that the diffusion of impurity (P or B) into the overlay inhibits the diffusion of Sn - are unfounded for concentrated (Pb-10 w/o Sn) alloys.
2. Quantitative analysis of previously produced samples indicate that only 0.1 w/o Sn was present in the overlay and not 10 w/o Sn as claimed. This confirms that Johnson's effect is probably only valid for dilute (Pb-0.1 w/o Sn) alloys.
3. As a consequence of 1 and 2 the claims that Cu-P and Cu-B diffusion barriers prevent the nucleation of Cu_3Sn and Cu_6Sn_5 compounds are also unfounded.
4. Furthermore, a similar approach based on Pb-P barrier and the co-deposition of Ni impurities with Pb-Sn overlay has also proved to be futile.
5. An alternative barrier based on amorphous Ni-P alloy has been identified. The compound growth rate on amorphous Ni-P barrier overlayed with Sn was found to be up to one third less than that on a conventional Ni barrier.

6. Only Ni_3Sn_4 compound grows on a amorphous Ni-P barrier whereas, Ni_3Sn_4 and NiSn_2 compounds grow on the Ni barrier. The latter compound is observed after the Ni_3Sn_4 has acquired a critical thickness.
7. During the early stages of heat treatment, an incubation period was found for both the Ni-P/Sn and the Ni/Sn systems. This incubation period was denoted by extensive intermixing which is a precursor to compound formation.
8. The Ni_3Sn_4 compound on the Ni-P barrier grows non-parabolically for the first 900h of heat treatment and thereafter tends to grow parabolically. For the Ni barrier, non-parabolic growth is observed for the first 400h and thereafter the combined growth of duplex compounds displays parabolic nature.
9. The appx values of interdiffusion coefficients calculated for Ni_3Sn_4 compound from the Ni-P/Sn and Ni/Sn systems were found to be $1.51 \times 10^{-11} \text{ cm}^2\text{s}^{-1}$ and $1.93 \times 10^{-11} \text{ cm}^2\text{s}^{-1}$ respectively, whereas that for NiSn_2 compound was found to be one order of magnitude lower, i.e. $2.86 \times 10^{-12} \text{ cm}^2\text{s}^{-1}$.
10. The Ni-P barrier overlayed with Pb-20 w/o Sn alloy retains its amorphous nature for longer duration of heat treatment. During this period the extent of

interdiffusion is markedly less compared to that in Ni/Sn and Ni-P/Sn systems.

11. It is thought that the onset of partial crystallisation of the Ni-P barrier is brought about by the diffusion of Sn in the barrier. For the Ni-P/Pb-Sn system, crystallisation is prolonged until the concentration of Sn in excess of 40 at/o is acquired in the barrier.

5.7 SUGGESTIONS FOR FURTHER WORK

In the main there are three general aspects to this project which warrants further investigation.

1. The need to evaluate the performance of a amorphous Ni-P barrier from engine tests, in terms of mechanical properties and structural integrity of the Ni-P barrier and additional benefits offered by way of enhanced corrosion protection.
2. Improvement of the amorphous Ni-P barrier by codeposition of a second metal, metalloid or both.
3. A detailed investigation of the crystallisation process in the Ni-P/Pb-Sn system.

REFERENCES

1. Lewis, W.R., 'Tin and its Uses' No77, p.10, 1968
2. Baker, R.G., Metals and Materials, Jan.1985, p.45
3. Ulrich Engel, SAE paper No.860354, 1986
4. Kalubowila, P.W., PhD Thesis, CNAA, 1984
5. Kalubowila, P.W. and Wach, S.P., UK Patent GB 2114156A
6. Kalubowila, P.W. et al., UK Patent GB 2117403A
7. Dybkov, V.I., J. Mat. Sci., 21, 1986, p.3078
8. Dybkov, V.I., J. Mat. Sci., 21, 1986, p.3085
9. Semlitsch, M., 5th. Intl. Cong. on X-Ray Opt. and Microanalysis, Tübingen, Sept. 1968
10. Semlitsch, M., Microchemica Acta (wein), Suppl. IV, 1970, p.157
11. Kay, P.J. and Mackay, C.A., Trans. Inst. Met. Fin., 54, 1976, p.68
12. Kay, P.J. and Mackay, C.A., Trans. Inst. Met. Fin., 57, 1979, p.169
13. Unsworth, D.A. and Mackay, C.A., Trans. Inst. Met. Fin., 51, 1973, p.85
14. Greenfield, L.T. and Forrester, P.G., Tin Res. Inst. Pub. No.155, 1965
15. Edges, E.S., ed., 'Tin and its Alloys', London, Edward Arnold, 1960, ch.8
16. Pratt, G.C., Intl. Met. Rev., 18, 174, 1973, p.62
17. Hillgers, W., 'Bearing Metals and their Uses', Goldschmidt Informiert, 2, 70, No11, 1972
18. Thwaites, C.J., 'Developments in Plain Bearing Technology', Intl. Tin Res. Inst., Pub. No513
19. Brit. Patent 1325291
20. Hunsicker, H.V., SAE Quart. Trans., 1, 1, 1947, p.6
21. Lloyd, K. and Love, P.P., Proc. Conf. on Tin Consumption, Intl. Tin Council, London, 1972, p.101
22. Desvaux, M.P., Tribology, 5, 2, 1972, p.61

23. Bierlein, J.C., et al., Intl. Autm. Eng. Cong., Detroit, 1969, Pub. No 690113
24. Eppich, R.E. et al., Mat. Eng. Cong., Tech. Report No P9-S.2, 1969
25. Pratt, G.C. and Lytwynec, M.D., SAE Paper No 86035, 1983
26. Eastham, D.R. and Crooks, C.G., Intl. Cong. on Metals Eng. (Met.Fin.), University of Aston in Birmingham, Sept. 1981, P.7/1
27. UK Patent GB 2060692A
28. Yamada, K. et al., 10th Intl. Cong. on Combustion Engines, Washington, 1973
29. Zuidema, H.H., 'Performance of Lubricating Oils', New York, (Reinhold), 1959
30. Miskinova, T.A. and Gindin, L.G., 'Protection of Metals', 1, 165, 1965
31. Wilson, R.W. and Shone, E.B., 'Anti-Corrosion', Aug., 1970
32. Pratt, G.C. and Whitney, W.J., SAE Paper No 830063, 1983
33. Flynn, C.P. ed., 'Point Defects and Diffusion', Clarendon, Oxford, 1972, p.19
34. Manning, J.R., 'Diffusion Kinetics for Atoms in Crystals', Van Nostrand, Princeton, 1968, p.1
35. Adda, Y. and Philbert, J., 'La Diffusie dans les Solides', Vol.1, Universitaire de France, 1966, p.20
36. Girifalco, L.A., 'Atomic Migration in Crystals', Blaisdell, New York, 1964, p.26
37. Shewmon, P.G., 'Diffusion in Solids', McGraw Hill, New York, 1964, p.9
38. de Groot, S.R. and Mazur, P., 'Non Equilibrium Thermodynamics', North Holland, Amsterdam, 1962, p.15
39. Franklin, A.D., 'Point Defects in Solids', Vol.1, ed. Crawford, J.H. and Slifkin, L.M., Plenum Press, New York, 1972, p.1
40. Barr, L.W. and Lidiard, A.B., 'Physical Chemistry', Vol.10, ed. Jost, W., Academic Press, New York,

- 1970, p.151
41. Peterson, N.L., Solid State Physics, Vol.22, ed. Seitz, F.W. et al., Academic Press, New York, 1968, p.409
 42. Howard, R.E. and Lidiard, A.B., Rep. Prog. Phys., 27, 1964, p.161
 43. Lazarus, D., 'Solid State Physics', Vol.10, ed. Seitz, F. and Turnbull, D., Academic Press, New York, 1960, p.71
 44. Anthony, T.R. 'Vacancies and Interstitials in Metals', ed. Seegar, A. et al., North Holland, 1970, p.935
 45. Owen, E.L. 'Properties of Electrodeposits, Their Measurements and Significance', ed. Sard, R. et al., The electrochemical Soc., Princeton, 1975, p.80
 46. Porter, D.A. and Easterling, K.E., 'Phase Transformation in Metals and Alloys', Reinhold, N. Y., 1981, p.60
 47. Seitz, F., 'Fundamental Aspects of Diffusion in Solids', Pittsburgh, 1948
 48. Huntington, H., Phys. Rev., 58, 1940, p.143
 49. Huntington, H., Phys. Rev., 61, 1942, p.325
 50. Feder, R. and Nowick, A.S., Phys. Rev., 109, 1958, p.1959
 51. Simmons, R.D. and Baluffi, R.W., Phys. Rev., 117, 1960, p.52
 52. Simmons, R.D. and Baluffi, R.W., Phys. Rev., 129, 1963, p.1533
 53. Simmons, R.D. and Baluffi, R.W., Phys. Rev., 119, 1960, p.600
 54. Simmons, R.D. and Baluffi, R.W., Phys. Rev., 125, 1962, p.862
 55. Feder, R. and Nowick, A.S., Phil. Mag., 15, 1967, p.805
 56. Metselaar, R., J. Mat. Edcn., 6, 1-2, 1984, p.229
 57. Le Clair, D.E., 'Diffusion in Body Centred Cubic Metals', Am. Soc. Metals, 1965, p.3
 58. Seegar, A. and Mehrer, H., 'Vacancies and Interstitials in Metals', ed. Seegar, A. et al., North Holland, 1970, p.1

59. Seegar, A., J. of Less Common Metals, 28, 1972, p.38
60. Grube, G. and Jedele, A, Zeit. Electrochem., 38, 1932, p.779
61. Heumann, T., Zeit. Physik. Chem., 201, 1952, p.168
62. Wagner, C., Acta Met., 17, 1969, p.99
63. Creydt, M. and Fisher, R., Metall. Wissenschaft u Technik, 10, 1971, p.1124
64. Tu, K.N. and Thompson, R.D., Acta Metall., 30, 1982, p.947
65. Castell-Evens, J.V., Trans. Inst. Met. Fin., 1969, 47, p.71
66. Gabe, D.R. and Mort, R.J., J. Iron Steel Inst., 1965, 203, p.64
67. Cogan, S.F. et al., J. Mat. Sci., 19, 1984, p.497
68. Vertes, A. et al., J. Radanal. Nuc. Chem., 111, 2, 1987, p.283
69. Cantor, B., Proc. Conf. Rapidly Quenched Metals, eds. Steeb, S. and Warlimont, H., Elsevier Sci. Pub., B.V., 1985, p.595
70. Cahn, R.W., J. Vac. Sci. Tech., A4, 6, 1986, p.3071
71. Luborsky, F.E., ed. Amorphous Metallic Alloys, Butterworths, London, 1983, p.487
72. Ahmadzadeh, M. and Cantor, B., J. Non. Cryst. Solids., 43, 1981, p.189
73. Buschow, K.H.J. et al., Solid Stat. Commun., 43, 1982, p.171
74. Akhtar, D. et al., Scr. Metall., 16, 1982, p.417
75. Akhtar, D. and Misra, R.D., Scr. Metall., 19, 1985, p.603
76. Jost, W., 'Diffusion in Solids, Liquids and Gases', Academic Press, N.Y., 3rd edn., 1960, chs. 1, 9.
77. Hauffe, K., 'Reactionen in und an festen Stoffen', Springer, Berlin, 1955, Part 2.
78. Arkharov, V.I., Fiz. Metall Metalloved, 8, 1959, p.193

79. Schroder, B. and Leute, V., J. Phys. Chem. Solids, 41, 1980, p.827
80. Fromhold, A.T. and Sato, N., Oxid. Metals, 16, 1981, p.203
81. Fujiwara, Y. et al., High Temp. High Press., 12, 1980, p.643
82. Lopes Gomes, J.E. and Huntz, A.M., Oxid. Metals, 14, 1980, p.471
83. Kidson, J.V., J. Nucl. Mater., 3, 1961, p.21
84. Gurov, K.P. et al., 'Vzaimnaya Diffuziya v Mnogofaznykh Metallicheskiykh Sistemakh', Nauka, Moscow, 1981, chs. 3 and 6
85. Kofstad, P., 'High Temperature Oxidation of Metals', Wiley, N.Y., 1968, chs. 1, 5-7
86. van Loo, F.J. and Rieck, G.D., Acta Metall. 21, 1973, p.61
87. Arkharov, V.I. et al., Oxid. Metals, 3, 1971, p.251
88. Evens, U.R., 'Corrosion and Oxidation of Metals', Edward Arnold, London, 1960, ch.20
89. Loria, J., Comp. Rend, 227, 1949, p.547
90. Loria, J., Comp. Rend, 231, 1950, p.522
91. Loria, J., Comp. Rend, 234, 1952, p.91

92. Nicolet, M.A., Thin Solid Films, 52, 1978, p. 415
93. Engel, U., SAE Technical Paper Series, 860648, SAE Congress, 1986.
94. Campisano S.U. et al., Philos. Mag., 35, 1977, p. 1333
95. Baglin, J.E et al., in Ion Beam Surface Layer Analysis, Edts. Meyer, O., Linker G., and Kapperler, F., Plenum Press, New York, 1976, p.385
96. Harris, J.M. et al., J. Vac. Sci. Technol., 12, 1975, p.524
97. Nowicki, R.S. and Wang, I., J. Vac. Sci. Technol., 15, 1978, p.235

98. Tu, K.N and Rosenberg, R., Thin Solid Films, 13, 1972, p.163
99. Kirsch, R.G. et al., Appl. Phys. Lett., 29, 1976, p.772
100. Hiraki, A. et al., Phys. Status Solidi, A, 7, 1971, p.401
101. Hiraki, A. et al., J. Appl. Phys., 43, 1972, p.3643
102. Hiraki, A. et al., J. Vac. Sci. Technol., 9, 1972, p.155
103. Wittmer, M. et al., Solid Stat Electron., 20, 1977, p.433
104. Wittmer, M. et al., J. Vac. Sci. Technol., 14, 1977, p.935
105. Wiley, J.D. et al., IEEE Trans. Ind. Electron., IE29, 1982, p.154
106. Koster, U. and Herold, U., in Topics in Applied Physics, eds. Guntherodt, H. and Beck, H., Springer, Berlin, 1980, p.225
107. Donald, I.W. and Davies, H.A., Philos. Mag., A42, 1980, p.277
108. Chen, H.S. et al., Appl. Phys. Lett., 32, 1978, p.461
109. Rosenblum, M.P. et al., Appl. Phys. Lett., 37, 1980, p.184
110. Anderson, W.T. et al., Thin Solid Films, 104, 1983, p.57
111. Suni, I. and Nicolet, M.A., Thin Solid Films, 107, 1983, p.73
112. Thomas, R.E. et al., Thin Solid Films, 150, 1987, p.245
113. Zhu, M.F. et al., J. Appl. Phys., 56, 10, 1984, p.2740
114. Nelson, C.W., Proc. Intl. Symp. on Hybrid Microelectronics, Intl. Soc. of Hybrid Microelectronics, Montgomery, 1969, p.413
115. Fournier, P.R., U.S. Patent 3,879,746, 1975
116. Wittmer, M., Appl. Phys. Lett., 36, 1980, p.456

117. Finstad, T.G., Thin Solid Films, 51, 1978, p.411
118. Cheung, N.W. et al., J. Appl. Phys., 52, 1981, p.4297
119. Tu, K.N. and Chance, D.A., J. Appl. Phys., 46, 1975, p.3229
120. Cunningham, J.A. et al., IEEE Trans. Reliab., 19, 1970, p.182
121. Harris, J.M. et al., J. Electrochem. Soc., 123, 1976, p.120
122. Fukuoka, T. et al., U.K. Patent GB 2060 692A, 1980
123. Hodes, E. et al., U.K. Patent GB 2137 288A, 1983
124. U.K. Patent 1365 354, 1974
125. Bower, R.W., Appl. Phys. Lett., 23, 1973, p.79
126. Howard, J.K. et al., U.S. Patent 4201 999, 1980
127. Chu, W.K. et al., U.S. Patent 4206 472, 1980
128. Chang, C.A., J. Mat. Res., 2, 4, 1987, p.441
129. Gehring, A.P. et al., Extnd. Abst. 10th Int. Symp. on the Reactivity of Solids, Dijon, France, 1984
130. Watanabe, T. and Tanabe, Y., J. Met. Fin. Soc. Japan, 32, 1981, p.600
131. Ramanik, P. and Bhattacharya, R.N., J. Electrochem. Soc. 127, 1980, p.2086
132. Popereka, M.Y., Electrodepo. Surf. Treat., 2, 1973/74, p.447
133. Panicker, M.P. et al., J. Electrochem. Soc., 125, 1978, p.566
134. Baranski, A.S. et al., J. Electrochem. Soc., 130, 1983, p.579
135. Takeda, Y. et al., J. Electrochem. Soc., 128, 1981, p.1221
136. Lee, C.H. and Kroger, F.A., J. Electrochem. Soc., 129, 1982, p.936
137. Furuya, H. et al., J. Met. Fin. Soc. Japan, 32, 1981, p.631 and p.637
Furuya, H. et al., J. Met. Sci. Soc. Japan, 19,

- 1983, p.341
138. Omi,T. et al., J. Electrochem. Soc., 119, 1972, p.168
Cote,P.J. et al., J. Electrochem. Soc., 121, 1974, p.776
Omi,Y. et al., J. Met. Fin. Soc. Japan, 31, 1980, p.85
139. Watanabe,T. and Tanabe,Y., Met. Sci. Eng., 23, 1976, p.97
Ratagopal,C. et al., Met. Fin., 82, 1984, p.59
140. Koiwa,I. et al., Proc. 69th Annual meeting of J. Met. Fin. Soc. Japan, 1984, p.52
141. Scholder,R. et al., Z. Anorg. Allg. Chemie., 232, 1973, p.1
142. Bestgen,H. in ref. 69, p.443
143. Ogburn,F. and Johnson,C.E., Plating, 60, 1973, p.1043
144. Ratzker,M. et al., Plating and Surf. Fin., Sept. 1986, p. 74
145. Toth-Kadar,E. et al., Surf. Coatings Tech., 31, 1987, p.31
146. Brenner,A., Electrodeposition of Alloys, Acad. Press, Vol.2, p.457
147. Walsh,F.C. and Gabe,D.R., Surface Tech., 13, 1981, p.305
148. Electrodeposition of Tin-Lead Alloys, Intl. Res. Inst., Pub.No. 325, Aug.1961
149. Hoshino et al., J. Electrochem Soc., 133, 4, p.68.
150. European Patent Appln., 0160761 A1, 1984.
151. Dingley et al., The Bulletin of Bismuth Institute, 2nd Quarter, 20, 1978.
152. Hansen, M., 'Constitution of Binary Alloys', McGraw Hill Book Co.,N.Y., 1958.
153. Huntington, H.B., Point and Defects Interaction in Metals', Yamada Science Foundation, University of Tokyo Press, 1982, p.589.
154. Bene', R.W., J. Appl. Phys., 61, 5, 1987, p.1826.
155. Bene', R.W., Appl. Phys. Lett., 41, 6, 1982, p.529.

156. Tu, K.N. and Rosenberg, R., Jap. J. Appl. Phys., Suppl. 2, Pt.1, 1974, p.633.
157. Marinkovic and Simic, Thin Solid Films, 98, 1982, p.95.
158. Mehner, H. and Vertes, A., J. Radioanal. Nuc. Chem., 89, 1985, p.153.
159. Vertes, A. et al., J. Radioanal. Nuc. Chem. Artcls., 3, 2, 1987, p.283.
160. Harman, A. C., Proc. Internepcon., Brighton, 1978, p.42, Edt. Mansfield, H. G., Kilver Communs., UK.
161. Tomlinson, W. J. and Rhodes, H. G., J. Mat. Sci., 22, 1987, p.1769.
162. Williams, D. S. et al., Metall. Trans. A, 12, 1981, p.639.
163. Williams, D. S., Thin Solid Films, 142, 1986, p.47.
164. Pittermann, U. and Ripper, S., (Ref.69, p.385).
165. Smoluchowski, R., Phys. Rev., 62, Dec.1942, p.539.
166. X-ray Powder Diffraction File, ASTM STP 48, American Society for Testing and Materials, Philadelphia, 1982.
167. Hansen, M., 'Constitution of Binary Alloys', McGraw Hill Book Co., N.Y., 1958.

THE BRITISH LIBRARY DOCUMENT SUPPLY CENTRE

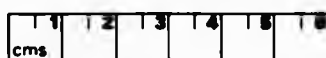
TITLE DIFFUSION PROBLEMS AND DEGRADATION OF BEARING OVERLAYS

AUTHOR Prakash Shashikant Patel

INSTITUTION C.W.A.A. City of London Polytechnic
and DATE 1989

Attention is drawn to the fact that the copyright of this thesis rests with its author.

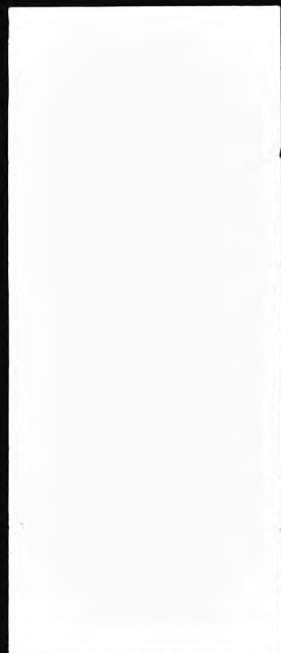
This copy of the thesis has been supplied on condition that anyone who consults it is understood to recognise that its copyright rests with its author and that no information derived from it may be published without the author's prior written consent.



CAM. 9

THE BRITISH LIBRARY
DOCUMENT SUPPLY CENTRE
Boston Spa, Wetherby
West Yorkshire
United Kingdom

REDUCTION X 21



DX

96473